# GROWTH AND CHARACTERIZATION OF SPRAY DEPOSITED LEAD ZINC SULPHIDE THIN FILMS

**Thesis**

**Submitted in partial fulfilment of the requirements for the degree of**

**DOCTOR OF PHILOSOPHY**

**By**

**VEENA . E**

**(Reg No: PH13F04)**


**DEPARTMENT OF PHYSICS**

**NATIONAL INSTITUTE OF TECHNOLOGY KARNATAKA,**

**SURATHKAL, MANGALORE-575025**

**MAY, 2018**

# DECLARATION

I hereby declare that the Research Thesis entitled "**Growth and characterization of spray deposited lead zinc sulphide thin films"** which is being submitted to the National Institute of Technology Karnataka, Surathkal in partial fulfilment of the requirements for the award of the Degree of **Doctor of Philosophy** in **Physics** is a *bonafide report of the research work carried out by me*. The material contained in this Research Thesis has not been submitted to any University or Institution for the award of any degree.

Reg. No. 135035PH13F04

Department of Physics

Place: NITK, Surathkal

Date:

# CERTIFICATE

This is to *certify* that the Research Thesis entitled "**Growth and characterization of spray deposited lead zinc sulphide thin films"** submitted by Veena E. (Reg. No. **135035PH13F04**) as the record of the research work carried out by her, is accepted as the Research Thesis submission in partial fulfilment of the requirements for the award of degree of **Doctor of Philosophy**.

**Prof. Kasturi V. Bangera**

Research Guide

Chairman-DRPC

## ACKNOWLEDGEMENT

The work presented in this thesis would not have been possible without my close association with many people who were always there when I needed them the most. I take this opportunity to acknowledge them and extend my sincere gratitude for helping me to finish my Ph.D.

On this occasion, I would like to express my deep and sincere gratitude to my research supervisor Prof. Kasturi V. Bangera for providing an opportunity to do research under her supervision. My thanks are due to her inspiring guidance, fruitful suggestions, constant support and encouragement at every stage of my work in spite of her ill health. I heartily acknowledge for her motherly care, kindness and generous which helped timely completion of my thesis.

There are no words to express my respectful thanks and gratefulness to Prof. G. K. Shivakumar who has been there for giving fruitful advice in channelizing the research work.

I sincerely thank my research panel members Dr. M. N. Sathyanarayan (present HOD) and Prof. Airody Vasudeva Adhikari for their valuable suggestions and excellent advice in accomplishing this work.

I must thank my research seniors Dr. Sowmya Palimar, Dr. Sadanand Kumar, Dr. Shashidhar for their suggestions. I also thank my present colleagues Mr. Santhosh T.C.M., Mr. Bharath S.P. (XRD characterization), Miss Vallem Sowjanya and Mr Biswajit Barman for their help, encouragement and wishes.

The help received from Manipal Institute of Technology for providing SEM and UV – VIS spectrometer facility is greatly acknowledged.

I thank all faculty members, research students, teaching and non teaching staff of the department of physics, for their kind and sincere support during my research period. I am grateful to the present and previous Head of the Department for supporting me to attend various conferences and workshops which in turn helped me to understand the current research trends.

I am grateful to my mother, father, mother in law, husband, sibling and my teacher Mrs. Kamalamma, Mr. Eshwarappa, Mrs. Lakshmidevamma, Mr. Chethan Kumar, Miss Chaitra, Mr. Naik D. C. and Mr. Prabhu Kumar who have provided me with moral and emotional support in my life. I am also grateful to my remaining family members and friends who have supported me along the way.

A very special gratitude goes out to National Institute of Technology Karnataka for helping and providing the financial assistance for my research work.

And finally, last but by no means least, I cannot find words to thank the supreme father, he was remembered every time I did not.

Mrs. Veena E.

# ABSTRACT

Ternary thin films are attractive for many applications due to their band gap tunability. In the present study, the stoichiometric n-$Pb_xZn_{1-x}S$ (x = 0, 0.2, 0.4, 0.5, 0.6, 0.8 and 1) were deposited on glass substrates using spray pyrolysis technique. The structural, optical and electrical studies have been made in order to understand the band gap tunability of prepared films. The optical band gap energy of $Pb_xZn_{1-x}S$ thin films varied from 0.40 eV to 3.54 eV and the transition has been changed from indirect to direct with different Pb: Zn mole fractions. It has been observed that the complete indirect to the direct transition of energy band gap occurred in $Pb_xZn_{1-x}S$ ($x \leq 0.5$) thin films. The resistivity and activation energy of the films were increased with an increase in the band gap indicating the formation of a mixed films of PbS and ZnS in the ternary phase.

Photoconductivity of the films was thoroughly studied and the possibility of using the lead zinc sulphide thin films as UV-IR photo detectors was investigated. Heterojunctions p-Si/n-PbS, p-Si/n-ZnS and p-Si/n-$Pb_xZn_{1-x}S$ were fabricated considering their usefulness in the fabrication of optoelectronic devices. A detailed electrical characterization of these heterojunctions was performed to understand the conduction mechanism in operation and also to determine various technically important parameters. The results confirmed the formation of a continues solid solution of PbS and ZnS in the ternary phase which can be a suitable candidate for optoelectronic applications.



**Keywords**:

Composite materials; Chemical synthesis; Electrical properties; X-ray diffraction.

# CONTENTS

## CHAPTER 3

## PREPARATION AND CHARACTERIZATION OF LEAD SULPHIDE THIN FILMS

**LIST OF TABLES**

**NOMENCLATURES**

**ABBREVATIONS**

| | |
|---|---|
| PLD | Pulsed laser ablation |
| KrF | Krypton fluoride |
| ArF | Argon fluoride |
| Nd-YAG | Neodymium-doped yttrium aluminium garnet |
| MBE | Molecular beam epitaxy |
| DC | Direct current |
| RF | Radio frequency |
| CVD | Chemical vapour deposition |
| LPCVD | Lower pressure chemical vapour deposition |
| PECVD | Plasma enhanced chemical vapour deposition |
| MOCVD | Metal organic chemical vapour deposition |
| LECVD | Laser-enhanced chemical vapour deposition |
| PVD | Physical vapour deposition |
| LVDT | Linear variable differential transformer |
| AC | Alternating current |
| TEM | Transmission electron microscope |
| SEM | Scanning electron microscope |
| HRTEM | High resolution transmission electron microscope |
| UV | Ultraviolet |
| IR | Infrared |
| PbS | Lead sulphide |

| | |
|---|---|
| ZnS | Zinc sulphide |
| PbZnS | Lead zinc sulphide |
| CBD | Chemical bath deposition |
| SILAR | Successive ionic laser adsorption and reaction |
| PH | Potential of hydrogen |
| PL | Photoluminescence |
| PbMgS | Lead magnesium sulphide |
| Mg | Magnesium |
| VIS | Visible |
| NIR | Near infrared |
| Pb | Lead |
| Cd | Cadmium |
| PC | Personal computer |
| XRD | X-ray diffraction |
| Zn | Zinc |
| EDAX | Energy dispersive analysis from X-Ray |
| XRA | X-ray absorption |
| XRF | X-ray fluorescence |
| FWHM | Full width half maximum |
| TC | Texture coefficient |
| T | Temperature |

| | |
|---|---|
| R | Resistance |
| K | Boltzmann constant |
| Pb $(CH_3COO)_2$ | Lead acetate |
| CS $(NH_2)_2$ | Thiourea |
| $CH_3COOH$ | Acetic acid |
| $NH_3$ | Amonia |
| $CO_2$ | Carbon dioxide |
| D | Crystallite size |
| $V_{DC}$ | Direct current potential |
| JCPDS | Joint Committee on Powder Diffraction Standards |
| ZnO | Zinc oxide |
| Zn $(CH_3COO)_2$ | Zinc acetate |
| $Cd_{1-x}Zn_xS$ | Cadmium zinc sulphide |
| f(θ) | Nelson relay function |
| SCLC | Space charge limited conduction |
| a, b and c | Lattice parameters |
| A | Absorbance |

**SYMBOLS AND UNITS**

| | |
|---|---|
| *d* | Interplanar distance (Å) |
| *λ* | Wavelength of X-ray |
| *2θ* | Diffracted angle/Bragg angle (Degree) |

| | |
|---|---|
| $N$ | Reflection number |
| $\Delta E$ | Change of band gap |
| $v$ | Frequency of radiation (Hz) |
| $I$ | Intensity of radiation |
| $\alpha$ | Absorption coefficient |
| $\rho$ | Resistivity ($\Omega$ cm) |
| $\Omega cm$ | Ohm Centimetre |
| $n$ | n-type |
| $p$ | p-type |
| $\mu$ | Carrier mobility ($cm^2/Vs$ ) |
| $cm^2/Vs$ | Centimetre square per volt second |
| $\Phi_b$ | Barrier height |
| $“$ | Inch |
| $A$ | Amperes |
| $I$-$V$ | Current-voltage (A-V) |
| $t$ | Thickness (nm) |
| $cm$ | Centimetre |
| $nm$ | Nano meter |
| $Å$ | Angstrom |
| $Cu\ K_\alpha$ | Characteristic X-Ray emission from transition K shell of copper |
| $J$ | Joule |

| | |
|---|---|
| $\varepsilon o$ | Permittivity |
| $E_a$ | Activation energy (eV) |
| $E_g$ | Energy band gap (eV) |
| $eV$ | Electron volt |
| $F_t$ | Thermophoretic force |
| $t_q$ | Thickness of the quartz crystal |
| $M$ | Molarity |
| $V$ | Volt |
| $^{\circ}C$ | Degree Celsius |
| $C$ | Velocity of light |
| $Cm^2$ | Centi meter square |
| $ml$ | mili leter |
| $Cm^{-3}$ | Per Centi meter cube |
| $Hrs$ | Hours |
| $At\%$ | Atomic percentage |
| $S/cm$ | Siemen per Centimetre |
| $K\,\Omega$ | Kilo Ohm |

# CHAPTER 1

# INTRODUCTION

## 1.1 THIN FILMS

Thin film is a physical phenomenon which is advanced due to the consequence of its planar geometry, unique structure and size. The occurrence of the metastable structure, quantum mechanical tunneling through super and normal conducting metal insulator junctions, the limit in size of electron and photon transport in metals, semiconductors and insulators, plasma resonance absorption and micromagnetic properties, epitaxial growth, are some of the remarkable contributions of the thin film phenomena in solid state physics. The technical interests which, stimulate in the study of thin films have also been rewarded in the form of useful inventions, such as a variety of passive and active microminiaturized components and devices, radiation detectors, solar cells, magnetic memory devices, interference filters, phototransistors, electrolysis photodiodes, surface acoustic; gas sensors, wave devices, transparent electrodes, high radiation resistance, laser emission and infrared photodetectors (Chopra 1969, Leaver et al. 1971).

The modern era in which we live in is within quest of materials that would satisfy the thirst of the ever blooming technology. The advance in science is always inadequate for the vision of the mankind. But most of the ideas of the vision have been realized. Thin films have a greater say in this revolution. The modern society has been changed by the ability of

engineering communities and material science. Implementing the novel materials by an extraordinary combination of mechanical, chemical and physical properties has changed the modern society. In the last decade, there is a rapid growth in the detailed study of the thin films below one micron of thickness. The advance of this technology has brought the researchers group to work effectively with scientific confidence. In addition, the development of the thin film technology is contributing to the multiple areas of research in chemical and physical (solid state) domain.

In last few decades majority of research work has been carried to reduce the size of electronic gadgets and increase their efficiency at the same time. This leads to the semiconductors used in the form of thin films and development of it in solid state electronics. Thin films are materials deposited on a substrate with smaller thickness range from few micrometers to nanometers which decide the properties of the film. Integration accomplished by fabricating many interconnected components on each supporting substrate forms thin film integrated circuits. Integration has many desirable results which include cost effectiveness, reproducibility, improved performance, and especially reliability (Berry et al. 1968). Unlike thin films, bulk devices have mixed properties which eventually limit their applications and require a lot of material for fabrication process which increases the production cost.

Thin films are different from a bulk material with some special characteristics such as (Kiyotaka et al. 2004):

- Bulk materials occupy a lot of space which results in the bigger devices, while thin film materials can be assembled on highly compact devices.
- Bulk devices require a lot of materials thus increasing the fabrication costs while thin films need very less material and so their fabrication cost is not high.
- Thin films have low density, low breakdown voltage and low dielectric constant compared to bulk materials.
- Thin films have lower melting point due to higher surface energy when compared to bulk materials.
- Selective transmission of reflection from interference takes place in thin films, unlike bulk materials.
- It has a high surface to volume ratio.
- It is also compact and has crystal-like properties.

- Due to tunneling, there is a large current density in thin films.
- Mechanical properties of thin films appear to be 200 times greater than the well-annealed bulk sample.

## 1.2 APPLICATIONS OF THIN FILMS

Thin films have wide application in electronic devices of the daily routine of modern civilization. Among various applications it can be classified into following domains (Anderson et al. 1965), namely:

- Electronics.
- Optics.
- Chemistry.
- Mechanics.
- Magnetics.

### 1.2.1 Electronics

Thin films provide a major contribution to the production of semiconductor technology. Semiconductor Technology is also termed as synonymous with thin films. Thin films are applicable during manufacturing of wireless devices, telecommunication devices namely routers and switches, integrated circuits (microprocessors, microcontrollers, and Programmable logical devices). It is also applicable in insulating and conducting films namely resistors, conductors, piezoelectric devices and many more devices.

### 1.2.2 Optics

Optics is a study of properties and behavior of light with help of optical instruments. Optical components like solar cells use antireflection coating techniques whereas mirror uses reflection coating technique. Antireflection coating will reduce unwanted reflections from different surface commonly used on photographic and spectacle lenses. Photosensitive thin film coating is used for analogue films and digital films.

### 1.2.3 Chemistry

Thin films are used as diffusion barriers which protect against corrosion and oxidation. It also used in liquid sensors and gas sensors.

### 1.2.4 Mechanics

In heavy machinery, engines and automobile manufacturers use thin films for friction reduction and it also provide adhesion.

1.2.5 Magnetics

Magnetic recording is storage of data on a magnetized medium namely Hard disks, SQUIDS, Video and audio tapes.

## 1.3 THIN FILM PREPARATION TECHNIQUES

There are mainly two methods for preparation of thin film based on the type of deposition as shown in Fig. 1.1(Anderson et al. 1965, Hass et al. 1971, Chopra et al. 1969, 1984, Berry et al. 2008).

Method1: Physical deposition process

Method2: Chemical deposition process

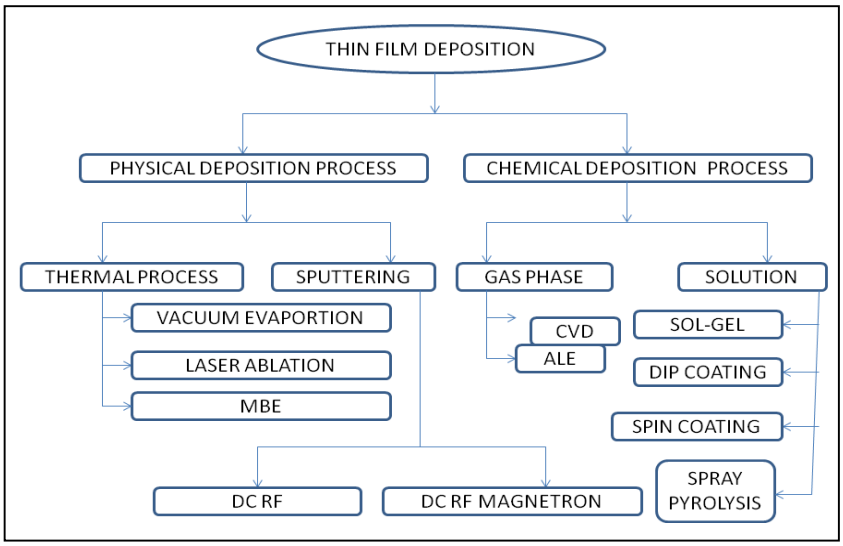


Fig. 1.1: Different preparation methods.

1.3.1 Physical deposition processes

1.3.1.1 Vacuum evaporation:

The thermal evaporation process comprises of evaporating source materials in a vacuum chamber below $10^{-6}$ torr and condensing the evaporated particles on a substrate. In this process, thermal energy is supplied to a source from which atoms were evaporated for deposition on a substrate. Heating of the source material can be accomplished by any of several methods. The simplest is resistance heating of a wire or strip of refractory metal to which the material to be evaporated has been attached. The evaporated atoms travel through reduced background pressure in the evaporation chamber and condense on the growth surface. The deposition rate or flux is a function of the travel distance from the source to the

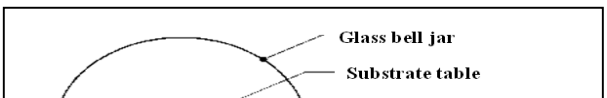

substrate, the angle of impingement onto the substrate surface, the substrate temperature and the base pressure.

Fig. 1.2 Vacuum evaporation technique.

1.3.1.2 Pulsed laser ablation

Pulsed laser deposition (PLD) is an improved thermal process used for the deposition of alloys or compounds with a controlled chemical composition. In laser deposition, a high-power pulsed laser (1 J/shot) is irradiated onto the target of source materials through a quartz window. In general, laser sources of PLD for magnetite thin films, are KrF (248 nm), ArF (193 nm) and Nd-YAG (266 or 355 nm). A quartz lens is used to increase the energy density of the laser power on the target source. Atoms that are ablated or evaporated from the surface are collected on nearby substrate surfaces to form thin films.

1.3.1.3 Molecular beam epitaxy (MBE)

This growth technique can provide film materials of extraordinarily good quality which are ideal for research purposes. However, the rate of growth is very low compared to other methods, which makes it of limited use for production of devices. In MBE, the deposition of a thin film can be accurately controlled at the atomic level in an ultra-high vacuum ($10^{-10}$ torr). A substrate wafer is placed in the ultra-high vacuum chamber. It is sputtered briefly with a low energy ion beam to remove surface contamination. This step is followed by a high temperature anneal to relax any damage done to the growth surface during preparation. The substrate is then cooled to the growth temperature, typically between 400$^{o}$C -700$^{o}$C and growth commences by directing atomic beams of the film material as well as a beam of dopant material if necessary toward the growth surface of the substrate. The beams are emitted from crucibles of the growth materials which have been heated to temperatures well above the substrate temperature to induce evaporation and condensation.

The film composition can be properly selected by accurate control of the atomic ratio of each metallic electron beam sources.

1.3.1.4 Sputtering process

The basic concept of sputtering is achieved by surface ejection of atoms from the surface by momentum transfer through bombarding ions. The major advantage of sputtering is a non-thermal physical process which is utilized for etching process and also deposition depends on ion energy. Different variants of the sputtering process such as DC, RF and DC/RF magnetron are used for thin films fabrication. The schematic diagram of DC and RF sputtering is shown in Fig.1.5.

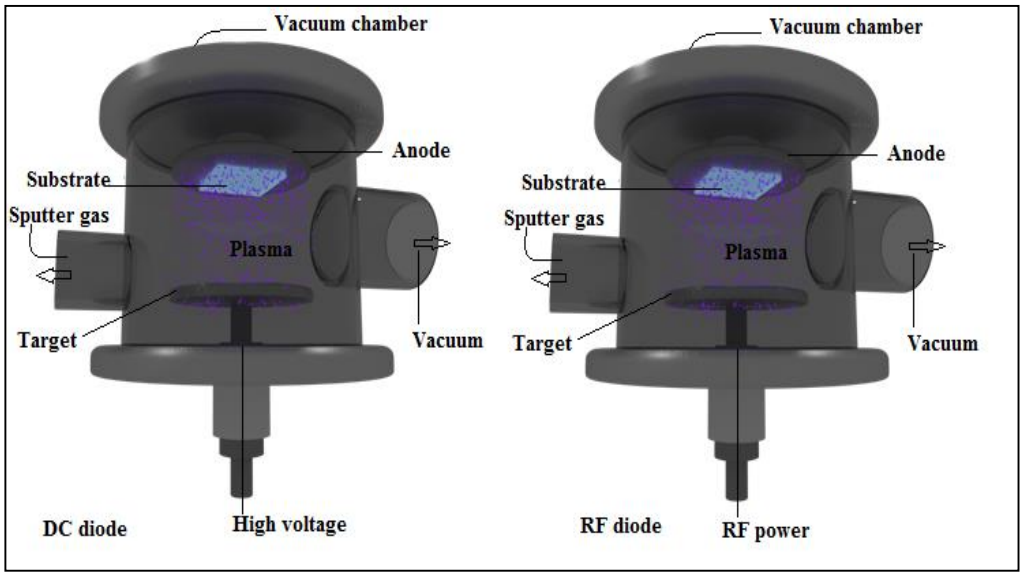


Fig. 1.5 Sputtering process.

1.3.2 Chemical deposition processes

1.3.2.1 Chemical vapor deposition (CVD)

It is the process of chemically reacting a volatile compound of a material to be deposited, with other gases, to produce a non-volatile solid that deposits atomistically on a suitably placed substrate. Among the reasons for the growing adoption of CVD methods is the ability to produce a large variety of films and coatings of metals, semiconductors, and compounds in a crystalline or vitreous form, possessing high purity and desirable properties. Furthermore, the capability of controllably creating films of widely varying stoichiometry

makes CVD unique among deposition techniques. Other advantages include the relatively low cost of the equipment and operating expenses, suitability for both batch and semi-continuous operation, and compatibility with other processing steps. Hence, many variants of CVD processing have been researched and developed in recent years, including low-pressure (LPCVD), plasma-enhanced (PECVD), metal-organic (MOCVD) and laser-enhanced (LECVD) chemical vapor deposition.

1.3.2.5 Spray pyrolysis

Spray pyrolysis is a chemical deposition method and an effective processing technique being considered in research to prepare thin and thick films, ceramic coatings, and powders. It has been developed in 1966 by Chamberlin and Skarmen for the deposition of inorganic films (Chamberlin et al. 1966). It has proved to be simple, reproducible and inexpensive, as well as suitable for large area applications. Besides the simple experimental arrangement, high growth rate and mass production capability for large area coatings makes them useful for industrial applications. It is an extremely easy technique for preparing films of any composition. Spray pyrolysis does not necessitate high-quality substrates or chemicals by using this technique one can control the film morphology and particle size in the nanometer range.

Even multilayered films can be easily prepared using this flexible technique. Deposition of very thin films is possible by judicious selection and optimization of spray machine parameters for forming “atomized” droplets and the reagent and solvent systems used to formulate the spray liquid. In principle, spray pyrolysis is a simple technique where an ionic solution (prepared by starting materials in appropriate stoichiometric proportions) containing the constituent elements of the compound, is sprayed over a heated substrate. Generally, the metals are in solution as their chlorides, nitrates or acetates. Droplets impact on the substrate surface spread into a disk-shaped structure and undergo thermal decomposition. The shape and size of the disk depend on the momentum and volume of the droplet, as well as the substrate temperature. Consequently, the film is usually composed of overlapping disks of metal salt being converted into oxides on the heated substrate. The substrates provide thermal energy for the thermal decomposition and subsequent recombination of the constituent species, followed by sintering and crystallization of the clusters of crystallites and thereby resulting incoherent film. The required thermal energy is

different for the different materials and also for the different solvents used in the spray process. The atomization of the spray solution into a spray of fine droplets also depends on the geometry of the spraying nozzle and the pressure of a carrier gas.

Thin film deposition using spray pyrolysis can be divided into three main steps namely:

Step1: Atomization of the precursor solution.

Step2: Transportation of resultant aerosol

Step3: Decomposition of the precursor on the substrate.

Factors affecting the deposition are

- Temperature of the Substrate
- Solution concentration
- Solution flow rate
- Nozzle to substrate distance
- Droplet Size
- Droplet velocity

Advantages of spray pyrolysis

- It has the capability to produce large-area, high-quality adherent films of uniform thickness.
- It does not require vacuum at any stage.
- Spray pyrolysis does not require high-quality targets or substrates.
- The deposition rate and the thickness of the films can be easily controlled over a wide range thereby changing the spray parameters.
- It operates at moderate temperature ($100^{o}C$-$500^{o}C$) thereby producing films even on less robust materials.
- There is no restriction on substrate dimensions.
- By changing the composition of the spray solution during spray, it can be used to make layered films and the films having compositional gradients throughout the thickness.

Disadvantages of spray pyrolysis

- Possible by-products interfering with film properties.
- Careful control of growth parameters is required.

## 1.4 THICKNESS MEASUREMENT

Thickness plays an important role in the film properties, unlike a bulk material. The physical properties of a thin film are highly dependent on their thickness. Reproducible properties are achieved only when the film thickness and the deposition parameters are kept constant. Hence, the determination of the film thickness and deposition rate is a fundamental task in thin film technology. In many applications it is necessary to have a good knowledge about the current film thickness even during the deposition process, as e.g. in the case of optical coatings. Therefore film thickness can be measured either by in-situ (applied during deposition) monitoring of the rate of deposition or by ex-situ (after the film deposition) (Hass et al. 1963).

### 1.4.1 Gravimetric Method

This is a method which is based on the determination of a mass. The film thickness $t$ can be calculated from the mass of the coating $m$ (determined by weighing the substrates before and after deposition), the bulk density of the material $\rho$ and the area $A$ on which the material is deposited is known

$$t = m/A\rho \qquad (1.1)$$

### 1.4.2 Electron microscopy

Thickness of the film is determined using metallographic cross sections of the electron microscope. In the transmission electron microscope (TEM) and scanning electron microscope (SEM) cross-sectional preparates can be investigated. The resolution and the metric range depend on the instrument and on the magnification. In the optical microscope thickness of the film up to some mm with a resolution of 0.1 µm can be determined. In the SEM a resolution of 5 nm can be achieved and in the high-resolution TEM (HRTEM) 0.1 nm are possible.

## 1.5 IMPORTANCE OF COMPOUND SEMICONDUCTOR THIN FILMS

The search for new materials to use in device technology is a never ending process. Discovery and study of new materials, whose properties can be tailored, constitute the core of the development of solid state technology. This idea brought to continue the study of compound semiconductors with alloy semiconductors. Alloy semiconductor compounds have attracted technological interest because of the provision of modifying their energy band gap with the difficulties in the formation of solid solution (alloy). According to Hume – Rothery rules solid solutions or alloys were formed in two forms depending on the atomic arrangement (Krishna reddy 2011). The ions in substitutional solid solution must be of the same charge, should have similar in size and valency (for metal atoms <15%).

$$\% \text{ difference} = ((r_{\text{solute}} \text{ X } r_{\text{solvent}})/r_{\text{solvent}}) \text{ X } 100\% \qquad (1.2)$$

A metal dissolves a metal of higher valency to a greater extent than one of lower valency (Smith et al. 2006). Structures of crystals should be similar. Also the solute and solvent should have similar electronegativity. If the electronegativity difference is too large, the metals tend to form intermetallic alloys which are a solid state compound exhibiting metallic bonding, defined stoichiometry and ordered crystal structure. The continuous variation of discrete structural, optical & electronic properties achieved in semiconducting materials in a controlled manner had enhanced their employability in the fabricating devices with pre-determined characteristics leading to obtain ternary alloy semiconductors. This method commonly adopted to grow ternary semiconductors is by mixing suitable binary semiconductors under appropriate solid solubility conditions. Chemical bonding & structural compatibility will provide a smooth restruction of energy bands and continuous change in characteristics with a variation of relative concentration of constituents in resulting materials. Ternary materials thus provide a possibility of tailoring their properties as per requirements and have projected themselves as an important semiconducting material for future advancements in the field of device fabrication. From the literature, it is found that the techniques which employed to prepare binary thin film semiconductors can be employed to deposit ternary semiconductor thin films.

## 1.6 IMPORTANCE OF LEAD ZINC SULPHIDE THIN FILMS.

II-IV-VI compound semiconductors are potential candidates which cover entire spectral range UV–IR region. This can be used in various applications such as thermo reflecting films for solar control coatings, optoelectronics, sensors and photoelectrochemical solar cells. II-VI semiconductors are important due to its high efficiency of radiative recombination, nearly matching band gaps with the visible region, and direct band gap, which is used in many applications such as photovoltaic and photoconductive devices (Basak et al. 2003), catalyzators (Mohammed et al. 2010), laser diode, humidity and temperature sensors (Wang et al. 2010), decorative coatings and photography. ZnS is one of the important II-VI group of compound semiconductors with direct band gap energy of 3.54 eV (UV region). It is a non-toxic, environmental friendly, inexpensive and chemically stable material which is suitable for industrial production (Sahraei et al. 2013, 2015). It is commercially used in an anti-reflection coating for heterojunction solar cells and nanogenerators (Afifi et al. 1995). It is electrically a poor conductor, doping is a must in order to improve its electrical conductivity.

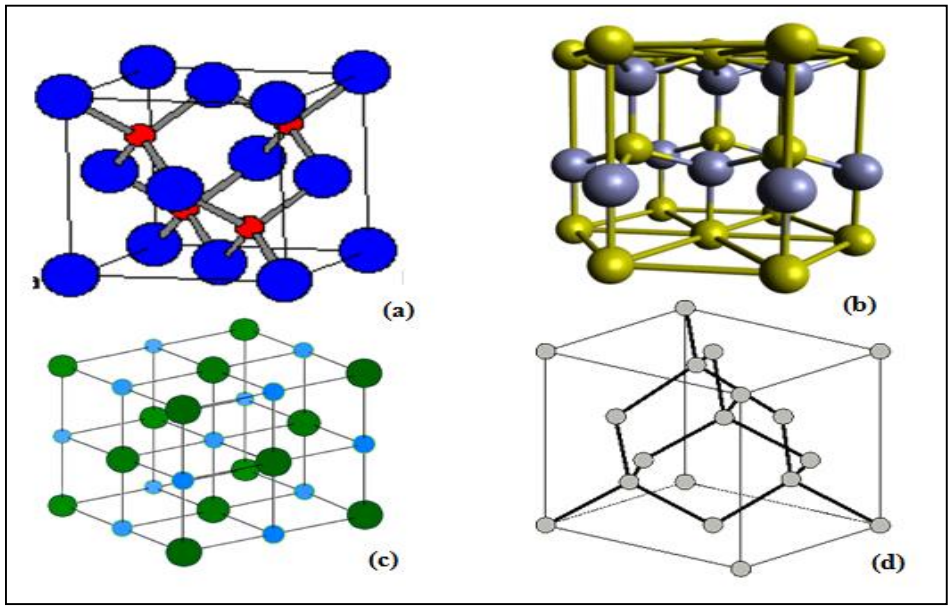


Fig.1.10 (a) Zinc-Blende, (b) Wurtzite, (c) Rock salt, and (d) Diamond structures.

Among IV-VI semiconductors PbS is both n-type and p-type with a narrow band gap (0.41 eV) (Junna Ji et al. 2015), large exciton Bohr radius (18 nm). It possesses a high dielectric constant, high mobility, positive temperature coefficient and small effective masses of electrons and holes (Al-Douri et al. 2008) which have been highly related to its ample range of thin film uses such as photo resistors, diode lasers, photothermal conversion

application (Popa et al. 2006) solar cells and thermoelectric applications (Junna Ji et al. 2015). With the combination of ZnS and PbS compounds the direct transition of an electron can be achieved and used in different applications in which both electrical and optical properties are necessary to improve the quality of devices. Common structures of PbS and ZnS compound semiconductors are rock salt, hexagonal, diamond, and wurtzite are given in Fig.1.10. Any of the below-mentioned structure can constitute for ternary $Pb_xZn_{1-x}S$ thin films.

## 1.7 LITERATURE REVIEW

The majority of the work carried out on semiconductors was focused mainly on compound semiconductors under the category II-VI, III-V, IV-VI, etc. An extensive work based on these semiconductors finds its application in thin film technology. Physical, structural, mechanical, magnetic, optical and electrical properties are enhanced when compared to bulk materials. But it was found that certain binary semiconductor lacked some of the above-mentioned property. Example, II-VI compound semiconductors are direct band gap compounds with comparatively poor conductivity. III-V compound semiconductors are used in many device applications but they have indirect energy band gap. IV-VI compound semiconductor exhibits good electrical conductivity but they show poor optical properties. Addressing this issue, ternary alloys such as II-IV-VI, II-III-V, etc. were considered as better alternative semiconductor materials for many device applications. The interesting conclusion drawn from the literature is that there is a drastic improvement in the physical properties of devices due to the introduction of ternary compound semiconductors. Although the majority of the works have been carried out on ternary alloy compound semiconductors, limited reports were observed for II-IV-VI semiconductor compounds. Of all II-IV-VI ternary compound semiconductor thin films, PbZnS ternary compound was selected because of its importance mentioned in section 1.7.

### 1.7.1. Lead sulphide (PbS) thin films

Thangaraju et al. (2000) studied spray pyrolytically prepared PbS thin films at various substrate temperatures and achieved polycrystalline films. They also investigated electrical properties and reported that PbS films are n-type semiconductors with a conductivity of the order $10^{-4}\Omega^{-1}cm^{-1}$.

Seghier et al. (2006) varied molarity of lead nitrate precursor from 0.165 to 0.185 per step of 0.005M and gives an idea to improve properties of lead sulfide thin films by varying lead precursor concentration.

Al-douri et al. (2008) reported thermally evaporated $Pb_xS_{1-x}$ films (x=0.50 and 0.53) have both direct and indirect optical transitions. Optical energy band gap decreased with increased Pb content and concluded helpful for optical devices.

Preetha et al. (2012) varied PH of the cationic precursor solution and revealed the existence of both direct and indirect band gap energy of SILAR deposited lead sulfide thin films. They succeeded to tune the band gap of a thin film over a wide range for photovoltaic applications.

Hussain et al. (2012) varied Pb:S molar ratio 0.05M, 0.075M, 0.1M, 0.125M and 0.150M by CBD technique. 0.1M was found to be suitable concentration to grow good quality thin films for devices.

Rajashree et al. (2014) investigated that substrate temperature is one of the main parameters of which properties of PbS thin films can be improved. They have reported 350 ˚C as an optimal temperature to grow homogeneous thin films.

Ravishankar et al. (2015) varied the molar concentration of precursor salts both cationic and anionic as 0.025M, 0.05M, 0.075M to 0.1M keeping ratio equal to 1. They reported spray pyrolysed lead sulfide films can also show an orthorhombic structure with 2.44-2.55eV band gap desirable for window layer in solar cell applications. Literature survey shows comparatively less work on maintaining a good stoichiometric ratio in fabricating PbS films which would favor good electrical conductivity.

### 1.7.2. Zinc sulphide (ZnS) thin films

Pike et al. (1993), Fifi et al. (1995) deposited ZnS thin films by spray pyrolysis technique and studied the effect of substrate temperature on growth and properties of the films. They reported that crystallinity of ZnS films will be achieved at a substrate

temperature more than 400˚C. They reported that the ZnS films are polycrystalline with both hexagonal and cubic structure.

Lo peza et al. (2005) studied the influence of precursors on the growth of ZnS thin films prepared by spray pyrolysis technique. The direct band gap measured was found to be 3.54 eV.

Fenollosa et al. (2008) studied the role of the precursor on morphology and Optical properties of ZnS thin films prepared by chemical spray pyrolysis. The films were prepared using different Zn:S ratios (between 1:1 and 1:6) and in different growth solutions: (A), zinc chloride and thiourea and (B) dehydrated zinc acetate and thiourea, both in distilled water. Thin film production conditions have a significant influence on absorption and the PL spectra. The good stoichiometry determined by the absorption spectra in the sample from solution A with a (1:4) ratio.

Prakasha et al. (2010) studied the effect of substrate temperature on structural, optical and thermal properties of chemically sprayed ZnS thin films. The films were grown at different substrate temperatures in the range, 300 - 400°C. The films are polycrystalline with cubic structure grown preferentially along the (111) axis. The optical studies exhibit direct allowed transition. He found that the energy band gap varies from 3.43 to 3.80 eV.

Saeed et al. (2011) studied structural and optical properties of ZnS thin films prepared by spray pyrolysis technique. He reported that the thin films grown by using $ZnCl_2$ precursor. Good optical transparency of about 65 % in the visible region (300-900nm).

Karim et al. (2012), Meshram et al. (2012) studied structural and optical properties of ZnS thin films prepared by spray pyrolysis technique. The optical properties of these films have been studied in the wavelength range 380-1000nm and direct band gap of 3.47eV-3.54eV was reported. Literature survey reveals that stoichiometry plays an important role in achieving good optical properties in the ZnS films. But limited study on the stoichiometry of the ZnS films has been reported. Hence, the present work focused on the preparation of stoichiometric ZnS films.

### 1.7.3. Lead zinc sulphide (PbZnS) thin films

Ternary derivative materials are attractive because it is possible to tune the lattice constant and band gap by controlling deposition parameters (Rajashree et al. 2016). In recent

past, many research groups have studied the structural, electrical and optical properties of derivative materials in thin film form involving Pb. Popescu et al. (2006) and Baroate et al. (2010) reported characteristics of chemically deposited films depends on the concentration and molar ratio of cadmium and lead salts. That can be utilized in photoelectron, chemical and solar cell applications. Rajashree et al. (2016) reported, properties of spray deposited PbMgS thin films depends on Mg concentration and suitable for optoelectronic applications especially in solar cells. Maskaevo et al. (2004, 2007) synthesized supersaturated zinc lead sulphide thin film and achieved substitution of 4.2 mol% of zinc into lead sites by the hydrochemical method. They established that the formation of these solid solutions makes lead sulphide films sensitive to the visible and near-IR radiation in a 0.4-2.8μm wavelength range. It was of considerable interest to obtain supersaturated ZnPbS solid solutions with still higher zinc content in PbS and to study the composition, morphology and properties of deposited layers.

Suhail et al. (2012) studied structural optical properties of ZnS, PbS, $Zn_{1-x}Pb_xS$, $Zn_xPb_{1-x}S$, and $PbZn_xS_{1-x}$ thin films by spray pyrolysis. He reported that all films are polycrystalline with cubic phase except ZnS films have cubic and hexagonal phase. Optical studies reveal that these films have a direct band gap and it is observed that the band gaps decrease with increase in the film thickness. The transmittance is high in VIS-NIR regions and the high transmittance properties make the film a good material for thermal control window coating for cold climates and anti-reflective coating. Refractive index increases in the film thickness, while the extinction coefficient decreases with increase in the thickness for all the films except ZnS films which are inverse. It has been observed that there is no detailed studies on electrical properties of lead zinc sulphide thin films.

Touati et al. (2015) studied Zn-doped PbS thin films prepared by CBD technique. They reported Zn:PbS films were polycrystalline and varied the optical energy band gap in the range of 0.72eV – 1.46eV. They suggested that the Zn:PbS thin films are a potential candidate as an absorber layer in the modern solar cell devices.

Abiodun et al. (2015) carried out studies on zinc lead sulphide thin films deposited by chemical spray pyrolysis technique and showed that the zinc can substitute lead in PbS lattice at higher mol% using chemical spray pyrolysis technique. Still the study was restricted to the

Rutherford backscattering spectrometry analysis and structural properties needing further studies.

Hence, a study of $Pb_xZn_{1-x}S$ (x = 0, 0.2, 0.4, 0.5, 0.6, 0.8 and 1) thin films with zinc substitution greater than 4.2 mol% in PbS is undertaken. The objective also includes a study of substitutional solid solution based on lead and zinc sulphides which make it possible to control their semiconducting, optical and electrical properties within broad limits by varying the lead and zinc composition.

## 1.8 SCOPE OF THE WORK

From the literature it has been observed that, in spite of the promising and novel opto-electronic properties of chalcogenide thin films, the use of II-IV-VI group material in device applications may be held back by the difficulty in preparing chemically stable material. Particularly, PbS, a IV-VI compound is potential for electrical properties with indirect and narrow band gap energy of 0.41 eV (IR region). Whereas, ZnS, a II-VI compound exhibits high efficiency radiative recombination and high transparency in UV-Visible region with direct band gap energy (3.54 eV). Hence, the combination of PbS and ZnS can enhance electrical properties along with wide spectral range from UV to IR region which is required for efficient optoelectronic devices. However, there are few reports of attempts made to achieve lead zinc sulphide films with zinc content which was limited to lower solubility of Zn into Pb sites ($\leq$ 4.2 mol%). In order to overcome the solubility limit of Zn into PbS films and to study properties beyond > 4.2 mol% of Zn in Pb sites spray pyrolysis technique has been used.

It was also observed that there is limited study on the stoichiometry of binary (PbS and ZnS) films. For the formation of an alloy a detailed study of binary compounds is required. Hence, the primary study is focused on the preparation of stoichiometric binary films using chemical spray pyrolysis technique. Further, the work on the preparation of different composition of PbZnS films by chemical spray pyrolysis technique is taken up. The studies include a detail analysis of structural, electrical and optical properties of the films, relating them with their binaries for possible device applications.

## 1.9 OBJECTIVES

Study on growth and characterization of spray pyrolysed $Pb_xZn_{1-x}S$ thin films.

- To prepare uniform sprayed PbS and ZnS films separately by optimizing the deposition parameters.
- To study the compositional, structural, optical and electrical properties of prepared PbS and ZnS films separately.
- To prepare uniform $Pb_xZn_{1-x}S$ thin films by optimizing the deposition parameters.
- To study the structural, optical and electrical properties of prepared $Pb_xZn_{1-x}S$ thin films with a different composition.
- To explore the possibility of $Pb_xZn_{1-x}S$ thin films for device applications.

# CHAPTER 2

# EXPERIMENTAL PROCEDURE

## 2.1 SPRAY PYROLYSIS TECHNIQUE

The spray pyrolysis technique is a chemical deposition method in which fine droplets of the desired material are sprayed onto preheated substrates. Continuous films are formed onto the hot substrate by thermal decomposition of the material droplets. Spray pyrolysis technique is the best technique among chemical methods to overcome the solubility limit, low cost experimental set up, high spatial selectivity. In spite of this, spray pyrolysis technique can be used for precise control over maneuvering the impurity concentration and it is helpful in preparing pin hole free, homogeneous, smoother thin films with desired thickness. Additional advantage of this method is it gives an opportunity to dope any kind of elements with stoichiometry.

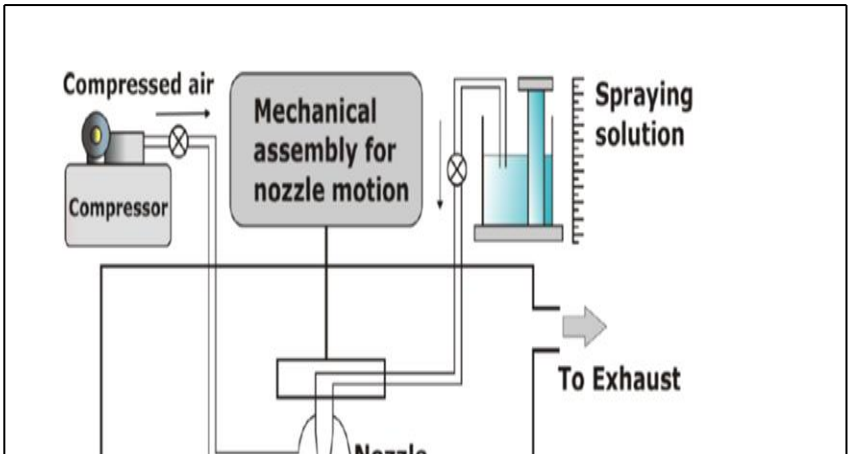

Fig. 2.1 Schematic representation of spray pyrolysis unit.

Fig. 2.2 Spray pyrolysis equipment (Holmarc mechatronics PVT LTD. HO-TH-04).

## 2.2 COMPONENTS OF SPRAY PYROLYSIS UNIT

The spray pyrolysis mainly consists of spray nozzle, liquid level monitor, hot plate, gas regulator value and airtight fibre chamber.

### 2.2.1 Spray nozzle

Spray nozzle is a specially designed nozzle made of glass consisting of different ports such as outer air port, inner liquid port and cylinder port. The outer air port is connected to an air compressor through a flow meter. The solution reservoir is placed well above the nozzle head level. The solution is fed to the liquid port by gravity and solution flow rate can be monitored by a value. When the value is activated, compressed air lifts a pneumatically operated air cylinder inside the nozzle allowing solution to be atomized. This arrangement prevents the solution flow out of the nozzle before atomizing air is admitted. The rotor controls the linear simple harmonic motion of the spray nozzle over the required length of the hot plate.

### 2.2.2 Liquid level monitor

The spray rate at a fixed air pressure depends upon the height of the solution measured with respect to the tip of the nozzle. The arrangement for the change in height of the solution forms the liquid level monitor system.

### 2.2.3 Hot plate

The iron disc served as a hot plate. Maximum temperature of 500˚C can be achieved with this arrangement. The chromel-alumel thermocouple is used to measure the temperature of the substrates. It is fixed at the center of the front side of the iron plate. The temperature of the hot plate is monitored with the help of temperature controller.

### 2.2.4 Air tight fiber chamber

Since the number of toxic gases is evolved during the thermal decomposition of sprayed solution. It is necessary to fix the spraying system inside with airtight fiber

chamber. The fiber avoids the corrosion of the chamber. The outlet of chamber is fitted to exhaust fan to remove the gases evolved during thermal decomposition.

In present study, parameters of spray pyrolysis technique like dispensing rate of the solution and speed of spray head movement which is difficult to control manually are controlled precisely by PC based automation. A positive displacement pump controlled by stepper motor and microprocessor is used to dispense solution as per requirement. The spray head movement is also controlled by stepper motor driven linear stages in X and Y direction. The temperature of the substrate heater plate is controlled independently through a controller. A desktop computer is used to control the operations through the serial port. Dedicated software for spray pyrolysis system can as well be used for documenting the relevant parameters used for sample preparation like temperature, air pressure, duration, etc.

## 2.3 CHARACTERIZATION TECHNIQUES

Properties of thin films are sensitive to their crystal structures. Further, defects and imperfections in crystal structure, precursor concentration, compositional variations and surface topography are also affect the properties of thin films. The prepared thin films can be characterized by various characterization techniques. Several highly sophisticated and powerful instrumental techniques have recently been developed for their analysis and surface characterization. XRD, EDAX, UV spectroscopy, SEM, two probe, Hall effect and photoconductivity etc. are some of the few techniques recently developed for material characterization and surface analysis.

### 2.3.1 Structural, morphological and compositional properties

#### 2.3.1.1 X-ray Diffraction (XRD)

X-ray diffraction is a non-destructive technique which can be used to study the structure, composition, and physical properties of materials. In general, the X-rays are directed to the sample to produce the constructive interference, when it satisfies the Bragg's law. Crystallite size

$$n\lambda=2d\sin\theta \qquad (2.1)$$

Where λ 

– wavelength of the X-rays, d – the distance between two lattice planes, θ – angle between the incoming X-rays and the normal to the reflecting lattice plane and n– order of reflection

The crystallite size is a very important structural parameter of a thin film. It is found that crystallite size of thin film has some dependence on deposition parameters, particularly rate of deposition and substrate temperature. If $\beta$ is the width of the diffraction line at the half of the maximum peak intensity (FWHM) for the diffraction angle, then according to Scherer's formula (Cullity 1956), the average crystallite size '*D*' of the films will be

$$D = \frac{k\lambda}{\beta \cos\theta} \qquad (2.2)$$

where, *K* is Scherrer's constant whose value is chosen as unity assuming the particle to be spherical (for cubic 0.94).

Fig. 2.3 XRD set up.

Quantitative information of the direction of preferred growth was obtained from Harris texture coefficient relation

$$TC_{(hkl)} = C \frac{{}^{I_{(hkl)}}/_{I_{o(hkl)}}}{\frac{1}{N}\sum_n {}^{I_{(hkl)}}/_{I_{0(hkl)}}} \quad (2.3)$$

where $I_{(hkl)}$ and $I_{0(hkl)}$ are the measured intensity and the standard intensity of *(hkl)* plane respectively, based on standard data, *N* is the reflection number and *n* is the number of diffraction peaks (Guneri et al. 2015, Chandra et al. 2015). $TC_{(hkl)}$ values represent the abundance of crystallites oriented in a given *(hkl)* direction. A sample with randomly oriented crystallite yields $TC_{(hkl)}$=1, while the larger this value the larger abundance of crystallites oriented at the *(hkl)* direction.

In the present study the structural characterization of the films was carried out by analyzing the X-ray diffraction patterns obtained using XRD (Rigaku mini flex 600) Cu $K_\alpha$ radiation in the 2θ range of angles between 20˚ to 60˚.

2.3.1.2 SEM and EDAX

SEM yields information about topography, morphology, crystallographic features at high magnifications. In the scanning electron microscope, the electron gun generates a stream of monochromatic electrons in vacuum. This beam is collimated by electromagnetic condenser lenses. The beam is then focused by an objective lens and scanned across the surface of the sample by electromagnetic deflection coils in a grid fashion. The impingement of high energy electrons on the surface results in the emission of electrons from the surface as secondary electron emission occurs from regions close to the surface,

whereas backscattered electrons emerge from regions beneath the surface. For the determination of topographical features, the scattered secondary electron mode is generally preferred. In the present investigation, a scanning electron microscope (JEOLJSM-6380LA) interface with EDAX operated at 15 KV was employed for studying the surface morphology and composition of the films. Films were coated with gold by JEOL sputter coating thickness of 10nm. Images were recorded at a different magnification.

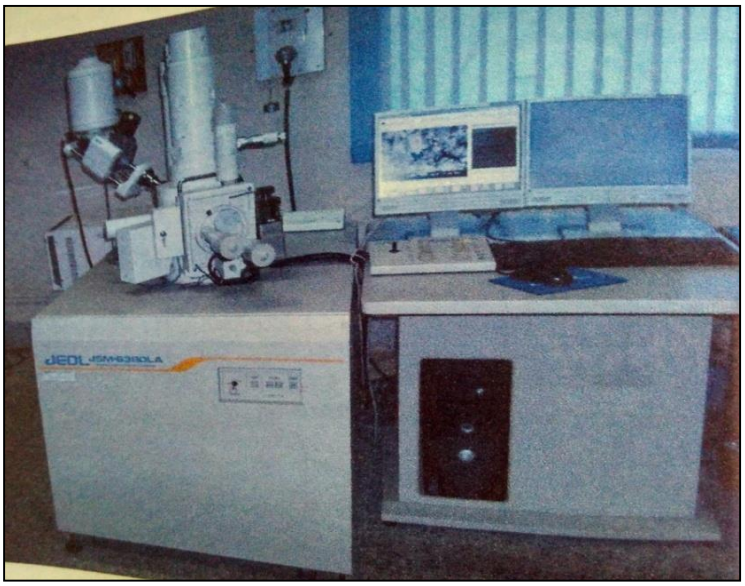

Fig. 2.4 SEM equipment.

2.3.2 Optical properties

2.3.2.1 UV-VIS-NIR spectroscopy

The most direct and probably the simplest method for determining the band structure of semiconductors is by measuring the optical absorption spectrum. Absorption is expressed in terms of a coefficient (αhυ), which is related to the energy gap '$E_g$' of the material is given by Bardeen et al. (1956)

$$\alpha = \frac{a\,(h\vartheta - E_g)^n}{h\vartheta} \qquad (2.4)$$

where a is a constant and $n$=1/2 for allowed direct transition and $n$=2 for allowed indirect transitions. The value of $\alpha$ is obtained from the relation given by equation 2.5

$$\alpha = 2.303\left(\frac{A}{t}\right) \quad (2.5)$$

where '$A$' is the absorbance and '$t$' is the thickness of the film (Barman et al. 2008). For allowed transition, for example if $\alpha^2$ is plotted against photon energy, a straight line for direct transition will be obtained. The intercept on the energy axis-gives the band gap of direct band gap semiconductor. Again if $\alpha^{1/2}$ is plotted against photon energy, a straight line for indirect transition will be obtained. For our experiments, a single beam UV-VIS spectrophotometer (Ocean optics Inc SD 2000 UV-VIS-NIR spectrometer; Spectral resolution 1 nm) was used.

Fig. 2.5 UV-VIS-NIR spectrophotometer.

### 2.3.3 Electrical properties

The use of thin films as resistors, contacts and interconnections has lead to extensive study of conductivity, temperature dependence, the effect of thermal processing stability and so on. Investigation of the critical resistivity as a highly structure sensitive properties make it possible to gain insight into the structural and electrical properties of the thin films which is important from both the theoretical and practical point of view. The contact methods are most widely used for the measurement of resistivity. These methods include two-point probe, four-point probe and the spreading resistance.

#### 2.3.3.1 I-V measurements

The current voltage (I-V) measurements of ohmic contact device were carried out by using Kiethley 2400 sourcemeter. Silver film deposited using PVD was used to make

contacts with 1mm gap between electrodes. I-V measurement was made between the contacts, using PC based I-V measurement system.

2.3.3.2 Two point probe method

The two-point probe method is simple, easy to use and useful for study of high resistive thin films. In this method constant voltage '*V*' is applied between two fixed position probes separated by '*l*' in cm and current passing through a sample of known dimension (cross sectional area '*A*' in $cm^{2}$) is measured with an appropriate current meter. For uniform sample resistivity is given by equation 2.6.

$$\rho = \frac{A(\frac{V}{I})}{l} = \frac{RA}{l} \qquad (2.6)$$

In case of semiconducting thin films, the resistivity decreases with increase in temperature (Broderick et al. 2003). The thermal activation energies '$E_a$' are calculated by using equation 2.7.

$$R = R_o \, exp \, (\frac{-E_a}{KT}) \qquad (2.7)$$

where *K* is the Boltzman constant and *T* is the temperature. Slope of the plot log *R* verses *1\T* leads to estimation of the activation energy (Sze 1985).

2.3.3.3 Hot probe method

It is a simple method, which is widely used to determine the type of conductivity of a semiconductor specimen (Axelevitch et al. 2013). Two fine metal probes are placed on the semiconductor sample and a multimeter is connected between them to measure the voltage. One of the probes is kept at room temperature and the other is heated to 80°C. Hot probe heats the semiconductor immediately beneath it so that the kinetic energy of free carriers in this region is increased. Therefore the carriers diffuse out of the hot region at a faster rate than they diffuse into this region from adjacent low temperature regions. If the semiconductor is n-type, electron will move away from the hot probe leaving a positive charge region of donors and the hot probe becomes positive with respect to the cold probe. The current will flow from the hot probe to the cold probe. In a p-type semiconductor the direction of the current flow is reversed. Thus the polarity of the hot probe indicates whether the semiconductor is n-type or p-type. This method is not applicable for intrinsic semiconductors where the number of electrons and holes are nearly equal. This method is not reliable when the resistance of the semiconductor is very high. In the present work, we often

used this technique to identify the conductivity of n-type PbZnS films. Later this was verified using Hall measurements.

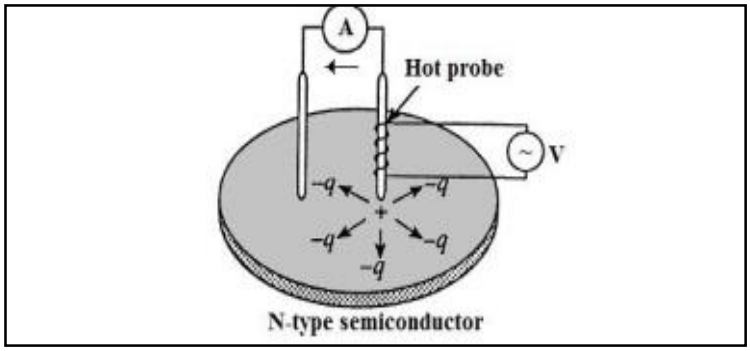


Fig. 2.6 Schematic diagram of hot probe technique.

2.3.3.4 Hall probe method

A Hall probe is a semiconductor-based detector which uses the Hall effect to allow the strength of a magnetic field to be measured (Fig.2.7). If an electric current flows through a conductor in a magnetic field, the magnetic field exerts a transverse force on the moving charge carriers, which tends to push them to one side of the conductor. A build up of charge at the sides of the conductors will balance this magnetic influence, producing a measurable voltage between the two sides of the conductor. The presence of this measurable transverse voltage is called the Hall effect after E. H. Hall who discovered it in 1879.

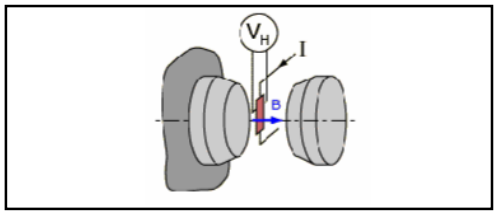


Fig. 2.7 Hall probe between magnetic poles.

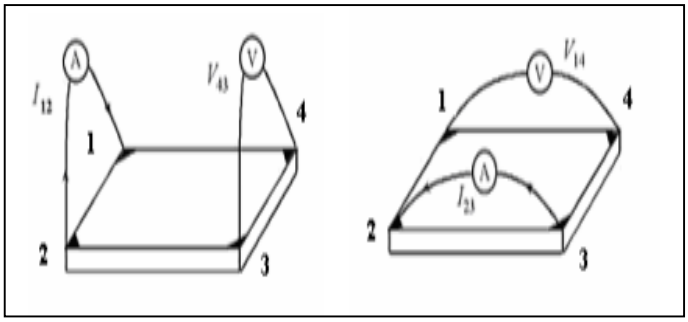

Fig. 2.8 Rectangular configuration for samples.

In order to determine the carrier density, a combination of a resistivity measurement and a Hall measurement is needed. A schematic diagram of a rectangular configuration is shown in Fig. 2.8.

The objective of the resistivity measurement is to determine the resistance *R*. $R_{12,34}$ and $R_{23,41}$ are related to the resistance *R* through the equation 2.9,

$$exp\ (-\pi R_{12,34}/R_s) + exp\ (-\pi R_{23,41}/R_s) = 1 \quad (2.8)$$

*R* is obtained as

$$R = \left(\frac{\pi}{ln2}\right) \frac{(R_{12,34}+R_{23,41})}{2} \quad (2.9)$$

which can be solved numerically for $R_s$, the bulk electrical resistivity can be calculated by using the relation

$$\rho = R, t = \frac{\pi t}{ln2} \frac{(R_{12,34}+R_{23,41})}{2} \quad (2.10)$$

where *t* is the thickness of the film.

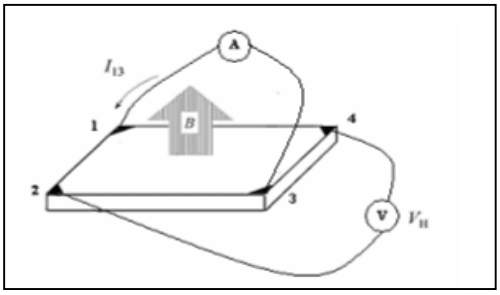


Fig. 2.9 Symmetric geometry of the films used for the Hall measurements.

To obtain the two characteristic resistances ($R_{12,34}$+$R_{23,41}$), initially DC current is applied through contact 1 to contact 2 and measures the voltage $V_{34}$ from contact 3 to contat 4 as shown in Fig. 2.9. Finally current applied through contact 2 to contact 3, the volatage $V_{41}$ from contact 4 to contact 1 are measured. Then

$$R_{12,34} = V_{34}/I_{12} \quad (2.11)$$

$$R_{23,41} = V_{41}/I_{23} \quad (2.12)$$

The hall coefficient is measured by applying a current through any one of contacts as mentioned in above procedure and $R$ should be measured before and after applying a magnetic field $B$ perpendicular to the surface of the sample. If $\Delta R$ is the difference between the two resistances then the hall coefficient $R_H$ of the sample is given by

$$R_H = \frac{d}{B}\Delta R \qquad (2.13)$$

From the determined value of $R_H$ the carrier concentration can be found by the equation, $n = \frac{1}{qR_H}$ (2.14)

where '$q$' is the elementary charge. The mobility '$\mu$' is related to '$\rho$' and '$n$' by the equation,

$$\mu = \frac{1}{\rho n q} \qquad (2.15)$$

2.3.4 Photoconductivity measurements

When a semiconductor is illuminated by light, an often increase in its conductivity is observed and it is called photoconductivity. This effect occurs in organic or inorganic materials. With the combination of different parameters such as spectral response, dark resistance, rise and decay time of the photoconductivity, etc., only few materials are useful for practical uses in photo detection.

Any transition that creates additional free carriers, it effectively increases the free life time as well as the photosensitivity of the material. The ratio of increase in conductivity of the material in the presence of light to the conductivity in darkness gives the values of photosensitivity and is given by the equation

$$\text{Photo sensitivity} = \frac{\Delta\sigma}{\sigma} = \frac{(I_{ph}-I_D)}{I_D} = \frac{(V_{ph}-V_D)}{V_D} \qquad (2.16)$$

$$\%\ \text{photosensitivity} = \frac{(V_{ph}-V_D)}{V_D} x100 \qquad (2.17)$$

where, $I_{ph}$ and $I_D$ are current under illumination and in dark, respectively. $V_{ph}$ and $V_D$ are the corresponding voltages respectively. Assuming, however, that the specimen resistance $R_{ph}$ and $R_D$ under illumination and dark is much larger than standard resistance used across which voltages are measured. In the present work the spectral response of the PbS and PbZnS films deposited at various substrate temperatures was studied using photoconductivity measurement setup comprising of a 150W Xenon arc lamp, a monochromator interfaced with a computer and a photomultiplier tube detector. The films were kept within a dark chamber.

The light from Xe arc lamp was allowed to pass through the monochromator to obtain monochromatic light of desired wavelength. This monochromatic light was then allowed to incident on the film sample. The resultant photocurrent was determined by measuring the difference between dark and illuminated currents.

# CHAPTER 3

# PREPARATION AND CHARACTERIZATION OF LEAD SULPHIDE THIN FILMS

In this chapter, the preparation of stoichiometric lead sulphide thin films using spray pyrolysis technique and characterization of these films are discussed. The characteristics of

thin films depend on the deposition technique employed and various deposition parameters such as substrate temperature, rate of deposition, ambiance and annealing treatment etc. In particular, properties of thin films synthesized using spray pyrolysis technique are dependent on the factors like precursors, concentration of precursors, flow rate of solution, spray rate, spray time, carrier gas flow rate and the distance between nozzle to substrate, etc. These parameters have to be optimized to get the required quality of the films.

## 3.1 PREPARATION OF LEAD SULPHIDE THIN FILMS

Lead sulphide thin films were deposited on glass substrates by varying the thickness, substrate temperature, lead (Pb) precursor concentration and annealing temperature. Aqueous solutions of lead acetate (Pb $(CH_3COO)_2$) and thiourea (CS $(NH_2)_2$) were utilized as precursor solution. Glass micro slides of the size 7.5 X 2.5 $cm^2$ were used as substrates. Before deposition, these substrates were washed with water, kept in (2 M) chromic acid for 24 h, washed with distilled water and then dried. The various preparative parameters such as spray rate, the nozzle to substrate distance and carrier gas pressure used, were optimized. After deposition, the films were allowed to cool at room temperature and cleaned with an air drier. The adhesion of the films on the substrate was good. Lead sulphide thin film is formed according the following chemical reaction:

$$Pb(CH_3COO)_2+SC(NH_2)_2+2H_2O \longrightarrow PbS\downarrow+2CH_3COOH\uparrow+2NH_3\uparrow+CO_2\uparrow \qquad (3.1)$$

## 3.2 OPTIMIZATION OF GROWTH PARAMETERS

### 3.2.1 Precursor optimization

In chemical methods, the precursor is an important parameter to improve the properties of thin films. Hence, prior to deposition selection of precursor for both cation and anion is a must. From the literature, it has been found that acetate, nitrate and chlorides of metallic salts can be used in the synthesis process. But, lead chloride does not dissolve in distilled water and dissolves only in acids. From the literature, it has been observed that thiourea is used as a common anionic precursor. Though researchers have used both lead acetate and lead nitrate as a cationic precursor, nitrates are corrosive and require high deposition temperature to get good quality thin films. Hence, in the present work thiourea is selected as an anionic precursor and lead acetate as a cationic precursor as it does not produce any byproducts which are hazardous to the environment and equipment.

3.2.2 Concentration of precursor

The concentration of the precursor is another important parameter to synthesize lead sulphide thin films. From the literature, it is found that the concentration of the precursor in the range between 0.005M to 0.5M is suitable to obtain device quality films and 0.1M is found to be suitable concentration of precursor to obtain the better electrical properties of the PbS films. Hence, by fixing 0.1M as the precursor concentration other parameters such as volume of the precursor, spray rate, the distance from the nozzle to substrate, the pressure of the carrier gas, substrate temperature have been optimized.

3.2.3 Volume of the precursor

The volume of the precursor solution of known concentration deposited for a finite time decides the thickness of the film. It has been varied from 5 ml to 35 ml keeping substrate temperature as 350˚C and other process parameters constant. The deposited films were uniform, pin-hole free and adherent to the glass substrate. Fig. 3.1 shows the variation of film thickness as a function of the volume of the spray solution.

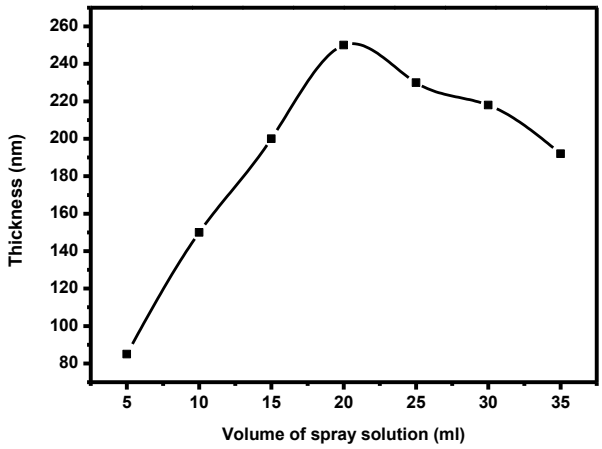


Fig. 3.1 Variation of PbS film thickness with the volume of spray solution.

The film thickness was found to be around 85±10 nm for 5 ml spray solution and it increased to 250±20 nm as the spray solution increased to 20 ml. However, a slight decrease in the film thickness was observed with further increase in the volume of the spray solution. This may be due to incomplete thermal decomposition of the spray solution resulting in the formation of powder on the surface of the film (Yogesh et al. 2016). Hence, the optimum volume of the spray solution was found to be 20 ml.

3.2.4 Spray rate

PbS films were deposited by varying the spray rate from 0.5ml/min to 2ml/min keeping substrate temperature as 350˚C and other process parameters constant.

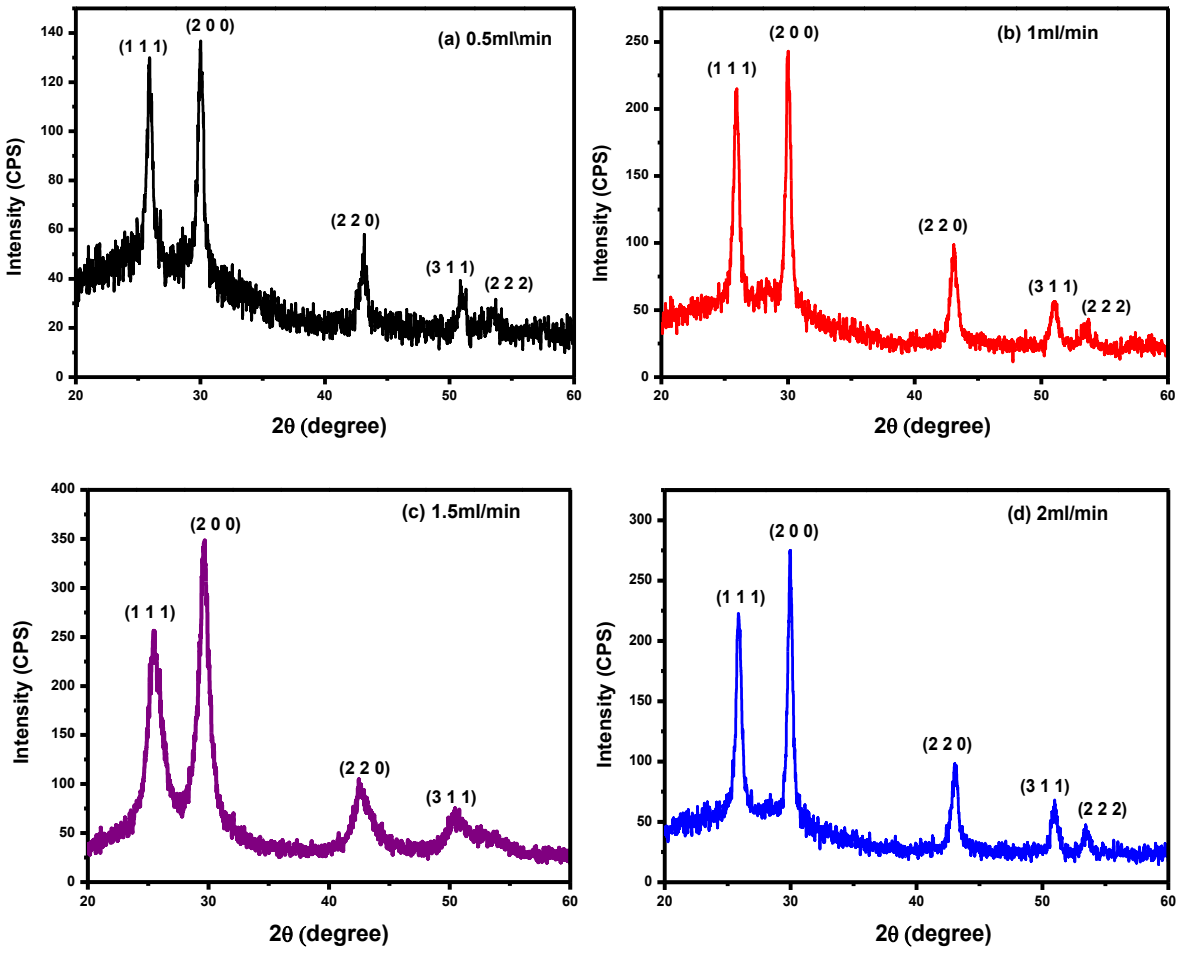


Fig. 3.2 XRD patterns of PbS films with spray rate variation.

Table 3.1 XRD data of PbS thin films with various spray rate.

| Spray Rate (ml/min) | (h k l) Value | 2θ (degree) | D (nm) | a (Å) |
|---|---|---|---|---|
| 0.5 | (2 0 0) | 30.07 | 16.23 | 5.937 |
| 1 | (2 0 0) | 30.07 | 20.68 | 5.938 |

| | | | | |
|---|---|---|---|---|
| 1.5 | (2 0 0) | 30.07 | 24.34 | 5.939 |
| 2 | (2 0 0) | 30.07 | 21.87 | 5.939 |

The XRD patterns of PbS films deposited at 350˚C with various spray rates are shown in Fig. 3.2. It is observed that films deposited with various spray rate exhibit polycrystalline nature with face-centered cubic structure. Crystallite size is calculated using equation 2.6 and results are shown in Table 3.1. The crystallite size of the films increases as the spray rate of the film increases from 0.5 ml/min to 1.5 ml/min and further increase in the spray rate, results in decrease in the crystallite size. This might be due to incomplete thermal decomposition of the spray solution causing powder formation on the surface of the films. The lattice parameter 'a' was calculated using equation 2.2. The calculated value of 'a' is in agreement with the standard value [JCPDS file number 00-005-0592].

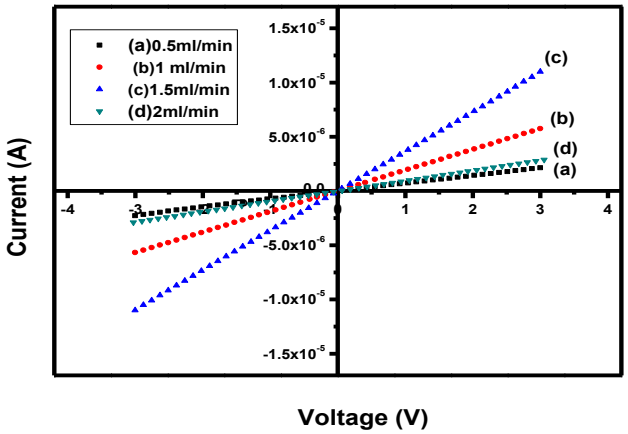


Fig. 3.3 I-V curves of PbS films for various spray rate.

The current-voltage characteristics of the films deposited at different spray rates are shown in Fig. 3.3. All the films show linear I-V characteristics satisfying ohmic conduction mechanism. The resistivity of the films decreased as the spray rate of the film increased from 0.5 ml/min to 1.5 ml/min, further increase in the spray rate resulted in increase in the resistivity of the films. This is in agreement with the results obtained from structural studies

showing a decrease in the crystallite size beyond 1.5 ml/min. Here, the optimum value of the spray rate was found to be 1.5ml/min.

### 3.2.5 Nozzle to substrate distance

As the nozzle to substrate distance was varied from 10 to 20 cm, the thermal gradient of vapor phase has been changed which lead to changes in the thermophoretic force acting on the liquid droplet. The complete vaporization of the byproducts from the droplet just above the substrate is the ideal condition for the best transportation of the main product species to the substrate. The thermal energy gained by the droplets depends on the temperature gradient in the air above the substrate surface. It will increase greatly with an increase in nozzle to substrate distance. This results in the preheating of the droplets by the carrier gas through heat radiation. It is known that preheating enhances the pyrolytic reaction in the droplets. At nozzle to substrate distance of 16 cm a chemical reaction takes place due to the preheating of the optimized droplet size and hence good quality films have been obtained. Above 16 cm the thermal energy gained by the droplet is very high. This causes the water molecule, which is an important oxidizing agent in the pyrolytic decomposition, to vaporize completely far away from the substrate. The particle melts then vaporizes and a chemical reaction will occur in the vapor phase. The molecules in the vapor phase condense as microcrystallites, which form a powdery precipitate on the substrate. This powder disturbs the formation of the film layer and diminishes the deposition efficiency. For nozzle-to-substrate distance less than optimized distance, cracks have been observed on the film surface; which clearly indicates that the solvent surrounding the solute does not evaporate completely and entrapped in the droplet, approaching towards the substrates. When droplet strikes the substrate, it explodes leaving behind the ruptured layers. Hence, the nozzle to substrate distance has been optimized at 16 cm to obtain good quality PbS thin films.

### 3.2.6 Carrier gas pressure

The pressure created using the carrier gas will also give continuous uniform film suitable to fabricate devices. Many researchers used various gasses to create pressure. For the present study, air is selected as a carrier gas to create pressure. To get continuous uniform films, carrier gas pressure is varied from 0.2 to 3 bar (1bar =1.0912 $kg/cm^2$). It has been observed that the films deposited at a pressure below 1.8 bar were found to be rough. This is

because at a lower pressure the size of the droplet is larger than the optimum droplet size for a particular temperature. So the heat absorbed from the surrounding will not be sufficient to vaporize the solvent entirely before reaching the substrate. The droplets hit the surface, where the solvent is vaporized entirely leading to the deposition of rough films. For the pressure above 1.8 bar, the droplet size will be much smaller than the optimum size hence the reaction takes place in the vapor phase will reduce the deposition efficiency and molecules condense as micro-crystallites and form the powdery precipitate on the substrates. For the pressure of 1.8 bar, it is observed that there is a formation of continuous films due to optimum droplet size so the thermal energy gained by the droplet is such that it vaporizes just above the substrate and gives continuous films. Hence, for the present study, the optimized pressure of 1.8 bar is selected to get continuous uniform films. Table 3.2 shows the optimized deposition parameters for the films.

Table 3.2 Preparative parameters for PbS thin films.

| **Parameter** | **Values** |
|---|---|
| Precursor | Lead acetate and thiourea |
| Concentration ratio (Pb:S) | 1:1 to 2:1(M) |
| Volume | 20 ml |
| Substrate temperature | 150 to 350˚C |
| Spray rate | 1.5 ml/min |
| Nozzle to substrate distance | 16 cm |
| Carrier gas | Air |
| Pressure of carrier gas | 1.8 bar |

## 3.3 EFFECT OF THICKNESS

To study the effect of thickness on structural, electrical and optical properties of PbS films, films of different thickness were prepared by varying the deposition time keeping all other parameters constant. The thickness of the films was calculated using gravimetric method and measurements were verified using cross-sectional view SEM micrographs.

### 3.3.1 Structural studies

XRD patterns of PbS thin films with different thickness are shown in Fig. 3.4. It is observed that films have face centered cubic structure with prominent (111), (200), (220) and (311) planes. The comparison of observed lattice parameters with the standard (JCPDS No.05-0592) confirms the formation of lead sulphide thin films. The position of the diffraction peaks is independent of the film thickness; however preferential orientation changes with film thickness as observed from the relative intensities of the peaks. The modifications in the peak intensity may be due to the re-alignment of crystallites with the increase in thickness Lakhdar et al. (2014). This can be understood easily; in the samples which are sufficiently thick there is much more matter which can diffract X-rays and the peak is more intense. This causes an improvement in crystallinity with an increase in film thickness as reported earlier from researcher groups Shewale et al. (2013), Bouderbala et al. (2008). The average crystallite size (D) of PbS thin films has been calculated using Scherer's formula (equation 2.6). The variation of average crystallite size with film thickness is tabulated in Table 3.3. It is seen that crystallite size increases up to 520 nm film thicknesses; however for the higher film thickness crystallite size seems to be saturated. This clearly shows that the thickness effect upon the crystallite size appears only in the thinnest films, the thickness of which is lower than approximately 600 nm to 700 nm. In this range the crystallinity is closely related to the film thickness. But a tendency to the saturation and independence versus film thickness was observed beyond the range indicating that the space required for the thermal movement is optimum at 520 nm film thicknesses.

Table 3.3 XRD data of PbS thin films with various thickness.

| **Thickness (nm)** | **(h k l) Value** | **2θ (degree)** | **D (nm)** | **a (Å)** |
|---|---|---|---|---|
| 150 | (2 0 0) | 30.07 | 16.23 | 5.939 |
| 240 | (2 0 0) | 30.07 | 21.32 | |
| 350 | (2 0 0) | 30.07 | 24.28 | |
| 430 | (2 0 0) | 30.07 | 29.87 | |
| 520 | (2 0 0) | 30.07 | 32.56 | |
| 610 | (2 0 0) | 30.07 | 32.30 | |

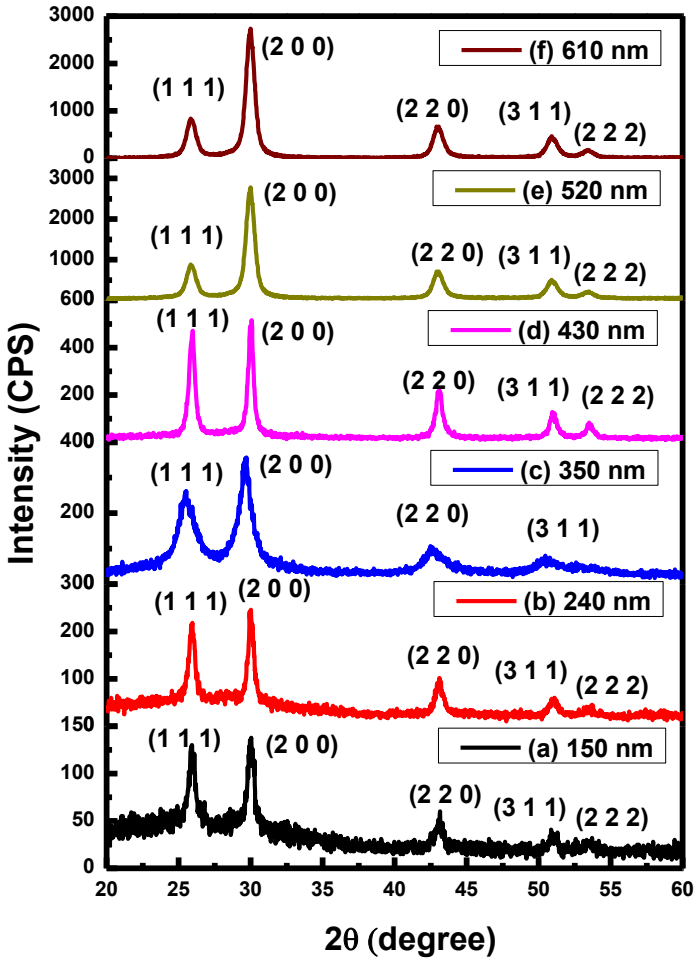


Fig 3.4 XRD pattern of PbS thin films with various film thickness.

3.3.2 Morphological and compositional studies

Fig. 3.5 shows EDAX spectra of the lead sulphide film with the optimized thickness 520 nm. It has been observed that the atomic % of lead and sulphur were 51.20 and 48.80 respectively with an error 0.5%.

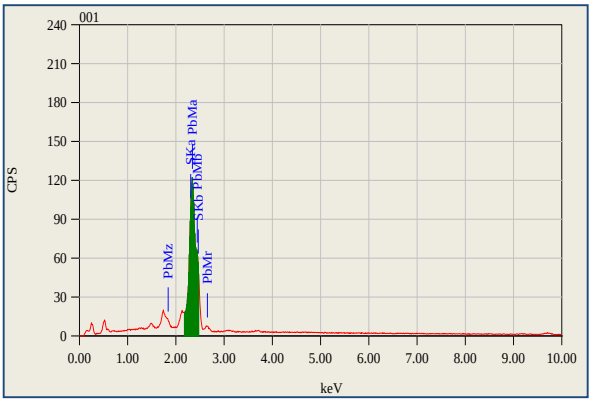


Fig 3.5 EDAX spectra of the PbS films with the thickness 520 nm.

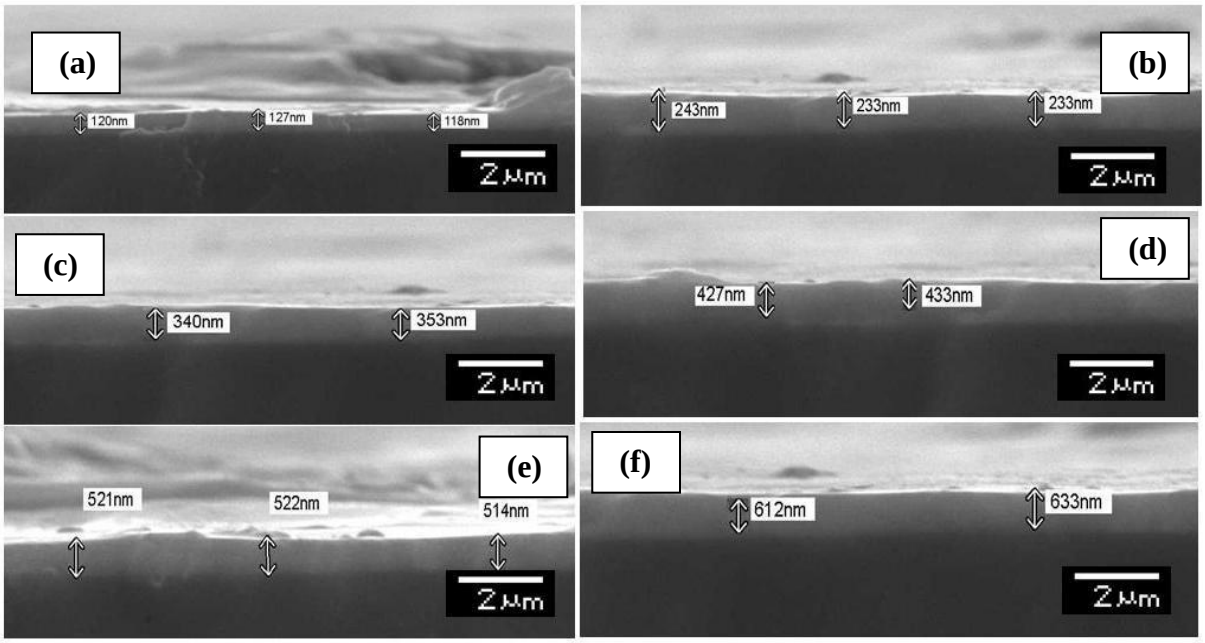


Fig. 3.6 Cross sectional view SEM micrographs for PbS films prepared with various thickness (a) 150 nm, (b) 240 nm, (c) 350 nm, (d) 430 nm, (e) 520 nm and (f) 610 nm.

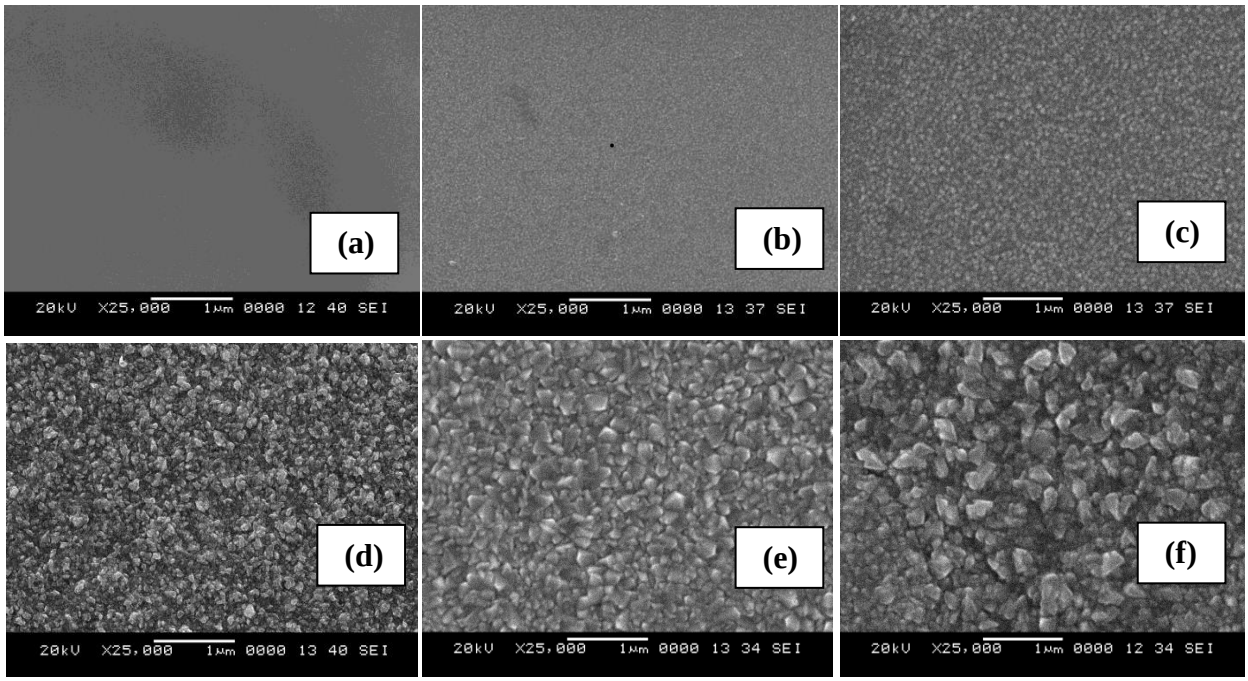


Fig. 3.7 In –plane scanning electron micrographs of the PbS thin films with various thicknesses (a) 150 nm, (b) 240 nm, (c) 350 nm, (d) 430 nm, (e) 520 nm and (f) 610 nm.

Fig. 3.6 shows the cross-sectional view SEM micrographs for PbS films prepared with different thickness. It is seen that the films deposited are compact and strongly adherent

to the substrate. The in–plane scanning electron micrographs of the PbS thin films with different thicknesses are shown in Fig. 3.7. All films exhibit crack-free, uniform and homogeneous surface morphology with an improvement in crystallite size via an increase in thickness. At lower thickness, the grain growth is restricted to two dimensions only; however, as the thickness increases additional space is provided for the crystals to grow in the third dimension. This may be a possible reason for the increase in crystallite size with film thickness (Shewale et al. 2013).

3.3.3 Electrical studies

The current –voltage (I-V) characteristics of PbS thin films are shown in Fig. 3.8. The PbS thin films show linear current-voltage response indicating that the conduction mechanism is ohmic with silver contact. The resistivity of the PbS thin films was calculated from the slope using the equation 2.15. The resistivity of PbS film decreased from 17.99 x$10^2$ Ω cm to 1.45 x$10^2$ Ω cm with an increase in film thickness from 150 nm to 520 nm. This may be attributed to the inverse dependence of film resistivity on thickness and crystallite size (Yadav et al. 2015). The increase in crystallite size with film thickness leads to decreased grain boundary scattering resulting in decrease in resistivity of the films (Bouderbala et al. 2008, Suchea et al. 2009). It has been noted that the resistivity of PbS films is in agreement with the reported resistivity value for the films grown by other chemical methods (Ravishankar et al. 2015). However, for further increase in film thickness resistivity seems to have reached the bulk value. The observed saturation indicates that the results obtained were consistent with crystallite size calculated from XRD data of the films.

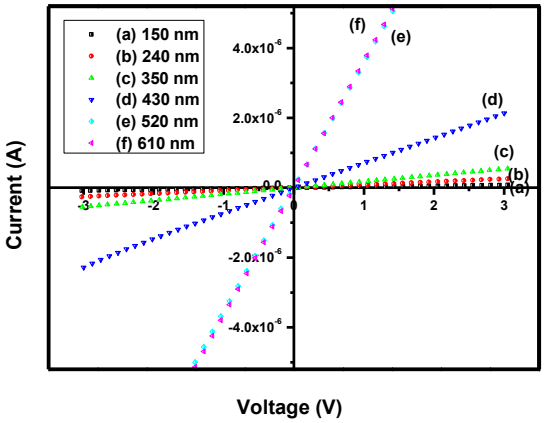


Fig. 3.8 I-V characteristics of PbS thin films with various thickness.

Fig. 3.9 shows Arrhenius plots (variation of log R with 1/T) for the PbS films. The resistance decreases with increase in temperature showing the semiconducting nature of the films. The nature of the plot gives single slope which indicates the presence of one type of conduction mechanism in intrinsic region. The activation energy of the films is found to be 0.2 ± 0.3 eV. The Hot probe measurement showed that PbS thin films are n-type semiconductors.

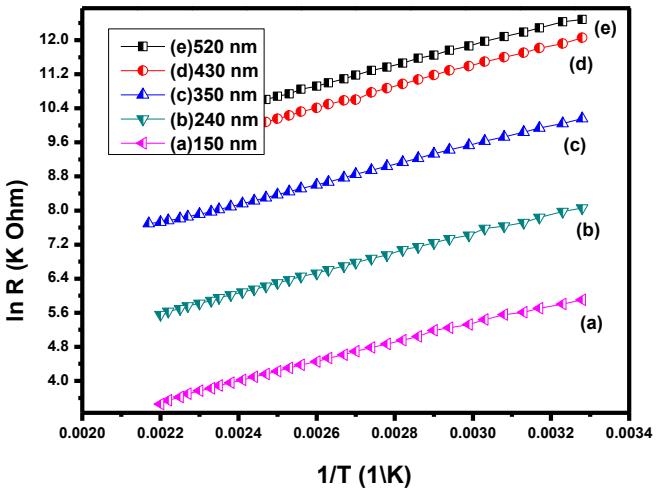


Fig 3.9 Variation of log R with (1/T) with various thickness of PbS films.

Table 3.4 Electrical properties of the PbS films with various thickness.

| **Thickness (nm)** | **Resistivity ($10^2$) Ω cm** | **Carrier concentration (/cm$^3$)** | **Mobility (cm$^2$/VS)** | **Energy band gap (eV)** |
|---|---|---|---|---|
| 150 | 17.99 | 2.14x10$^{16}$ | 16.23 | 1.34 |
| 240 | 13.79 | 2.90 x10$^{16}$ | 15.62 | 1.31 |
| 350 | 12.24 | 3.77 x10$^{16}$ | 13.54 | 1.28 |
| 430 | 4.92 | 1.08 x10$^{17}$ | 11.81 | 1.25 |
| 520 | 1.45 | 4.14 x10$^{17}$ | 10.41 | 1.22 |
| 610 | 1.50 | 4.07 x10$^{17}$ | 10.52 | 1.23 |

The carrier concentration and mobility determined for the films deposited with various thicknesses are summarized in Table 3.4. The values of carrier concentration and

Hall mobility for the spray deposited PbS thin films at 520 nm film thickness are $4.14x10^{17}$ $cm^{-3}$ and 10.41 $cm^2V^{-1}S^{-1}$, respectively. These values of carrier concentration and mobility are comparable with the values reported for PbS films deposited by CBD technique (Slonopas et al. 2014). It is apparent from the Table 3.4 that the hall mobility decreases with increase in the film thickness. In contrast, the charge carrier concentration of the films shows a gradual increase with an increase in the film thickness until the value of 520 nm. It is a well-known fact that the various factors, such as crystallinity, morphology, roughness, porosity, stress, composition and film substrate interface play a crucial role in determining the electrical properties of the films (Yadav et al. 2015). Hence, the variation in the electrical parameters of the film, with respect to thickness, can be attributed to the crystallinity as examined by XRD. Hall mobility measurements show that the films were n-type which confirms the results of hot probe measurements.

### 3.3.4 Optical studies

The optical transmittance measurements of PbS films were carried out at room temperature and normal incidence in the wavelength range of 300-3500 nm in order to investigate the feasibility of using PbS films for optoelectronic devices. As shown in Fig. 3.10 the films with thickness 150 nm exhibited the highest average optical transmittance of 70% in the near IR region. However, the optical transmittance found to decrease with increase in film thickness. The average optical transmittance of the 520 nm and 610 nm PbS films is approximately 42% in the near IR region. This apparent decrease in transmittance is attributed to absorption due to inter-band transition.

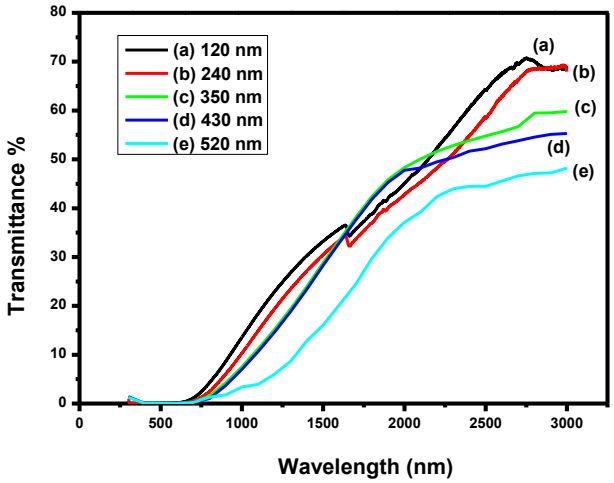


Fig. 3.10 Transmittance spectra of PbS films with various thickness.

In order to estimate the band gap of the PbS films with various thicknesses optical absorption of the films deposited on glass substrates has been studied at room temperature in the wavelength range of 300 – 3500 nm. The optical absorption data were analyzed for near edge optical absorption of the films by using the equation 2.14. The absorption coefficient is in the order of $10^6$ $cm^{-1}$. Fig. 3.11 shows the variation of $(\alpha h\nu)^2$ with $h\nu$ for PbS thin films with various thicknesses. The estimated values of band gap energy are given in Table 3.4. It is observed that the band gap is decreased from 1.34 eV to 1.22 eV as the film thickness changes from 150 nm to 520 nm. It was found that the optical band gap energy of PbS films decreases as the film thickness increases. The film thickness dependence of band gap energy can be due to factors like the (i) existence of amorphous phases in thin films, (ii) the quantum confinement effect and (iii) the change in barrier height owing to change in crystallite size in polycrystalline films. In the present case, the films were polycrystalline and the quantum confinement effect may not be appropriate since the crystallite sizes of the films in the present study are large. It can be considered that the thickness dependence of band gap energy is concerned with the crystallinity of the films (Bao et al. 2001). The decrease in band gap energy with film thickness is similar to its crystallite size dependence, which indicates the decrease in barrier height at the boundaries with an increase in crystallite size (Slater et al. 1956).

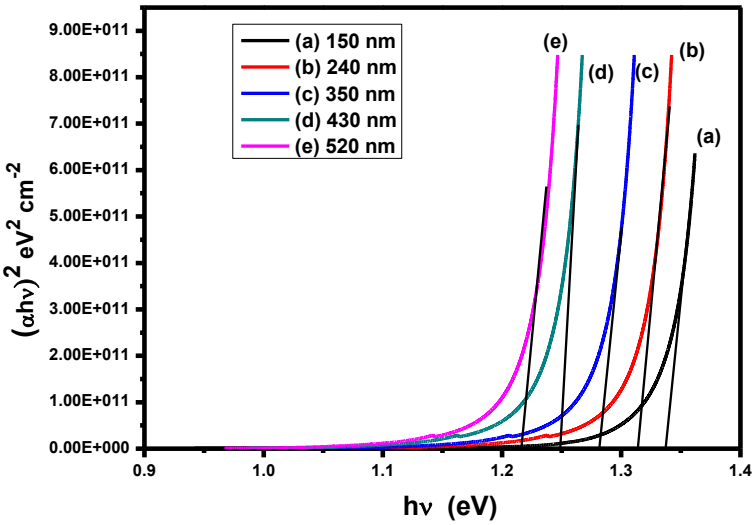


Fig. 3.11 Variation of $(\alpha h\nu)^2$ with $h\nu$ for various thickness of PbS thin films.

## 3.4 EFFECT OF SUBSTRATE TEMPERATURE

### 3.4.1 Structural studies

The XRD patterns of the films deposited at various substrate temperatures are shown in Fig. 3.12. It confirms the proper phase formation of the PbS films. The films have a face centered cubic structure with highly preferred orientation along (2 0 0) plane. This preferential orientation is strongly supported with an earlier report (Faraj et al. 2014). The lattice parameters and crystallite size of the films for (2 0 0) reflection were calculated from these XRD patterns are given in Table 3.5.

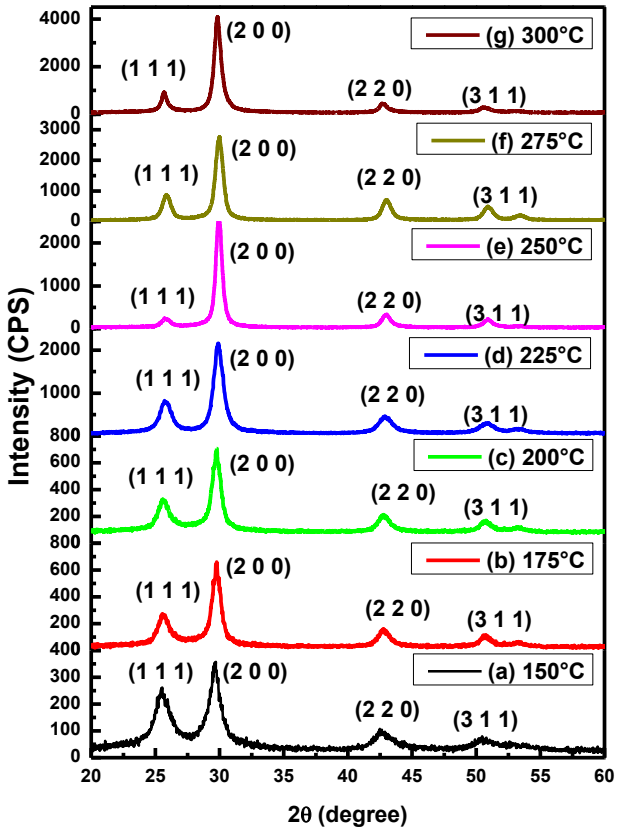


Fig.3.12 XRD patterns of PbS films deposited at different substrate temperatures.

Table 3.5 Lattice parameters and crystallite size of the films deposited at different substrate temperature.

| Substrate temperature (°C) | 2θ (deg) | (h k l) | $d_{cal}$ (Å) | $d_{std}$ (Å) | a (Å) | Crystallite size (nm) |
|---|---|---|---|---|---|---|

| | | | | | | |
|---|---|---|---|---|---|---|
| 150 | 29.77 | (2 0 0) | 3.001 | 2.969 | 6.002 | 6.9 |
| 175 | 29.72 | (2 0 0) | 3.006 | 2.969 | 6.012 | 9.8 |
| 200 | 29.72 | (2 0 0) | 3.006 | 2.969 | 5.938 | 10.8 |
| 225 | 29.86 | (2 0 0) | 2.989 | 2.969 | 5.979 | 11.9 |
| 250 | 29.91 | (2 0 0) | 2.987 | 2.969 | 5.974 | 13.3 |
| 275 | 29.91 | (2 0 0) | 2.987 | 2.969 | 5.974 | 15.4 |
| 300 | 29.85 | (2 0 0) | 2.991 | 2.969 | 5.938 | 16.3 |

The intensity of the peaks increases with increase in substrate temperature which reveals that crystallinity of the film improves at elevated substrate temperature. It might be due to the reduction of microstrain values at a higher temperature. The variation in crystallite size as a function of substrate temperature shown in Fig. 3.13 shows that the crystallite size of the typical PbS thin films were increases with increase in substrate temperature.

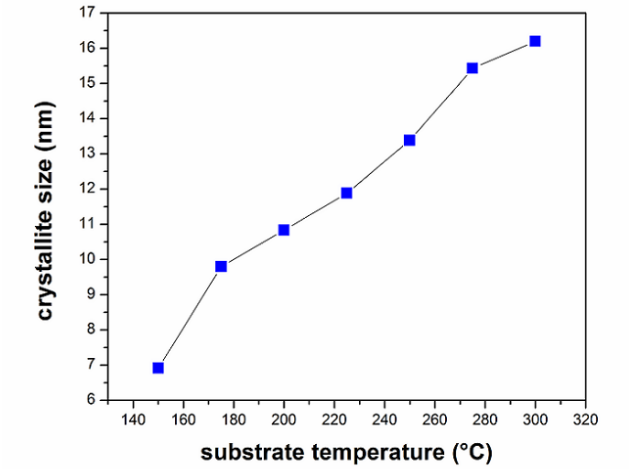


Fig. 3.13 Variation of a crystallite size of the PbS films with different substrate temperatures.

3.4.2 Compositional and morphological studies.

Table 3.6 shows the chemical composition of the films at different substrate temperatures. It shows that the films grown at low temperature are sulphur rich. This trend is due to the different rates of adsorption of lead and sulfur ions. When substrate temperature of these films is increased, the composition changed due to the evaporation of excess sulphur. Films deposited at a substrate temperature above 225°C films were found to be discontinuous and porous due to the evaporation of precursor solution. Here, the optimum value of the substrate temperature was found to be 225°C.

Table 3.6 Chemical composition of the PbS films deposited at different substrate temperatures.

| **Substrate temperature (°C)** | **Lead (At %)** | **Sulphur (At %)** | **Pb:S (At %)** |
|---|---|---|---|
| 150 | 42.79 | 57.21 | 0.75 |
| 175 | 43.76 | 56.24 | 0.79 |
| 200 | 44.03 | 55.97 | 0.78 |
| 225 | 45.36 | 54.64 | 0.83 |
| 250 | 46.86 | 53.14 | 0.88 |
| 275 | 47.19 | 52.81 | 0.89 |
| 300 | 48.06 | 51.94 | 0.93 |

The SEM images of the films deposited under various conditions are shown in Fig. 3.14. All films deposited at substrate temperature up to 225°C were smooth, homogeneous and free from voids. The morphology of the spray deposited PbS films are found to be comparable to the reported earlier (Sudad et al. 2013).

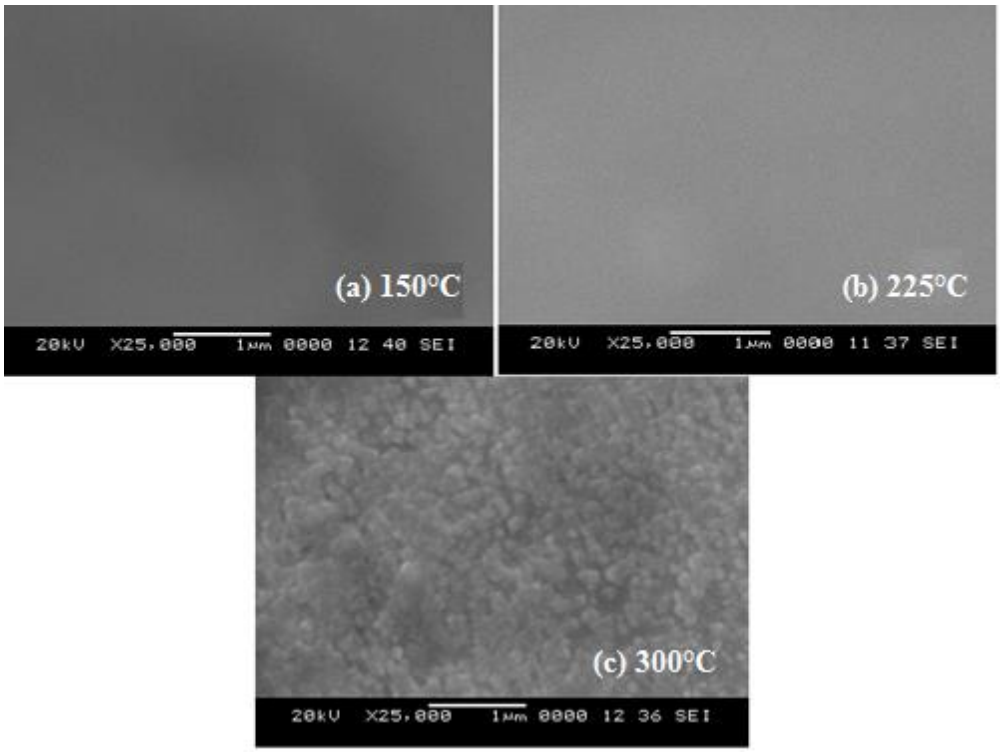


Fig. 3.14 SEM images of PbS films deposited at a different substrate temperature.

3.4.3 Electrical studies

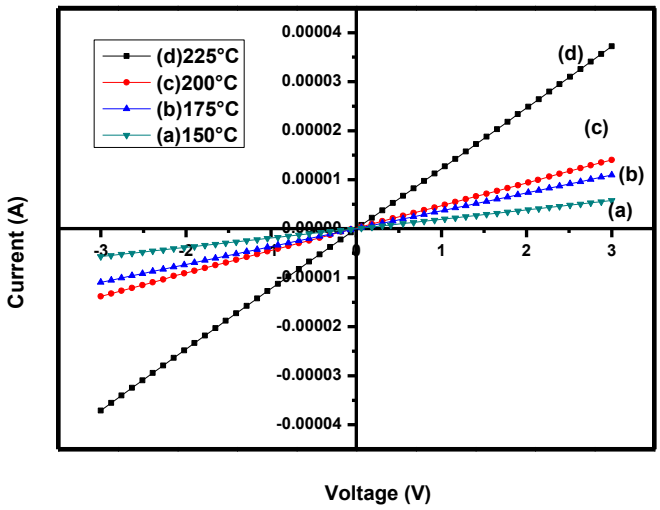


Fig. 3.15 I-V plots of the films deposited at different substrate temperatures.

I-V plots of the films deposited at different substrate temperatures from150°C to 225°C with silver contact are shown in Fig. 3.15. These plots indicate that silver makes ohmic contact with the semiconductor. It was found that the electrical conductivity of the films increased with increase in substrate temperature up to 225°C which is seen as a consequence of reduced defect content in the films. But, the electrical conductivity of the films decreased with increase in temperature above 225°C due to discontinuity and pores present on the deposited films. The conductivity of the film deposited at 225°C substrate temperature was in the order of $10^{-4}$ $\Omega^{-1}cm^{-1}$.

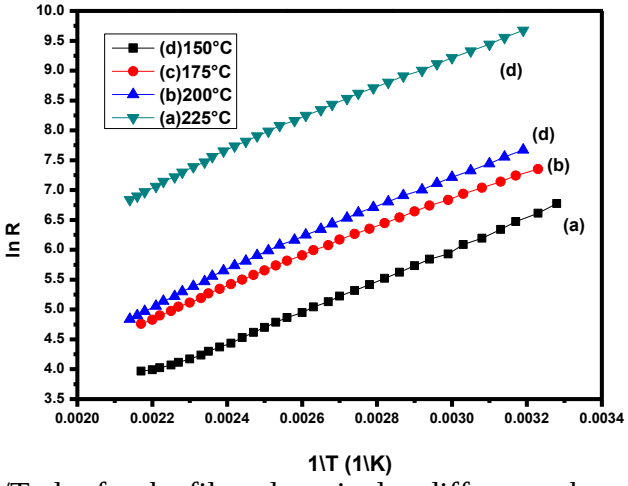


Fig. 3.16 ln R Vs 1/T plot for the films deposited at different substrate temperatures.

The plots of log R Vs 1/T were drawn as shown in Fig. 3.16. All these plots show single slope which is in the intrinsic conduction region where resistance decreases with temperature indicating that the films are semiconducting nature. The energy band gap of the films was determined from the plot. Very small change in the thermal activation energy has been observed. Energy band gap of the films deposited at 225°C substrate temperature was calculated to be 0.39 eV. Conventional hot probe technique was used to determine the majority carrier type in the PbS film, deposited at various substrate temperatures. It was observed that films deposited at substrate temperature in the range 150°C to 225°C were of p-type and above 225°C they were found to be n-type. In the case of films deposited at 150°C to 225°C excess of sulphur is responsible for the films to become p-type. However, even the films deposited at above 225°C which is relatively rich in lead content were found to be n-type.

## 3.5 EFFECT OF LEAD PRECURSOR CONCENTRATION

The precursor concentration of lead was optimized to achieve 50:50 (Pb:S) stoichiometric thin films keeping substrate temperature 225˚C. The atomic % of lead and sulphur in the PbS films were varied from 45(Pb):55(S) to 55(Pb):45(S) by varying only the lead precursor concentration from 1 to 2M.

### 3.5.1 Structural studies

XRD pattern of lead sulphide thin films with various lead precursor concentration is shown in Fig. 3.17. All PbS thin films have a face centered cubic structure with polycrystalline nature as evidenced by the presence of higher intensity peak (Fig. 3.17b) at 30.07˚ which corresponds to PbS as observed in standard JCPDS file 00-005-0592 (Rajathi et al. 2014). The 50:50 stoichiometric thin films with a sharp peak at 30.07˚ confirm the presence of PbS. Other peaks (111) and (220) at 25.64˚ and 42.75˚ correspond to different orientations of the crystallites in the thin films. The increase in lead precursor concentration from 1:1 to 2:1 (in steps of 0.25) results in shifting of crystallites orientation in PbS thin films from (200) to (111) indicating a three-dimensional growth of the crystallites. This change in crystallite orientation could be attributed to the variation in a number of $Pb^{2+}$ and $S^{2-}$ ions in the reactant solution at higher molar concentration. The results suggest that the microstructural characteristics of the sprayed lead sulphide films are dependent on the lead

precursor concentration and hence, the orientation of the crystallites can be tuned by varying the cationic precursor concentration. The lattice constant 'a' of the films was determined by equation 2.2 (Tohidi et al. 2013).

The crystallite size (D) of deposited thin films was calculated using equation 2.6 (Ravishankar et al. 2015). The formula was used on (111) diffraction peak for the determination of crystallite size of the films. It reveals that the increase in lead precursor concentration results in increased crystallite size as tabulated in Table 3.7. The increase in crystallite size and thickness is due to the enhancement of the horizontal velocity of adatoms and condensation of energetic lead and sulphur vapor on the substrate surface. The crystallites are found to be nanocrystalline in nature which explains that the PbS thin films have larger nucleation rate than the growth rate due to more number of nucleation centers that exist on the surface of the substrate as explained by Rajathi et al. (2014).

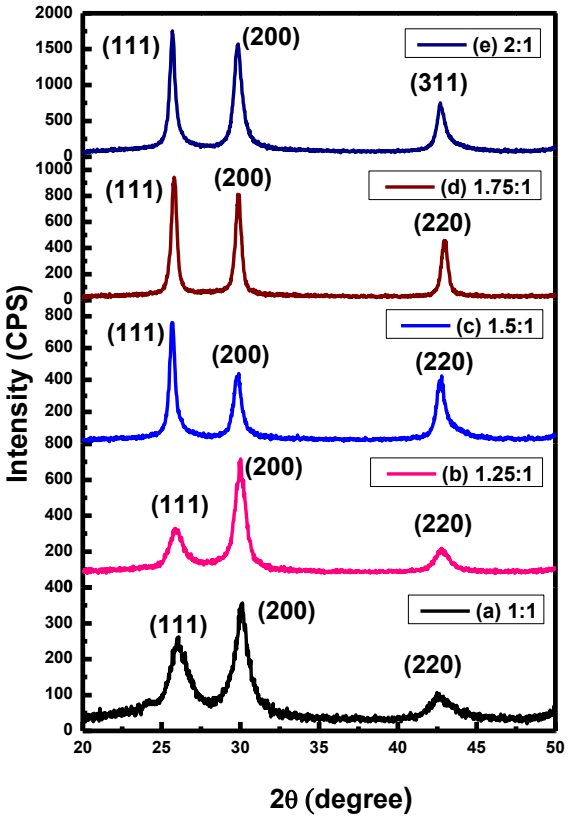


Fig.3.17 X-ray diffraction pattern of the PbS thin films with various precursor concentration ratios.

Table 3.7 Structural parameters of PbS thin films with various precursor concentration ratios.

| Pb:S ratio | Maximum intensity | | For (111) plane | | | | |
|---|---|---|---|---|---|---|---|
| | 2θ | (hkl) Plane | 2θ | d (Å) | a (std) (Å) | a (cal) (Å) | Crystallite size (D) (nm) |
| 1:1 | 30.09 | (200) | 25.96 | 3.445 | 5.939 | 5.944 | 5.00 |
| 1.25:1 | 30.07 | (200) | 25.86 | 3.429 | 5.939 | 5.939 | 10.42 |
| 1.5:1 | 25.64 | (111) | 25.64 | 3.451 | 5.939 | 5.977 | 18.58 |
| 1.75:1 | 25.64 | (111) | 25.64 | 3.451 | 5.939 | 5.977 | 26.94 |
| 2:1 | 25.72 | (111) | 25.72 | 3.469 | 5.939 | 6.008 | 39.14 |

The increase in nanocrystallite sizes results in narrowing of the diffraction peaks as observed in Fig. 3.17 (a-e). The precursor molar ratio exceeds 2:1, the thickness of lead sulphide film decreases. The result seems to confirm that the nucleation rate is mainly regulated by the concentration of $Pb^{2+}$ ions in solution which results in the development of PbS complex as reported by Seghaier et al. (2006) for lead sulphide thin films by varying lead nitrate precursor concentration using CBD technique.

3.5.2 Morphological and compositional studies

Table 3.8 Variation of composition in PbS film with various precursor concentration ratio.

| Pb:S precursor concentration ratio | Lead (At %) | Sulphur (At %) |
|---|---|---|
| 1:1 | 44.03 | 55.97 |
| 1.25:1 | 50.35 | 49.65 |
| 1.5:1 | 51.49 | 48.51 |
| 1.75:1 | 53.25 | 46.75 |
| 2:1 | 55.54 | 44.46 |

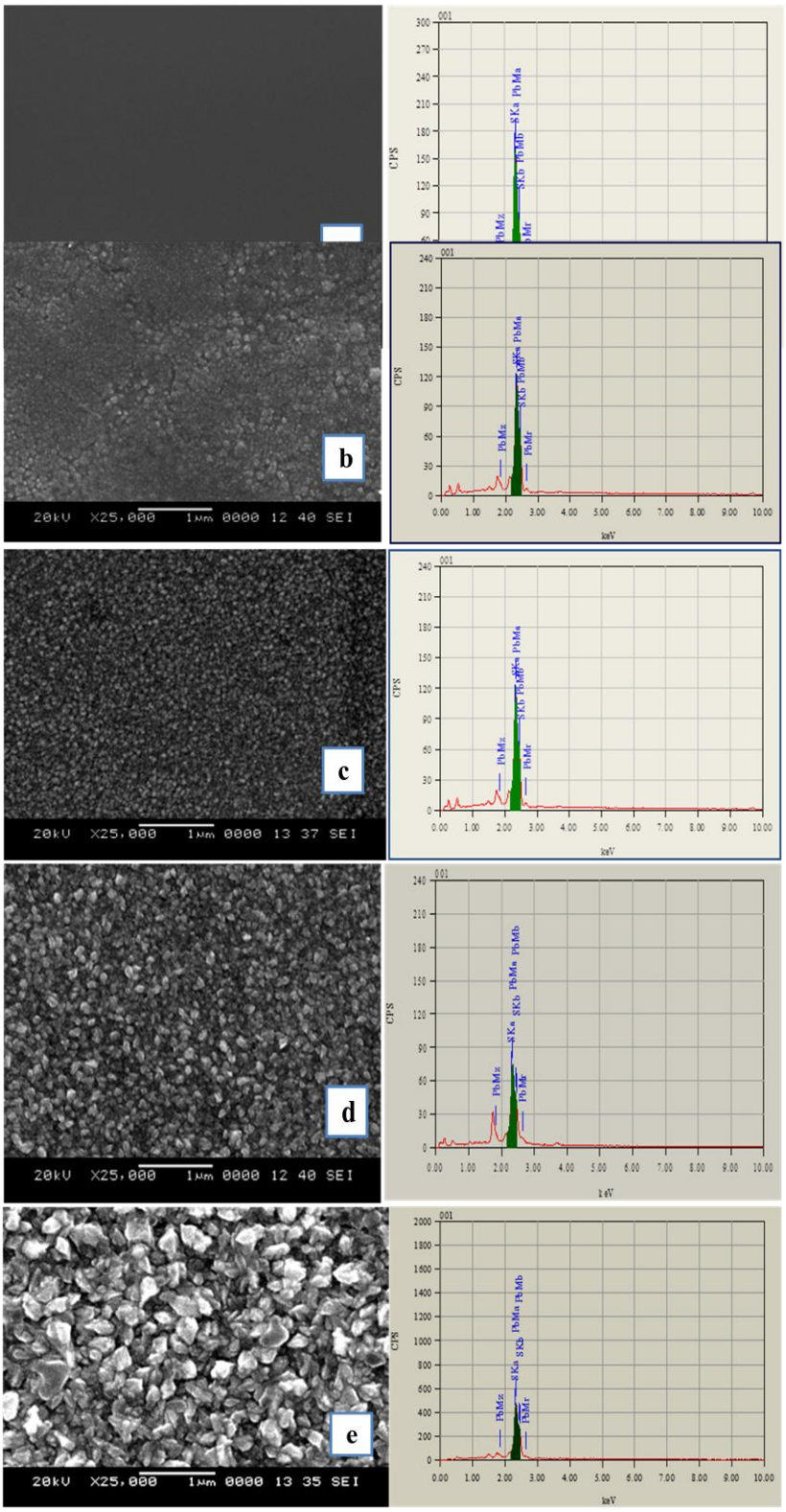


Fig. 3.18 SEM image and EDAX spectra of PbS thin films with precursor concentration ratio (a) 1:1 (b) 1.25:1 (c) 1.5:1 (d) 1.75:1 (e) 2:1.

The morphology of the nanocrystalline PbS thin films is shown in Fig. 3.18. The stoichiometric lead sulphide thin film (Fig. 3.18b) shows a uniform and smooth surface morphology over the entire substrate. For 1:1 molar concentration of precursor solutions, the resultant PbS thin films are found to be smooth. The grains are small and densely packed throughout the surface. The grains grow larger as the molar concentration of the lead precursor is increased. Larger grains of 40 nm have been observed for 2:1 molar concentration. The results suggest that the microstructural characteristics such as grain size, grain density, and grains packing of the lead sulphide thin films are influenced by the lead precursor concentration. It also validates the analysis from Scherer's formula (equation 2.6) that the nanocrystallite size increases as the lead precursor concentration increases (as given in Table 3.7). The atomic % of lead and sulphur with various precursor concentration of Pb is given in Table 3.8. The films prepared with 1.25:1 precursor concentration ratio are found to be stoichiometric.

### 3.5.3 Optical studies

Fig. 3.19 shows the optical absorption spectra of the PbS thin films for different lead precursor concentration as a function of wavelength ranging from 500 nm-3000nm. The absorbance spectrum of stoichiometric PbS thin films shows the presence of two absorption thresholds, one in NIR region and the other in mid-IR region. From Fig. 3.19, it is evident that the absorption increases linearly from 3000 nm to 1100 nm. At the second threshold near 1100 nm, the absorption increases steeply and peaks at 330nm. The absorption does not reach zero in visible region indicating that the sample is partially transparent. As the lead ion concentration increases from 45% to 55% by increasing the molar concentration of lead precursor solution the absorption threshold wavelengths get shifted as observed in Fig. 3.19.

The absorption peak shifts from 330 nm (for 50% Pb) to 880 nm (for 52% Pb). Although the change in lead concentration is feeble, the microstructural characteristics of both the films show marked difference i.e., the film (with 52% Pb) looks more granular with dense packing. The granularity possibly induces strain in the film resulting in a red shift of the absorption threshold and maximum absorption. The shift in absorption peaks is attributed to the increase in dangling bonds for higher Pb concentration which in turn increases the density of localized states for the films as reported by Douri et al. (2008) for thermal

evaporated PbS films. The trend of red shifting in absorption peaks continues as the lead precursor concentration is increased to 2:1 (in step of 0.25). The absorption threshold at mid-IR wavelength region remains almost unaltered with a change in lead ion concentration.

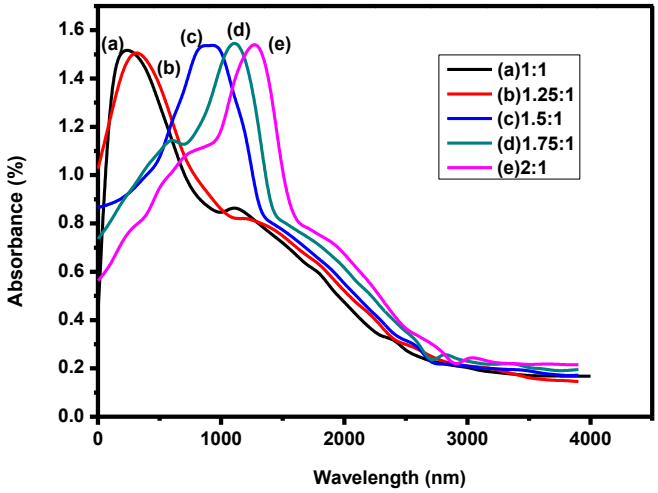


Fig. 3.19 Absorption spectra of the PbS films with various precursor concentration ratios.

The absorption coefficient α of the film was found to be in the order of $10^6$ $cm^{-1}$ which has been calculated using equation 2.14 (Beddek et al. 2016). Kennedy et al. (2014), Douri et al. (2008) and Schoolar (1965) reported that PbS thin film has both direct and indirect transitions. Hence, the energy band gap of PbS films was determined for both direct and indirect transition. The band gap of the material was determined using equation 2.13 (Tauc 1974). The optical band gap of the films has been calculated by extrapolating the linear part of $(\alpha h\nu)^{1/n}$ versus photon energy plot. Fig. 3.20 shows the Tauc's plot for both direct and indirect transition of the films deposited with various Pb concentrations. The band gaps of lead sulphide thin films as calculated from Tauc's plot are tabulated in Table 3.9. The direct band gap energy of PbS thin films varies from 1.22 eV for 45% Pb to 0.78 eV for 55% Pb concentration. However, the indirect band gap energy remains almost constant for all the Pb ion concentrations. The optical studies reveal that as the lead precursor concentration is increased from 1:1 to 2:1, the band gap energy of the PbS films reduces from 1.2 eV to 0.78 eV. As a result, optical absorption gets red shifted from visible to the near-IR range. This might be due to the creation of new states in $E_g$ that leads to an increase in the density of localized states which causes the shift in $E_g$ to lower photon energy (Hussain et al. 2012,

Douri et al. 2008). The energy gap values for different precursor concentration ratio are shown in Table 3.9.

Table 3.9 Variation of direct and indirect energy band gap of PbS films with various precursor concentration ratios.

| precursor concentration ratio | Direct bandgap energy (eV) | Indirect band gap energy (eV) |
|---|---|---|
| 1:1 | 1.22 | 0.41 |
| 1.25:1 | 0.96 | 0.40 |
| 1.5:1 | 0.91 | 0.39 |
| 1.75:1 | 0.86 | 0.38 |
| 2:1 | 0.78 | 0.37 |

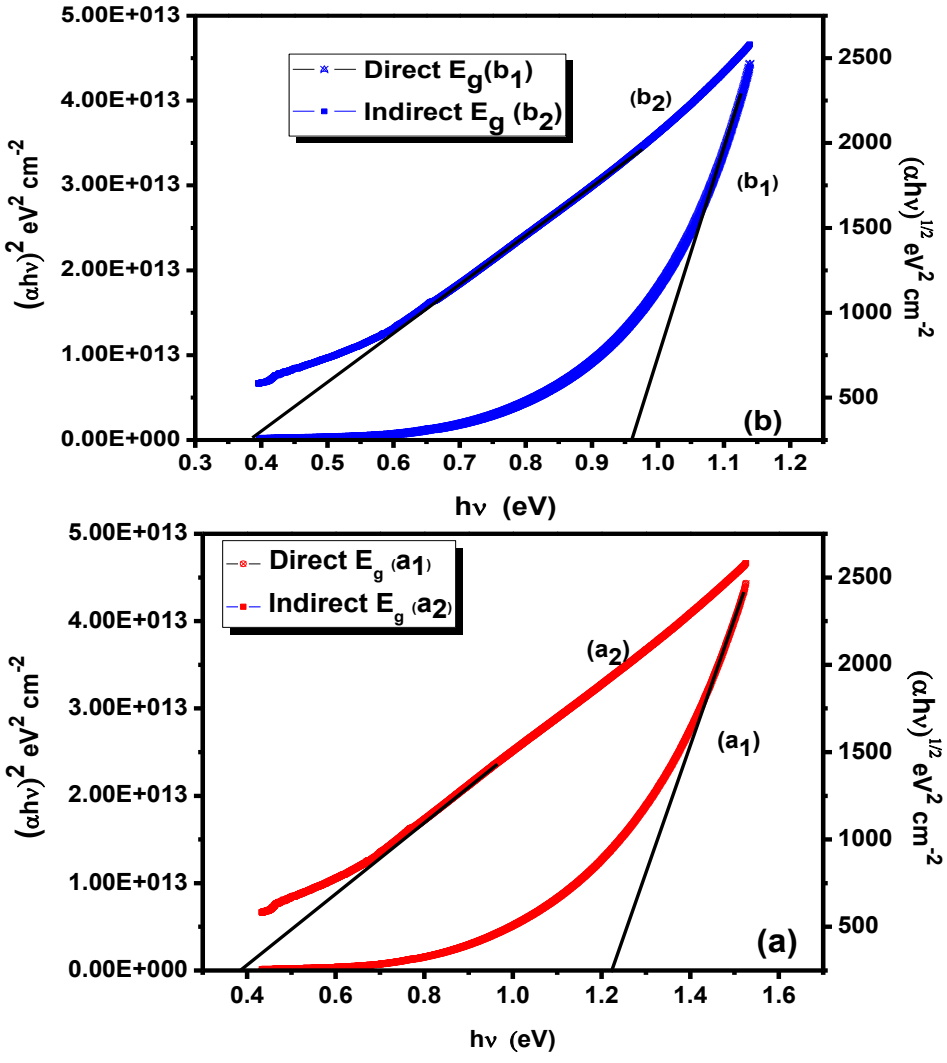

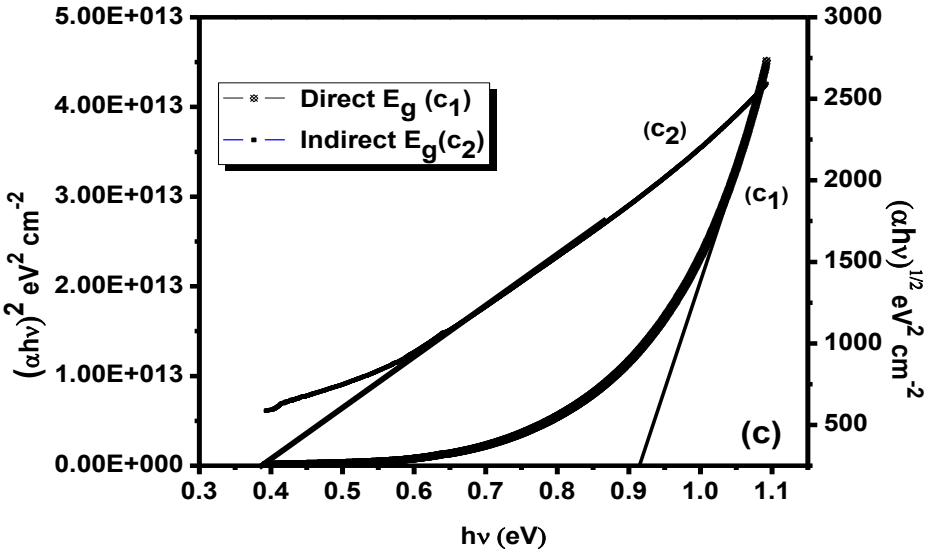
Direct $E_g$ ($c_1$)
Indirect $E_g$($c_2$)
($c_2$)
($c_1$)
(c)
$(\alpha h\nu)^2$ $eV^2$ $cm^{-2}$
$(\alpha h\nu)^{1/2}$ $eV^2$ $cm^{-2}$
hν (eV)

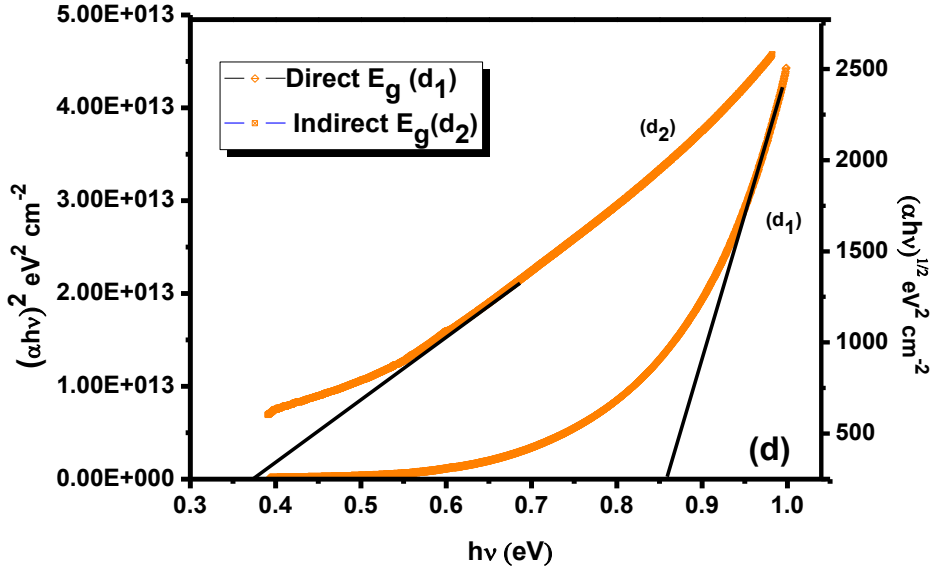
Direct $E_g$ ($d_1$)
Indirect $E_g$($d_2$)
($d_2$)
($d_1$)
(d)
$(\alpha h\nu)^2$ $eV^2$ $cm^{-2}$
$(\alpha h\nu)^{1/2}$ $eV^2$ $cm^{-2}$
hν (eV)

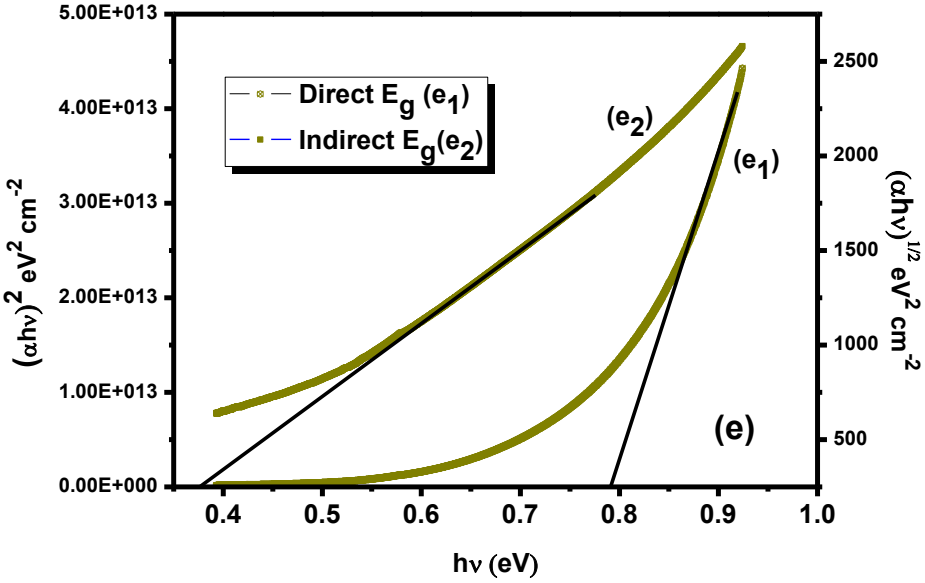
Direct $E_g$ ($e_1$)
Indirect $E_g$($e_2$)
($e_2$)
($e_1$)
(e)
$(\alpha h\nu)^2$ $eV^2$ $cm^{-2}$
$(\alpha h\nu)^{1/2}$ $eV^2$ $cm^{-2}$
hν (eV)

Fig. 3.20 Tauc's plots for Pb:S thin films of different precursor concentration ratio (a) 1:1 (b) 1.25:1 (c) 1.5:1 (d) 1.75:1 (e) 2:1.

The mode of optical transitions in these films have been confirmed by equation

$$\ln(\alpha h\nu) = \ln K + n \ln(h\nu - E_g) \quad (3.2)$$

The plot of $\ln(\alpha h\nu)$ v/s $\ln(h\nu - E_g)$ (Fig. 3.21) is a straight line with two linear regions whose slope gives the power factor n for the films. The value of n has been found as about 0.5 for lower wavelength region indicate direct transition. Whereas for higher wavelength is about 2 indicate indirect transition (Kennedy et al 2014, Chaure et al. 2008).

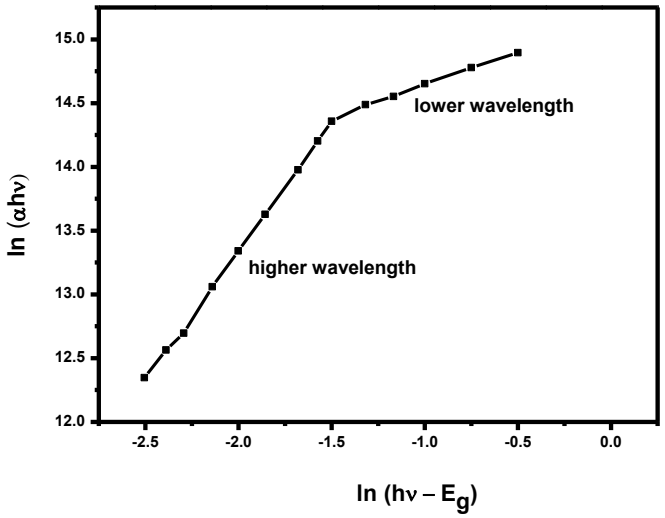


Fig. 3.21. The plots of ln (αhν) Vs. ln (hν-$E_g$) of stoichiometric PbS thin films.

3.5.4 Electrical studies

The current–voltage (I-V) characteristics of PbS thin films are shown in Fig. 3.22. The PbS thin films show linear current-voltage response indicating that the conduction mechanism is ohmic with silver contact. The resistivity of the PbS thin films was calculated using equation 2.15. The resistivity of films found to decrease with increase in lead precursor concentration, this is due to the improvement in crystallinity and larger crystallite sizes of thin films. The resistivity of PbS thin films found to be in the order of $10^2$ Ω cm which is listed in Table 3.10.

The Fig. 3.23 shows Arrhenius plot (variation of log R with 1/T) for the PbS films. The resistance decreased with increased temperature shows the semiconducting nature of the films. The nature of the plot gives single slope which indicates the presence of one type of conduction mechanism in intrinsic region. The thermal activation energy was calculated using equation 2.16 (Preetha et al. 2012).

The activation energy (as listed in Table 3.10) of the films is found to decrease with increase in lead ion concentration. The decrease in activation energy also reflects the decrease in the band gap energy of the thin films. Further, the resistivity of the PbS thin films also decreases with decreasing activation energy and band gap. The observed resistivity values of the spray deposited PbS thin films are better for wet chemically prepared PbS thin films. The Hot probe measurement showed the +ve value of $V_{DC}$ which indicates PbS thin films were n-type semiconductors with different lead precursor concentration.

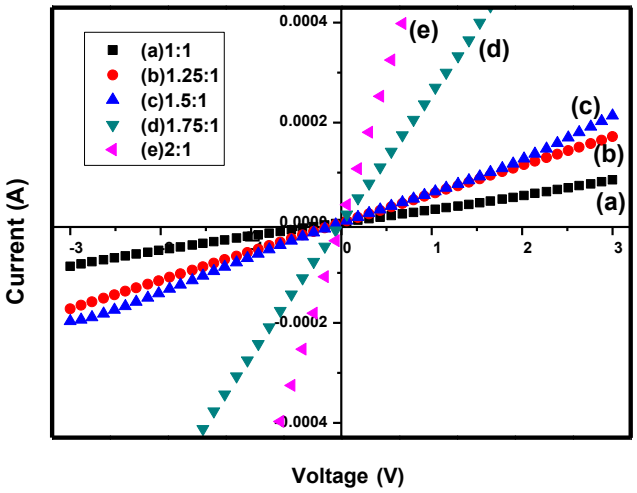


Fig. 3.22 I-V characteristics of the Pb:S thin films .

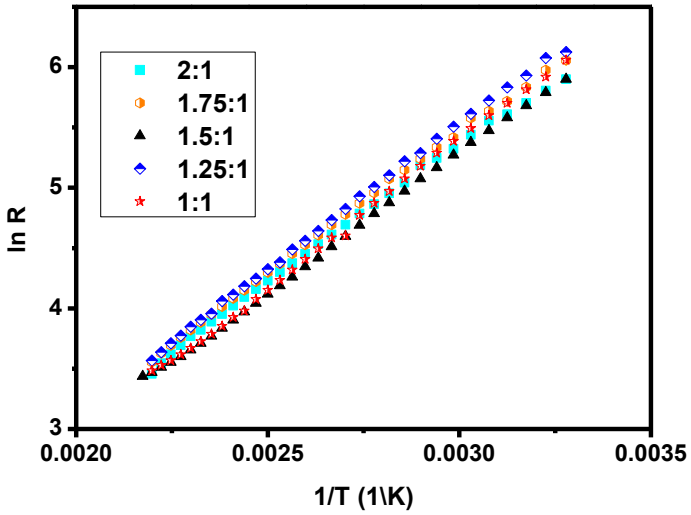

Fig. 3.23 Variation of ln R with 1\T for PbS films with various precursor concentration ratios.

Table 3.10 Activation energy and resistivity measured for PbS films with various precursor concentration ratios.

| **Pb:S precursor concentration ratio** | **Activation energy (eV)** | **Resistivity ρ ($X10^2$) in Ω cm** |
|---|---|---|
| 1:1 | 0.205 | 10.600 |
| 1.25:1 | 0.2 | 05.117 |
| 1.5:1 | 0.195 | 04.348 |
| 1.75:1 | 0.19 | 01.060 |
| 2:1 | 0.185 | 00.497 |

## 3.6 EFFECT OF ANNEALING

### 3.6.1 Compositional and morphological studies

The lead sulphide thin films that were prepared at different substrate temperatures ranging from 150°C to 350°C with an interval of 25°C. PbS films were found to be rich in sulphur content at a substrate temperature ranging from 150°C to 350°C. Since sulphur has a great affinity towards oxygen, its content readily decreases as the substrate temperature increases (Raviprakash et al. 2009). Unlike the homogeneous films deposited at lower substrate temperature, the films deposited at a substrate temperature above 225°C were non-homogeneous with some pores on the surface. These pores are due to re-evaporation of the precursor solutions during deposition at a higher temperature. This restricts to optimize the deposition temperature as 225°C. To grow thin films using the solution processing techniques, it becomes necessary to deposit the films at a suitable elevated temperature followed by thermal annealing at higher temperature for their decomposition and reaction. Therefore for solution based techniques, annealing process is indispensable. Considering the advantages offered by annealing, films were air annealed at temperature 300°C and 350°C for the different duration (1hr, 2hr, 3hr and 4hr) to obtain a stoichiometric film. The variation in the composition of the film has been tabulated in Table 3.11.

Fig. 3.24 and Fig. 3.25 show the representative EDAX spectra for PbS films annealed at 300˚C and 350˚C temperature, respectively. It was observed that as the annealing temperature increases, the sulphur content decreases hence stoichiometry was achieved at

350°C after 4hrs of annealing. This is due to the fact that when films were annealed at high temperature, evaporation of excess sulphur leads to the stoichiometry of the films. But as the annealing duration goes beyond 4hrs, the film becomes rich in lead content and films tended to peel off from the substrates.

Table 3.11 Composition of PbS thin films deposited at 225°C and annealed at different temperatures for different duration.

| Annealing temperature | Duration (hrs) | Lead (At %) | Sulphur (At %) |
|---|---|---|---|
| 300°C | 1 | 45.86 | 54.24 |
| | 2 | 46.18 | 53.82 |
| | 3 | 47.54 | 52.46 |
| | 4 | 48.32 | 51.68 |
| 350°C | 1 | 46.87 | 53.13 |
| | 2 | 47.94 | 52.06 |
| | 3 | 48.50 | 51.50 |
| | 4 | 49.56 | 50.44 |

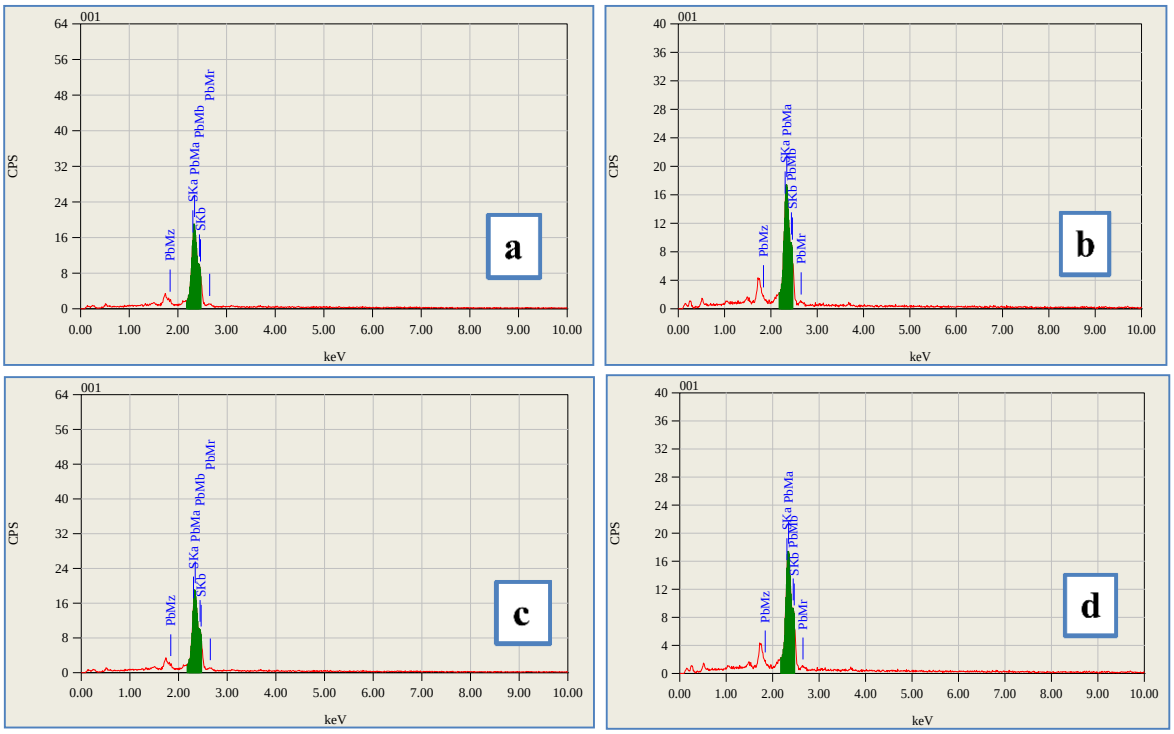

Fig. 3.24 EDAX spectra of PbS films annealed at 300˚C temperature for (a) 1hr, (b) 2hr, (c) 3hr and (d) 4hr

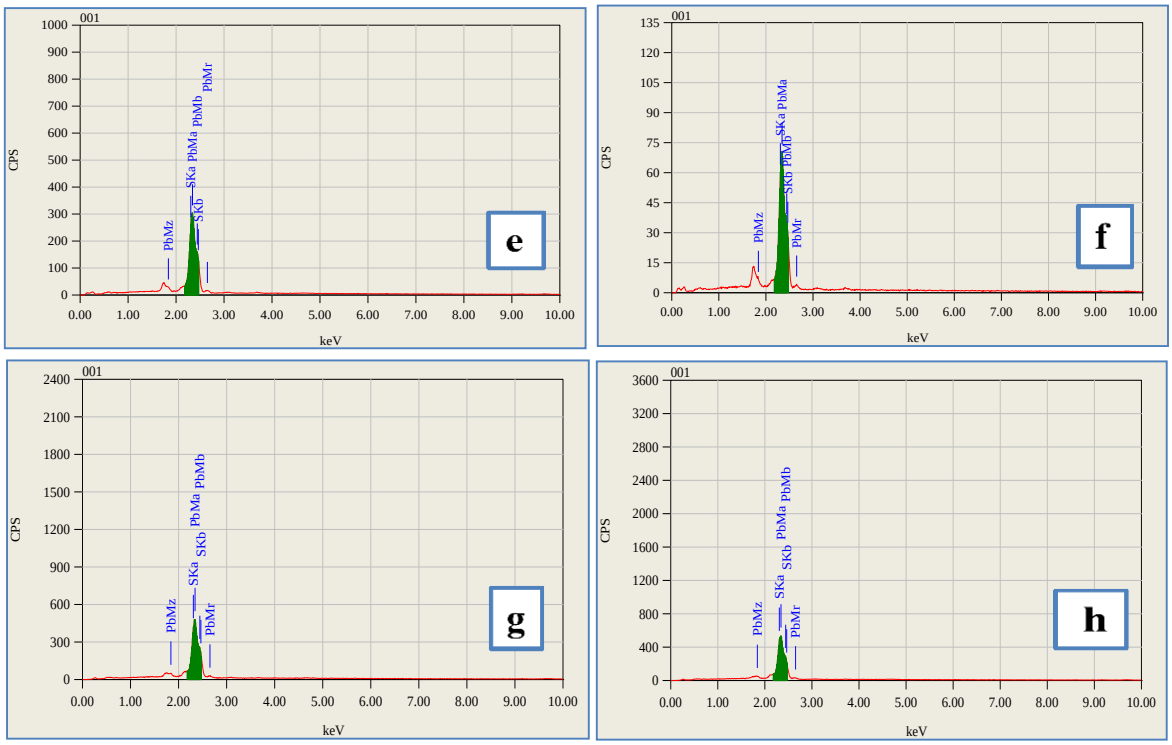


Fig. 3.25 EDAX spectra of PbS films annealed at 350˚C temperature for (e) 1hr, (f) 2hr, (g) 3hr and (h) 4hr.

Surface morphology of deposited films plays an important role in device fabrication. SEM images of the annealed PbS thin films at different temperature and duration are as shown in Fig. 3.26 and Fig. 3.27. The crystallinity of the film is directly proportional to the annealing temperature as XRD peaks were observed at higher annealing temperature. Fig. 3.26 (a) shows poor crystallinity of the films due to the dominance of the amorphous nature of sulphur. As shown in Fig. 3.26 (b) and (c), the duration of the annealing increases the seed-like structure due to increase in crystallinity. Fig. 3.26 (d) shows few rod-like structures at the 300˚C annealing temperature for 4hrs. This may be due to a reduction in surface energy of crystalline grains. At an annealing temperature of 350˚C for 1hr, films are agglomerated as shown in Fig. 3.27 (e) when annealing time increases agglomeration gets reduced and a rod-like PbS exhibit a diameter of 400 – 600 nm in the middle part these were

observed due to recrystallization process. This is due to the fact that at higher annealing temperature seeds were acted as nucleation center to grow nanorods.

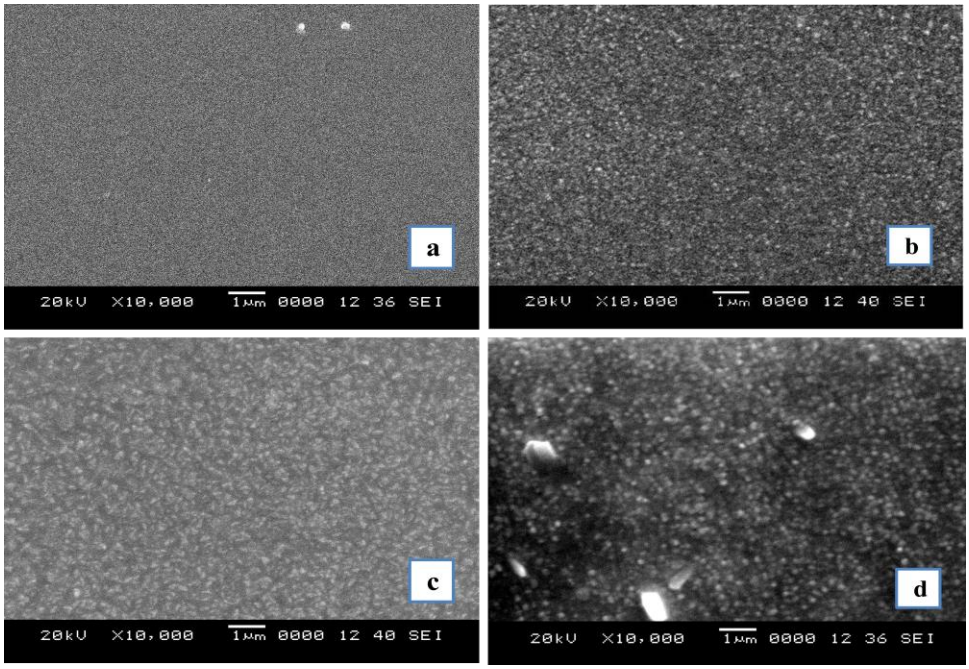


Fig. 3.26 SEM images of PbS films annealed at 300˚C temperature for (a) 1hr, (b) 2hr, (c) 3hr and (d) 4hr.

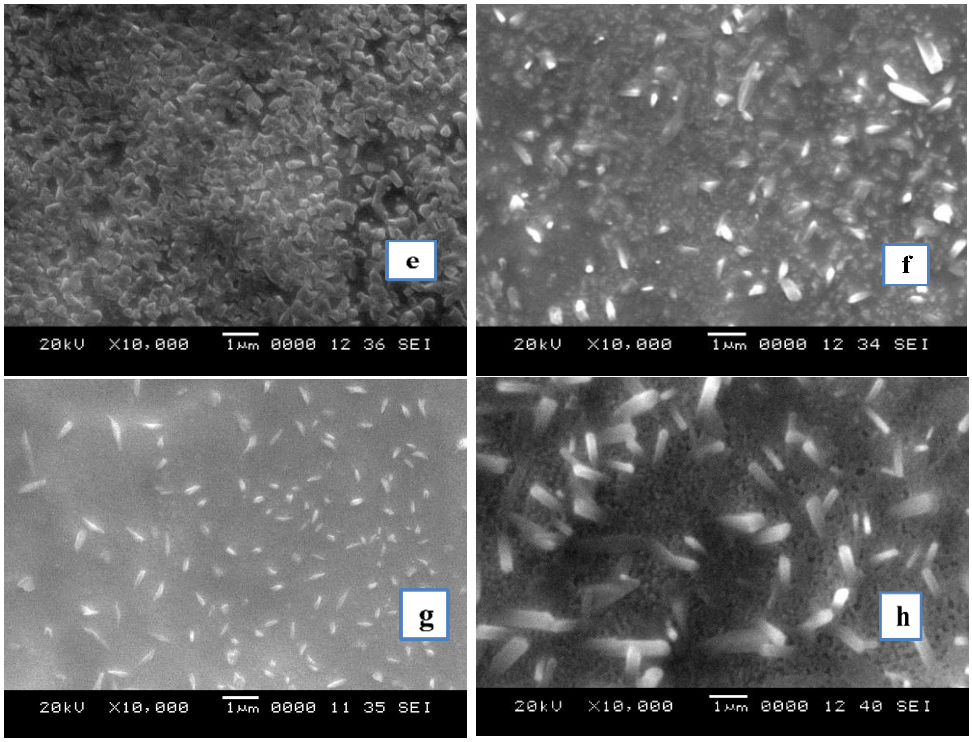

Fig. 3.27 SEM images of PbS films annealed at 350˚C temperature for (e) 1hr, (f) 2hr, (g) 3hr and (h) 4hr.

3.6.2 Structural studies

XRD analysis was carried out to identify crystalline structure and phase of the films. The effect of annealing on the crystallinity of the films is shown in Fig. 3.28 (A) and (B). Diffraction peaks were indexed with a face centered cubic rock salt type structure which was confirmed using standard data JCPDS No.05-0592. The narrow peaks showed that the material has good crystalline nature with a preferred orientation along (2 0 0) plane. This shows that films with a-axis orientation are perpendicular to the substrate surface which may be attributed to self-texturing as reported by other researchers group (Tong et al. 2011, Jiang et al. 2002). After annealing films, more Pb ions occupy the lattice position which will improve the crystallinity and also shows that the diffracted intensity mainly depends on the annealing time. The single axis orientation in thin films can be understood by the "survival of the fastest" model proposed by Drift (Drift 1967). According to this model, nucleation with various orientations can be formed at the initial stage of the deposition and each nucleus competes to grow but only nuclei having the fastest growth rate can survive i.e., an axis orientation will result (Fujimura et al. 1993). The absence of any other prominent diffraction peaks indicates that no other crystalline phase such as oxides or carbonates of Pb exist with detectable concentration within layers while the presence of broad diffraction peaks indicates that deposited films on the substrates are of nano-size and assumed to be strain free (Prasad Rao et al. 2012, Bayraktaroglu et al. 2008). It is also observed that the peaks became sharper and of higher intensity with increasing annealing time and temperature. There is a notable increase in the intensity of (200) peak for the air-annealed samples. The comparatively high intensity of XRD peaks implies that the crystalline quality is better for PbS thin films annealed at 350˚C for 4hrs. Quantitative information of the direction of preferred growth was obtained from Harris texture coefficient relation (Sagade et al. 2009, Kashani 1996). $TC_{(hkl)}$ values represent the abundance of crystallites oriented in a given *(hkl)* direction. A sample with randomly oriented crystallite yields $TC_{(hkl)}$=1, while the larger this value the larger abundance of crystallites oriented at the (hkl) direction. The calculated texture coefficients TC are presented in Table 3.12. It can be seen that highest TC is obtained for the (200) plane

of the PbS thin film annealed at 350˚C for 4hrs. The higher values of TC reveal that the film crystallinity improved after thermal annealing.

Table 3.12. Lattice parameters and crystallite size of the PbS films.

| | Duration (hr) | 2θ (deg) | (h k l) | $d_{cal}$ Å | $d_{std}$ Å | Lattice constant (a) Å | D (nm) | TC (2 0 0) |
|---|---|---|---|---|---|---|---|---|
| As deposited | - | 29.54 | | 3.024 | | 6.048 | 6.91 | 0.94 |
| | 1 | 29.63 | | 3.015 | | 6.030 | 9.56 | 1.39 |
| Annealed 350°C | 2 | 29.74 | (2 0 0) | 3.004 | 2.969 | 6.008 | 10.43 | 2.01 |
| | 3 | 29.82 | | 2.996 | | 5.992 | 11.90 | 2.50 |
| | 4 | 29.97 | | 2.982 | | 5.964 | 26.41 | 2.73 |

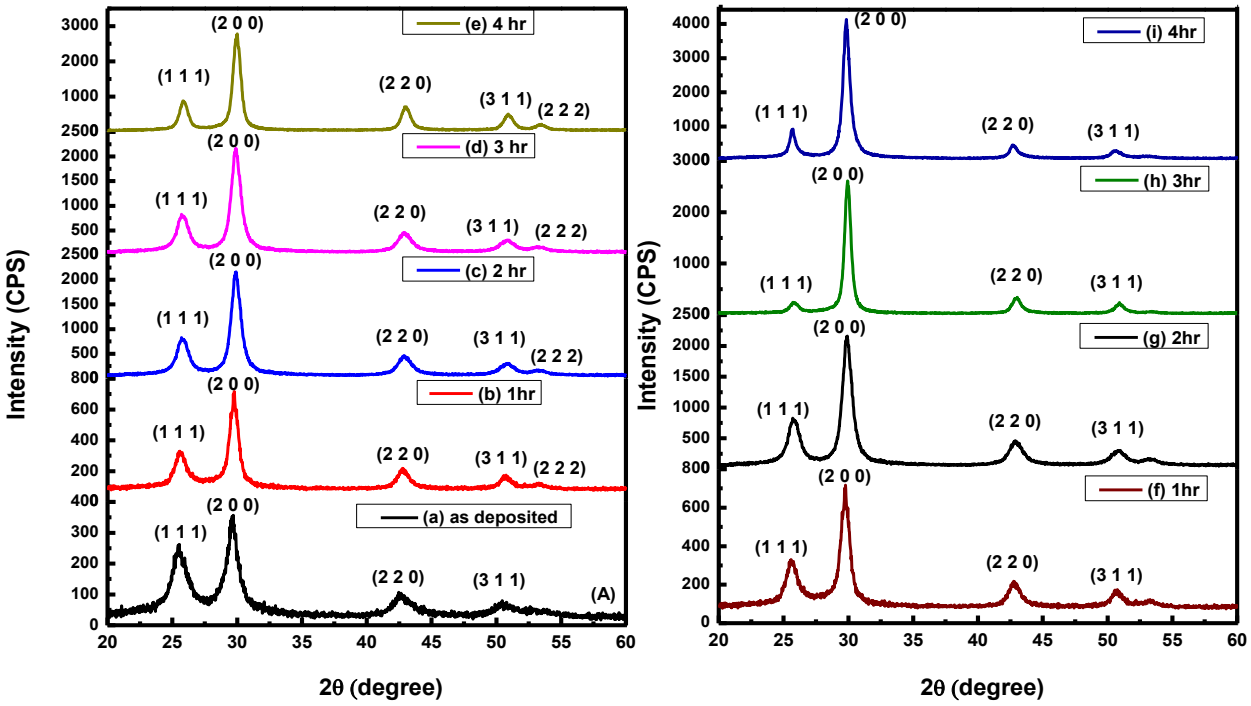


Fig. 3.28 XRD spectra of PbS films annealed at (A) 300˚C and (B) 350˚C temperature.

The crystallite size indicates the nanocrystalline nature of the film. This is due to quantum confinement which will be discussed in optical studies section. For PbS films deposited on glass, nucleation rate is considered to be larger than the growth rate due to the great number of nucleation centers on the surface of the substrate. This explains why PbS films deposited on glass are compact with a small size of crystallites (Obaid et al. 2013) which is in agreement with surface morphology results.

3.6.3 Optical studies

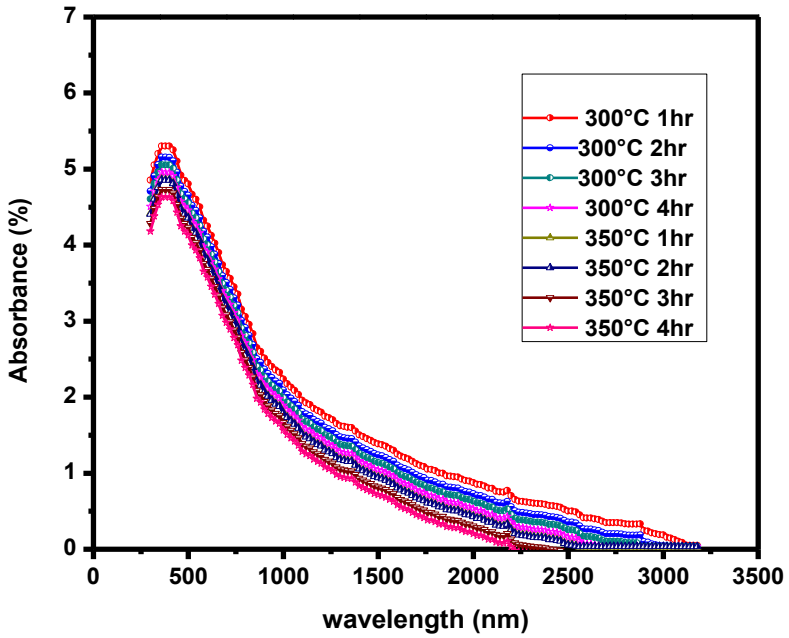


Fig. 3.29 Absorption spectra of annealed PbS films.

Absorbance measurements at near normal incidence were carried out over a spectral range of 500 nm-3500 nm on PbS thin films. Fig. 3.29 shows the absorption spectra of PbS thin films annealed at temperature 300˚C and 350˚C for different duration. Though there is a difference in absorbance, the shapes of the curves were observed to be similar. The absorbance of the annealed films was higher compared with that of as-deposited films which confirm the presence of more states available for the photon absorption as reported by Abbas et al. (2011) and Ezema et al. (2003) for chemical bath deposited PbS thin films. As-deposited films exhibit interference effect with sub-banding which is an evidence for smooth surface morphology; whereas annealed films exhibit non-interference effect with no resolved

sub-banding. It can be an evidence of the effect of quantum confinement (Martucci et al. 1999). The absorption coefficient is found to be in the order of $10^6$ $cm^{-1}$ for PbS thin films. Literature revealed the several investigations of the optical absorption edge in PbS thin films. However, several other studies reported measurements of absorption coefficient ($\alpha$) from$10^2$ to$10^4$ $cm^{-1}$ (Douri et al. 2011). Here we have achieved absorption coefficient of $10^6$ $cm^{-1}$ which is suitable for solar cell applications.

Fig. 3.30 and Fig. 3.31 show the Tauc's plots for the PbS films annealed at temperature 300˚C and 350˚C respectively for different duration. The optical energy band gap of the films was calculated by using the Tauc relation (equation 2.13). The calculated direct energy band gap values are tabulated in Table 3.13. The direct energy band gap of PbS films was found to be 1.22 eV and for the films annealed at 350°C for 4hrs was 0.98 eV which may be related to the structural changes for enhanced quantum confinement caused by localization of electrons and holes in a confined space. This results in quantization of the energy levels of the electrons and holes. The idea behind confinement is all about keeping electrons and holes trapped in a small area (Preetha et al. 2012). Earlier it was reported that decrease in energy band gap in polycrystalline semiconductors is due to stoichiometric deviations, quantum size effect, change in preferred orientation of the films, dislocation density, and disorder at the grain boundaries (Revathi et al. 2010). In the present study, PbS thin films exhibit bandgap larger than that of bulk PbS due to quantum confinement effects. Khan et al. (2010), Yuan et al. (2011) have attributed such changes to the formation of nanostructured particles in which a shift in the band gap for other thin films was observed.

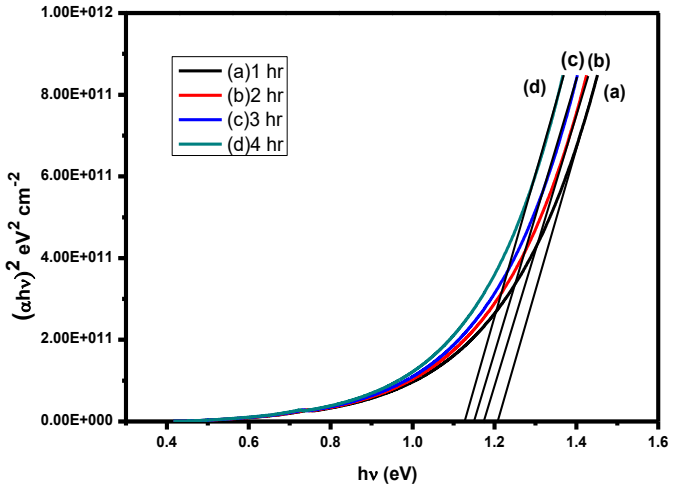

Fig. 3.30 Tauc's plot of PbS films annealed at 300˚C temperature for different duration.

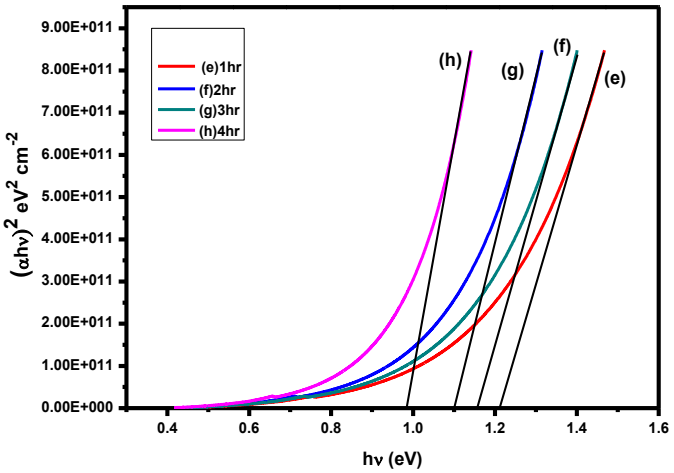


Fig. 3.31 Tauc's plot of PbS films annealed at 350˚C temperature for different duration.

Table 3.13 Energy band gap of the PbS films annealed at different temperatures and duration.

| **Annealing Temperature (˚C)** | **Duration (hr)** | **Band gap (eV)** |
|---|---|---|
| 300 | 1 | 1.22 |
| | 2 | 1.18 |
| | 3 | 1.16 |
| | 4 | 1.13 |
| 350 | 1 | 1.21 |
| | 2 | 1.15 |
| | 3 | 1.09 |
| | 4 | 0.98 |

3.6.4 Electrical studies

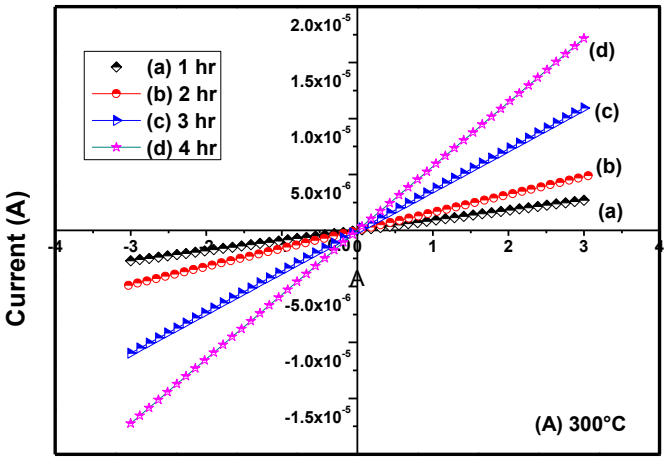

Fig. 3.32 I-V plot of PbS films annealed at 300˚C temperature for different duration.

The electrical properties of PbS films were investigated through resistivity measurements and current–voltage measurements with silver as an ohmic contact. The I-V plots of the PbS films annealed at 300˚C and 350˚C are as shown in Fig. 3.32 and Fig. 3.33 respectively. The linear nature of I-V characteristics confirms that silver makes ohmic contact with PbS indicating that the work function of silver is higher than the PbS thin film (Ibrahim et al. 2014). The electrical conductivity of the heat treated PbS thin films at room temperature in the order of $10^{-2}$ $\Omega^{-1}$ $cm^{-1}$. It increases from 0.12 $X10^{-2}$ $\Omega^{-1}$ $cm^{-1}$ to 22.2 $X10^{-2}$ $\Omega^{-1}$ $cm^{-1}$ as the annealing temperature increases from 300˚C to 350˚C for the samples annealed for 4hrs.

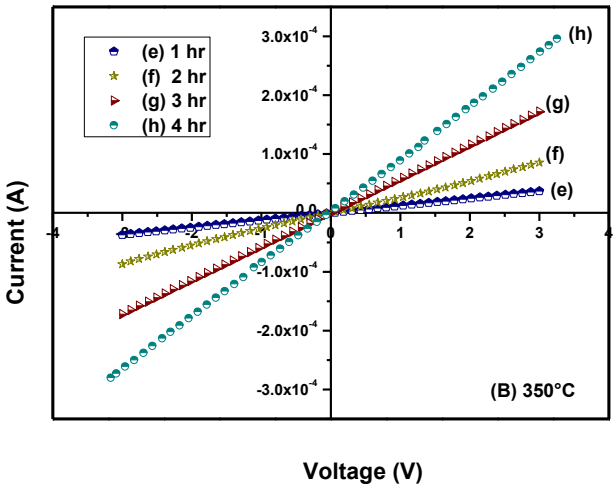


Fig. 3.33 I-V plot of PbS films annealed at 350˚C temperature for different duration.

The hot probe experiment provides a simple and efficient way to distinguish between n-type and p-type semiconductors (Gode et al. 2014). The hot probe is connected to the positive terminal of the meter while the cold probe is connected to the negative terminal. When the cold and hot probes are in contact with the n-type semiconductor, a positive voltage is obtained in the voltmeter, whereas, for p-type semiconductor films a negative voltage is obtained. PbS films annealed at 300˚C showed p-type conductivity even for different annealing duration. At an annealing temperature of 350˚C, films annealed for 1hr showed p-type and as the annealing duration increased, conductivity of the films changed to n-type since there is an increase in the lead content. The electrical resistance was found to decrease with increase in temperature showing semiconducting nature of the films. Fig.3.34

showed the variation of ln R with (1/T) from which the activation energy was calculated were tabulated in Table 3.14.

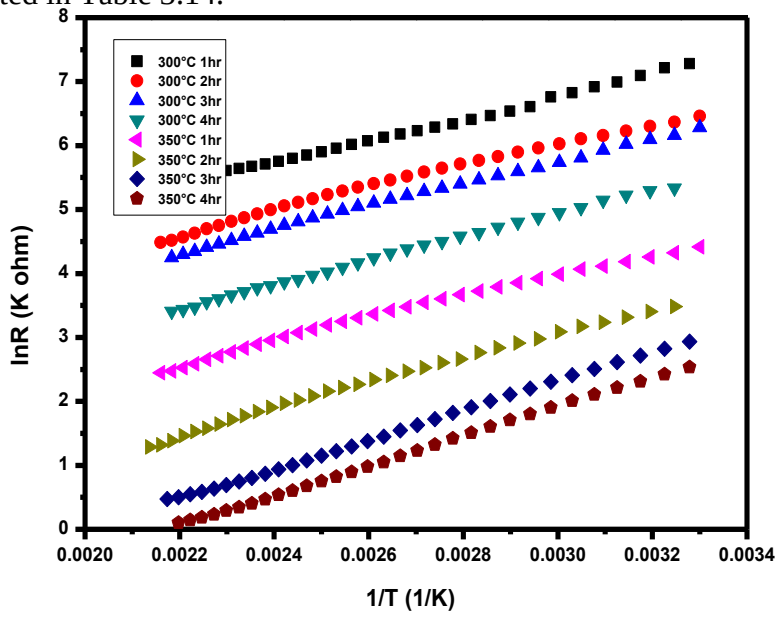


Fig. 3.34 Variation of ln R with 1/T for annealed PbS films.

Table 3.14 Electrical parameters of PbS thin films annealed at different temperature and duration.

| **Temperature (°C)** | **Duration (hrs)** | **Activation energy (eV)** | **Type** |
|---|---|---|---|
| 300 | 1 | 0.146 | P |
| | 2 | 0.149 | P |
| | 3 | 0.150 | P |
| | 4 | 0.15 | P |
| 350 | 1 | 0.16 | P |
| | 2 | 0.17 | n |
| | 3 | 0.20 | n |
| | 4 | 0.22 | n |

# CHAPTER 4

# PREPARATION AND CHARACTERIZATION OF ZINC SULPHIDE THIN FILMS

This chapter deals with the preparation of stoichiometry zinc sulphide thin films using spray pyrolysis technique and corresponding results obtained by characterization of these films. As mentioned in the chapter 3, the characteristics of thin films depend on factors like deposition technique employed, deposition parameters such as substrate temperature, the rate of deposition, ambiance and annealing treatment. In particular, properties of thin films synthesized using spray pyrolysis technique are dependent on the factors like precursors, concentration of precursors, flow rate of solution, spray rate, spray time, carrier gas flow rate and the distance between nozzle to substrate.

## 4.1 PREPARATION OF ZINC SULPHIDE THIN FILMS

Zinc sulphide thin films were deposited on glass substrates by varying thickness, substrate temperature and zinc precursor concentration. Aqueous solutions of zinc acetate Zn $(CH_3COO)_2$ and thiourea CS $(NH_2)_2$ were utilized as precursor solution. The procedure used for the synthesis of lead sulphide thin films was followed to synthesize zinc sulphide thin films and growth parameters were similarly optimized. After deposition, the films were allowed to cool at room temperature and cleaned with an air drier. The adhesion of the films on the substrate was found to be good. Zinc sulphide thin film is formed according the following chemical reaction.

$$Zn(CH_3COO)_2+SC(NH_2)_2+2H_2O \longrightarrow ZnS\downarrow+2CH_3COOH\uparrow+2NH_3\uparrow+CO_2\uparrow \quad (4.1)$$

## 4.2 OPTIMIZATION OF GROWTH PARAMETERS

### 4.2.1 Volume of the precursor

Since volume of the precursor depends on deposition time and thickness of the films, it is varied from 5 ml to 35 ml keeping substrate temperature of 450˚C and other process parameters constant (as mentioned in Table 4.3). The deposited films were uniform, pin hole

free and adherent to the glass substrate. Fig. 4.1 shows the variation of film thickness as a function of the volume of the spray solution.

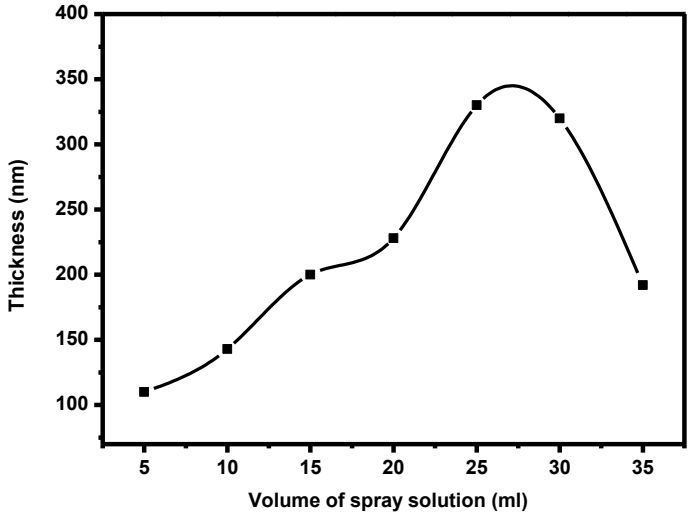


Fig. 4.1 Variation of ZnS film thickness with volume of spray solution.

The film thickness of approximately 110±10 nm was obtained for a 5 ml spray solution and it increases to 330±20 nm as the spray solution increases to 25 ml. However, a slight decrease in the film thickness was observed with further increase in the volume of the spray solution. This may be due to incomplete thermal decomposition of the spray solution which resulted in the formation of powder on the surface of the film (Yogesh et al. 2016). Hence, the optimum volume of the spray solution was found to be 25 ml.

4.2.2 Spray rate

ZnS films were deposited by varying spray rate from 0.5ml/min to 2ml/min keeping substrate temperature of 450˚C and other process parameters constant (as mentioned in Table 4.3). The XRD patterns of ZnS films deposited at 450˚C for various spray rates have been shown in Fig. 4.2. It is observed that films deposited with various spray rate exhibit polycrystalline cubic structure. Crystallite size is calculated using equation 2.6 and results are shown in Table 4.1. The crystallite size of thin films increases from 3.9 nm to 10.68 nm as the spray rate of the film increases from 0.5 ml/min to 1.5 ml/min, further increase in the spray rate results in decreasing the grain size. This might be due to incomplete thermal decomposition of the spray solution which causes powder formation on the surface of the

films. The lattice parameter ‘a’ was calculated using equation 2.2 is in agreement with the standard value [JCPDS file number # 01-080-0020].

Table 4.1 XRD data of ZnS thin films deposited with various spray rates.

| Spray Rate (ml/min) | (h k l) Value | 2θ (degree) | D (nm) | a (Å) |
|---|---|---|---|---|
| 0.5 | (1 1 1) | 28.56 | 3.59 | 5.406 |
| 1 | | | 5.78 | |
| 1.5 | | | 10.68 | |
| 2 | | | 10.05 | |

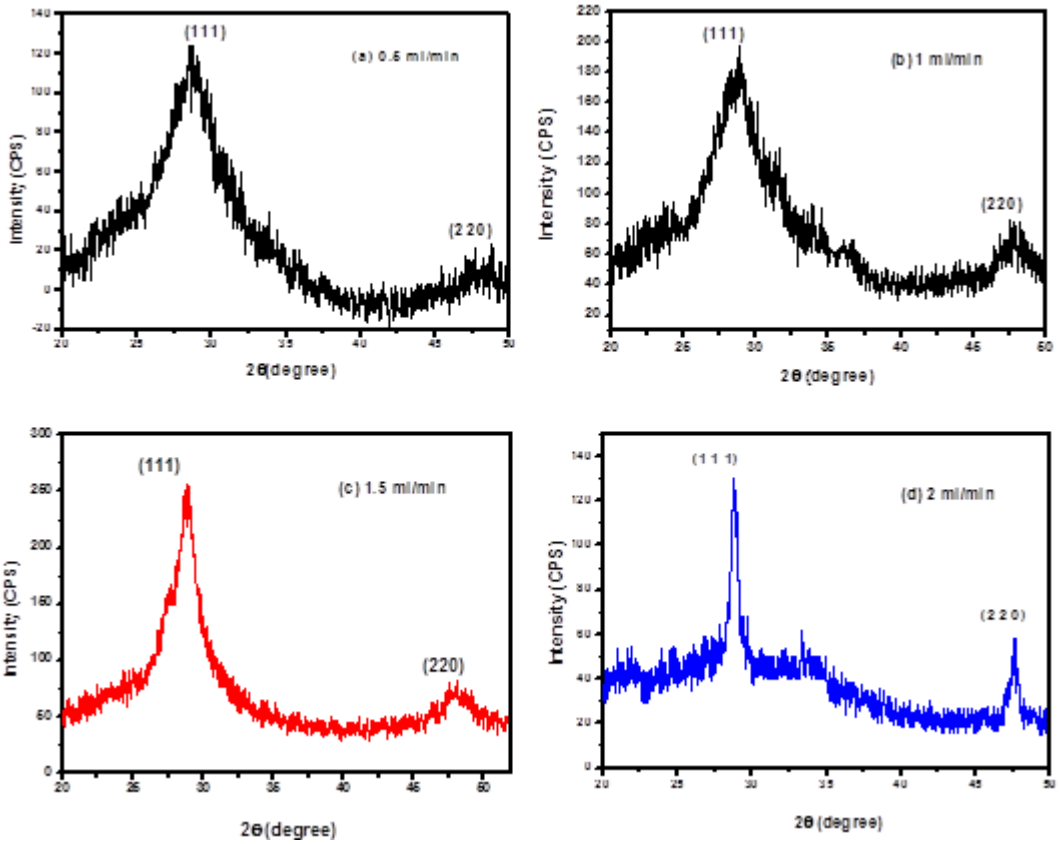


Fig. 4.2 XRD patterns of ZnS films deposited with various spray rates.

Transmittance spectra of the films prepared with various spray rates has been shown in Fig. 4.3. The optical transmittance of the films increased from 73% to 84% as the spray

rate increased from 0.5ml/min to 1.5ml/min. Further, increase in the spray rate resulted in decrease in the transmittance of the films which evidences with the results obtained from structural studies. The films deposited with the spray rate of 1.5ml/min show better optical transmittance in the visible region, which reveal that films has less defects and better crystallinity. Moreover, there are interference effects in transmittance spectra indicating the formation of uniform zinc sulphide films.

For a direct allowed transition, the band gap of thin films was determined using the equation 3.13. Tauc's plots of ZnS thin films deposited with various spray rate is shown in Fig. 4.4. The energy band gap of ZnS thin films is found to be in the range of 3.54 ±0.03eV for the different spray rate used.

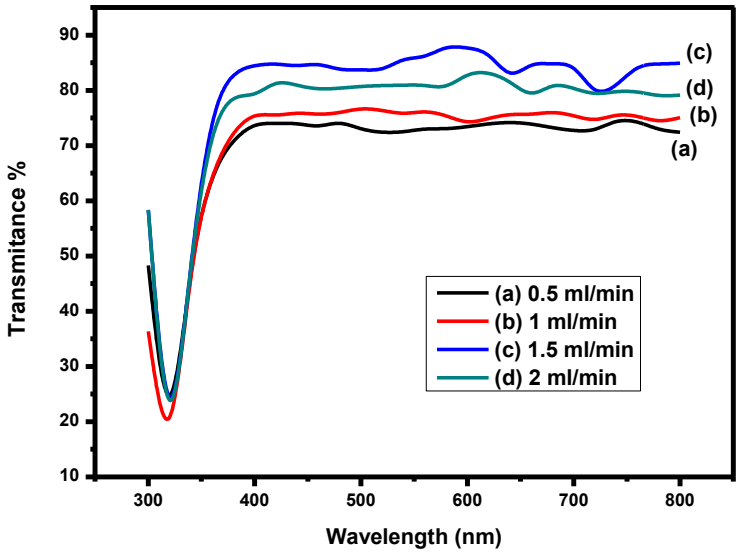


Fig. 4.3 Transmittance spectra of ZnS films with various spray rate.

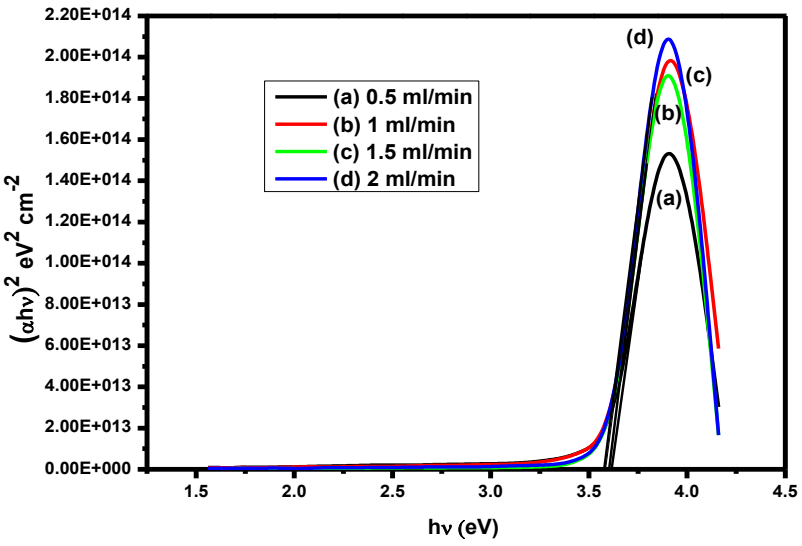

Fig. 4.4 Tauc's plots of ZnS films with various spray rate.

4.2.3 Thickness

ZnS thin films with various thickness were prepared by keeping the substrate temperature as 450˚C and other process parameters constant (as mentioned in Table 4.3). The film thickness was calculated using gravimetric method and measurements were verified using cross-sectional SEM images as shown in Fig. 4.5.

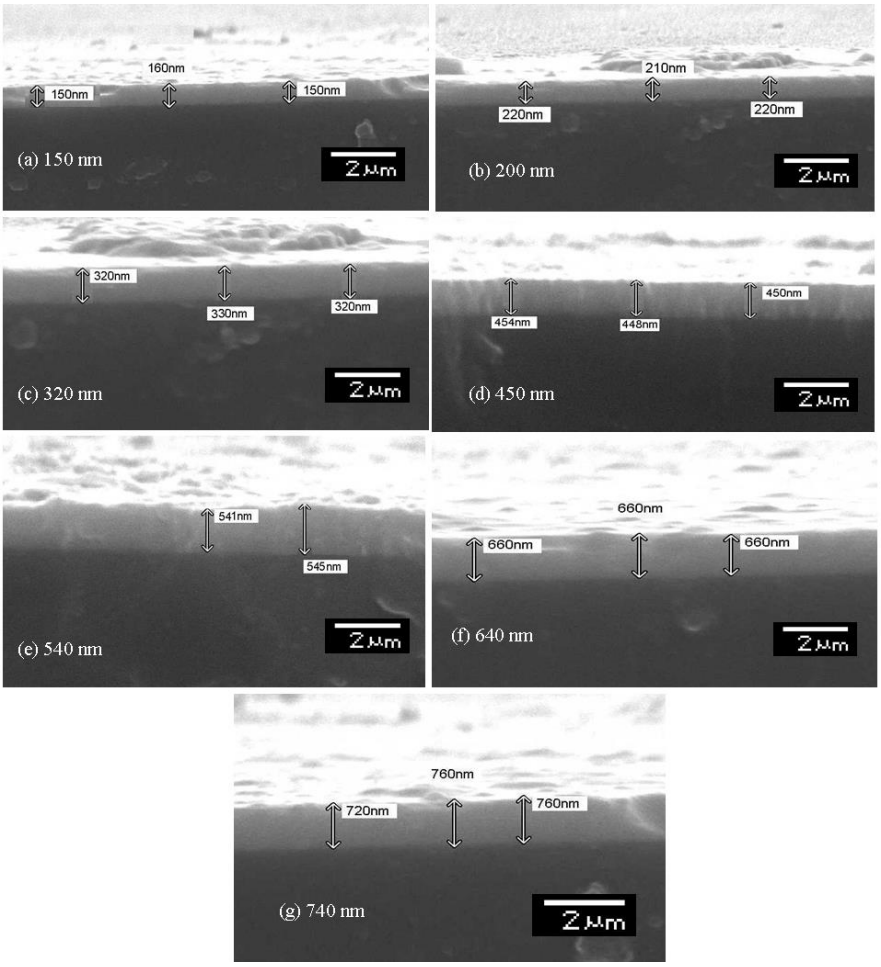


Fig. 4.5 Cross-sectional SEM images of ZnS films with various thickness.

The XRD patterns of ZnS films with various thickness are shown in Fig. 4.6. From the figure it has been observed that all the films exhibit cubic structure with polycrystalline

nature oriented along (111) plane. The comparison of observed and standard lattice parameters confirms the formation of zinc sulphide thin films. The position of the diffraction peaks is independent of the film thickness; however intensity of the oriented peak increased with film thickness. The modifications in the peak intensity may be due to the re-alignment of crystallites with the increase in thickness. The large thickness may provide sufficient space for the thermal motion of particles; which may, in turn, helps for better alignment of crystallites. This causes an improvement in crystallinity with an increase in film thickness (Shewale et al. 2013). The average crystallite size (D) of ZnS thin films has been calculated using Scherer's formula (equation 2.6). The variation of average crystallite size with film thickness is tabulated in Table 4. 2. It is seen that crystallite size increased from 3 nm to 13 nm as the thickness of the films increased from 450 nm up to 650 nm. However, further increase in the film thickness results in extra peaks which are related to ZnO due to the oxidation of sulphur. The mechanisms and kinetics of oxidation depend on surface area, the presence of any impurities, crystallite and aggregate sizes of the materials (Basak et al. 1973). Hence, thickness of the films was found to be optimum at 650 nm.

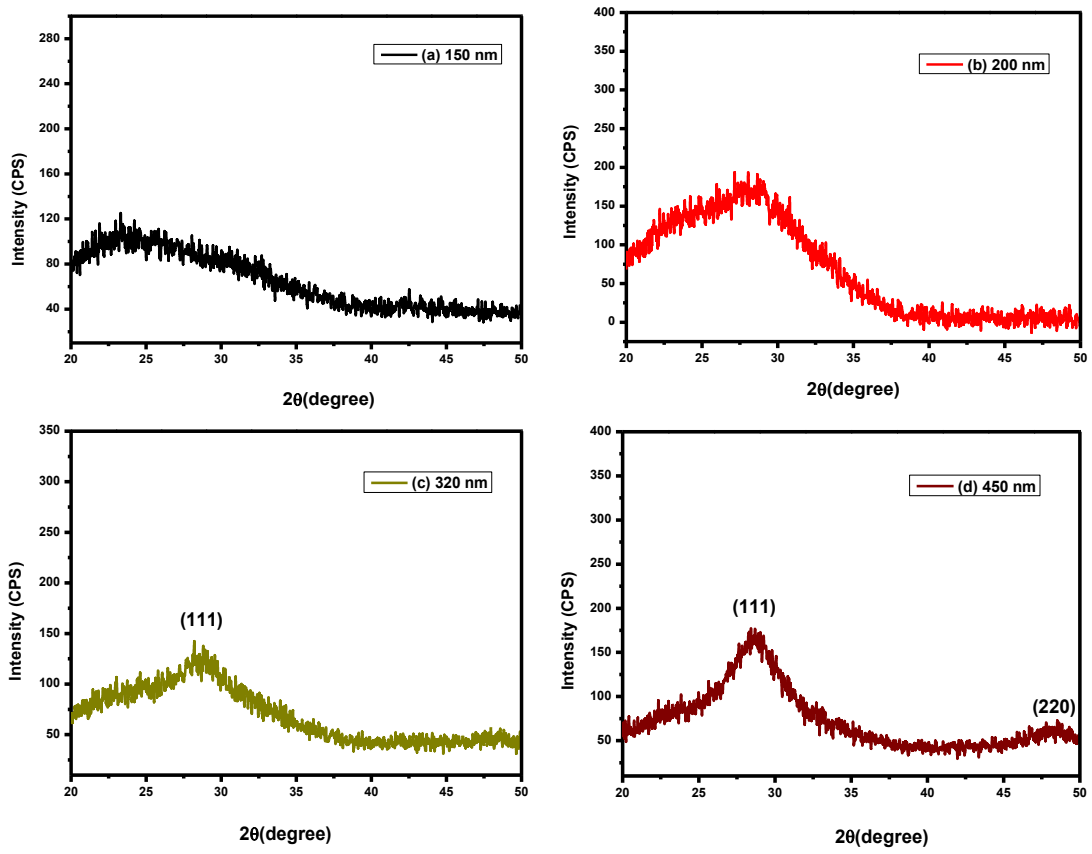

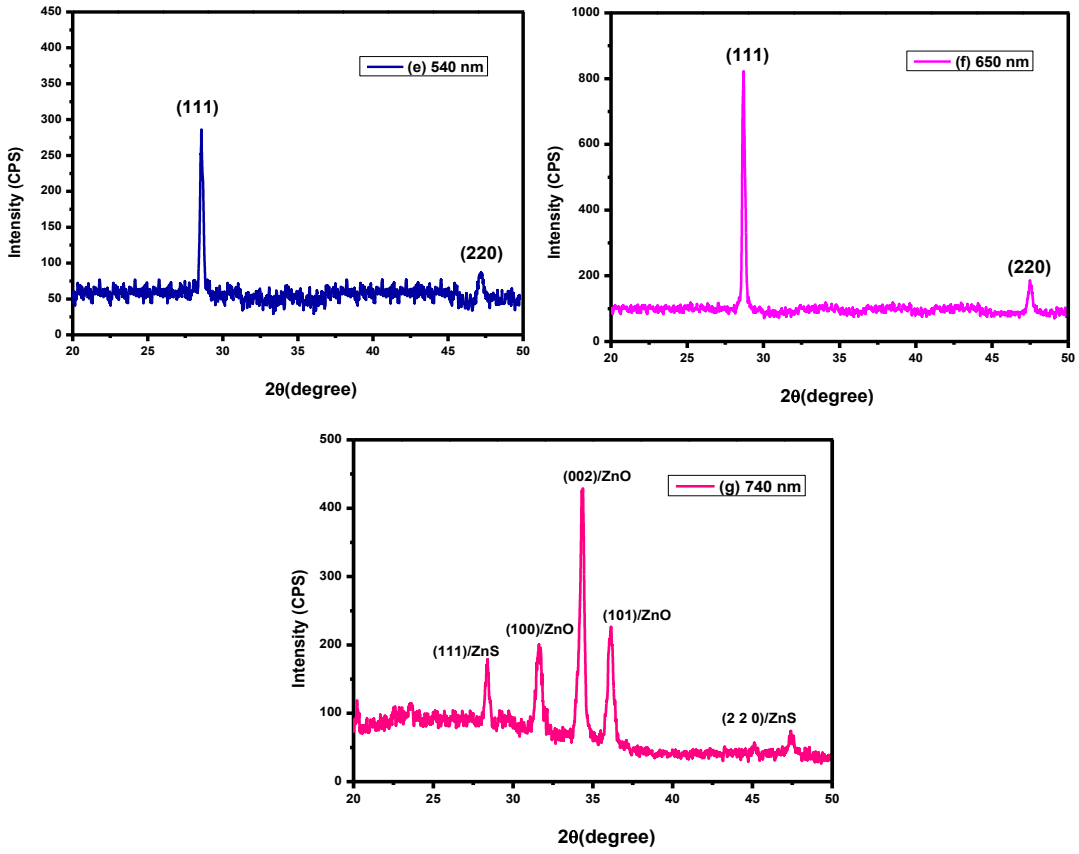


Fig 4.6 (a-g) XRD patterns of ZnS thin films with various thickness.

Table 4.2 XRD data of ZnS thin films with various thickness.

| **Thickness (nm)** | **(h k l) value** | **2θ (degree)** | **D (nm)** | **a (Å)** |
|---|---|---|---|---|
| 150 | (1 1 1) | 28.61 | - | 5.404 |
| 200 | | | - | |
| 320 | | | - | |
| 450 | | | 3.20 | |
| 540 | | | 11.35 | |
| 650 | | | 13.62 | |

Fig. 4.7 shows EDAX spectra of the zinc sulphide film with the optimized thickness of 650 nm. It can be observed that the atomic % of zinc and sulphur were 59.12 and 40.88 respectively with an error of 0.3%. The purity of the ZnS thin films could be evidenced by

the absence of peaks other than that of ZnS. Table 4.3 shows the optimized deposition parameters for the films.

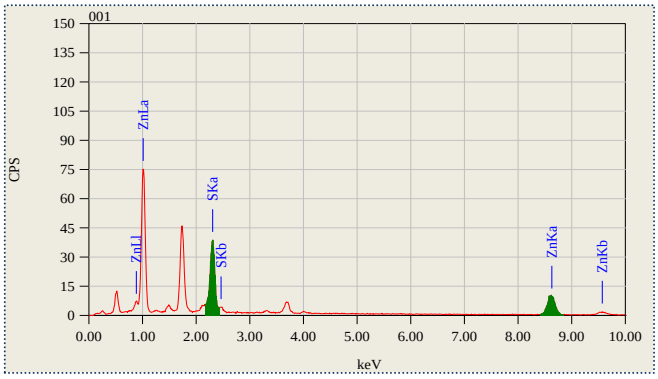


Fig 4.7 EDAX spectra of the ZnS film with the thickness 650 nm.

Table 4.3 Preparative parameters for ZnS thin films.

| Parameter | Values |
|---|---|
| Precursor | zinc acetate and thiourea |
| Concentration | 1:1 to 0.25:1 |
| Volume | 25 ml |
| Substrate temperature | 300˚C to 450˚C |
| Spray rate | 1.5 ml/min |
| Nozzle to substrate distance | 16 cm |
| Carrier gas | Air |
| Pressure of carrier gas | 1.8 bar |

## 4.3 EFFECT OF ZINC PRECURSOR CONCENTRATION

The precursor concentration of zinc was optimized to achieve 50:50 (Zn:S) stoichiometric thin films by keeping substrate temperature of 450˚C. The atomic % of zinc and sulphur in the ZnS films were varied from 59.92(Zn):40.08(S) to 47.10(Pb):52.90(S) by varying only the zinc precursor concentration from 1 to 0.25M.

### 4.3.1 Compositional and morphological studies

Zinc sulphide thin films were prepared by varying the substrate temperature from 300°C to 450°C with an interval of 50°C. ZnS films obtained at a substrate temperature of

450°C are found to be highly transparent and films were found to be rich in zinc content. Hence, a substrate temperature of 450°C was selected for further studies to get stoichiometry with varying zinc precursor concentration. The variation in the composition of zinc and sulphur was evaluated by EDAX analysis is given in Table 4.4.

Table 4.4 Composition of ZnS thin films deposited at different substrate temperatures.

| **Substrate temperature(°C)** | **Zinc (At %)** | **Sulphur (At %)** |
|---|---|---|
| 300 | 53.46 | 46.54 |
| 350 | 55.76 | 44.24 |
| 400 | 57.54 | 42.46 |
| 450 | 59.92 | 40.08 |

Table 4.5 Atomic % of ZnS thin films with various Zn precursor concentrations.

| **Zn:S precursor concentration ratio** | **Zinc (At %)** | **Sulphur (At %)** |
|---|---|---|
| 1:1 | 59.92 | 40.08 |
| 0.5:1 | 56.74 | 43.26 |
| 0.33 :1 | 50.48 | 49.52 |
| 0.25 :1 | 47.10 | 52.90 |

The atomic % of ZnS thin films with various Zn precursor concentrations is shown in Table 4.5. The zinc sulphide thin films with Zn:S precursor concentration ratio 0.33:1 was found to be stoichiometric. The growth of thin films using solution processing techniques involves the coating of wet precursors which should be performed in advance and followed by thermal annealing at high temperature for their decomposition and reaction. Therefore, for solution based techniques, annealing process is unavoidable. Owing to the advantages offered by annealing, stoichiometric films were annealed for 30 min and 60 min at the synthesized temperature itself to maintain stoichiometry. Films were found to maintain stoichiometry after annealing for 30 min. Table 4.6 shows the chemical composition of the ZnS films annealed at 450°C for 30 min and 60 min.

Table 4.6 Variation in chemical composition for annealed ZnS thin films.

| Ratio | Substrate temperature (˚C) | Annealed temperature (˚C) | Duration (min) | Zinc (At %) | Sulphur (At %) |
|---|---|---|---|---|---|
| 0.33:1 | 350 | 350 | 30 | 50.48 | 49.52 |
| | | | 60 | 50.80 | 49.20 |

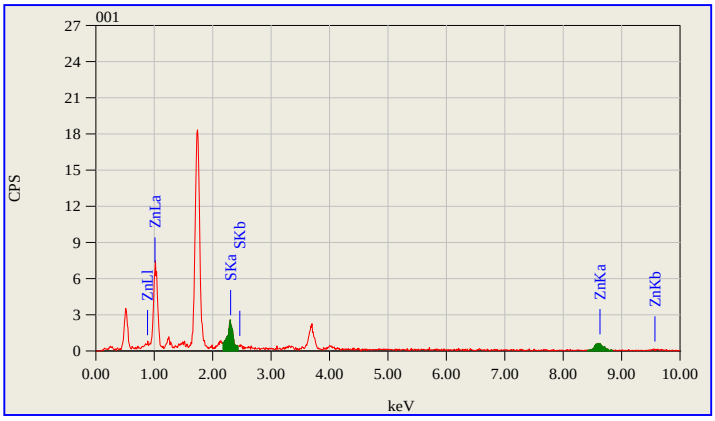


Fig 4.8 EDAX spectra for the ZnS films with precursor concentration ratio of 0.33:1.

Fig. 4.8 shows EDAX spectra of the stoichiometric zinc sulphide film with precursor concentration ratio of 0.33:1. It has been observed that the atomic % of zinc and sulphur were 50.48 and 49.52 respectively with an error of 0.5%. The purity of the ZnS thin films could be evidenced by the absence of peaks other than that correspond to ZnS.

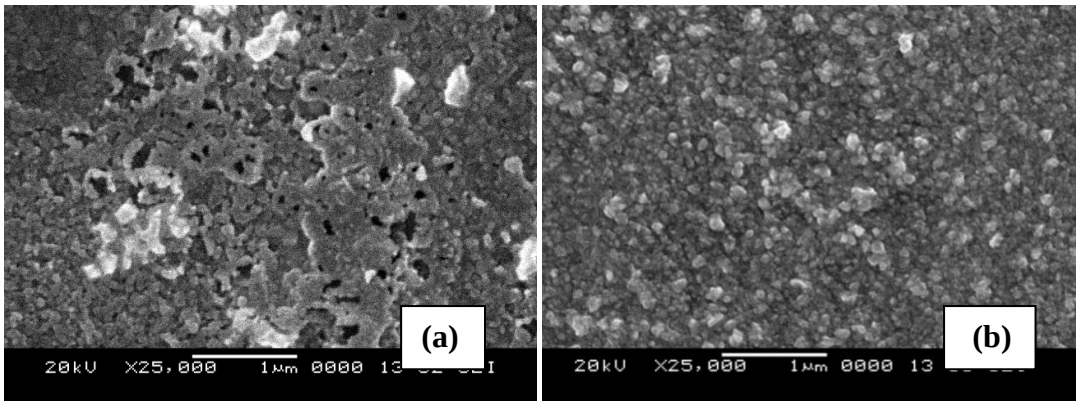


Fig. 4.9 SEM images of ZnS thin films with precursor concentration ratio of (a) 1:1 and (b) 0.33:1.

Fig. 4.9 shows the influence of cationic precursor concentration on the morphology of the films. It can be observed that films deposited at 1:1 molar ratio (Fig. 4.9a) are having pin-hole, porous and non homogeneous. As the precursor concentration ratio is reduced to 0.33:1 morphology of the films changed. The stoichiometric zinc sulphide thin film (Fig. 4.9b) shows homogeneous, granular and smooth surface morphology over the entire substrate. No significant changes observed due to annealing on the morphology of the films.

4.3.2 Structural studies

XRD pattern of ZnS thin films prepared with precursor concentration ratios 1:1 and 0.33:1 are shown in Fig. 4.10. It has been observed that the films exhibit polycrystalline cubic structure with preferential orientation along (1 1 1) plane which was confirmed using standard data JCPDS # 01-080-0020 (Akhtar et al. 2015).

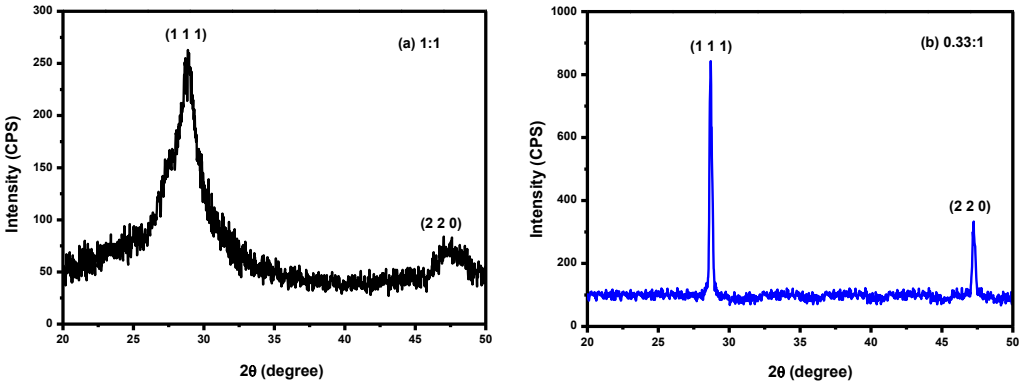


Fig. 4.10 XRD patterns of ZnS thin films with precursor concentration ratio (a) 1:1 and (b) 0.33:1.

The crystallite size (D) of deposited thin films was calculated using Scherer's formula (Ravishankar et al. 2015). It reveals that the decrease in zinc precursor concentration results in increased crystallite size as tabulated in Table 4.7. This change in crystallite size could be attributed to the variation in number of $Zn^{2+}$ and $S^{2-}$ ions in the reactant solution at lower molar concentration (Fenollosa et al. 2008). The results suggest that the micro structural characteristics of the sprayed zinc sulphide films is dependent on the zinc precursor concentration and hence, structural properties can be tuned by varying the cationic precursor concentration which can be evidenced by morphological studies of the films. Further, the lattice constant 'a' of the films was determined by the equation 2.2 (Thohidi et al. 2013). No significant changes observed in structure due to annealing the films.

Table 4.7 Structural parameters of ZnS thin films with various precursor concentration of zinc.

| **Zn:S precursor concentration ratio** | **Substrate temperature (˚C)** | **2θ (degree)** | **$d_{cal}$ (Å)** | **$a_{std}$ (Å)** | **a (Å)** | **Oriented (hkl) texture** | **D (nm)** |
|---|---|---|---|---|---|---|---|
| 1:1 | 450 | 28.65 | 3.076 | 5.345 | 5.329 | (111) | 5.9 |
| 0.33:1 | | 28.56 | 3.086 | | 5.344 | (111) | 13.7 |

4.3.3 Optical studies

The transmittance spectra of the ZnS films deposited with Zn:S precursor concentration ratio 1:1 and 0.33:1, in the wavelength range of 300-1100 nm as shown in Figure 4.11.

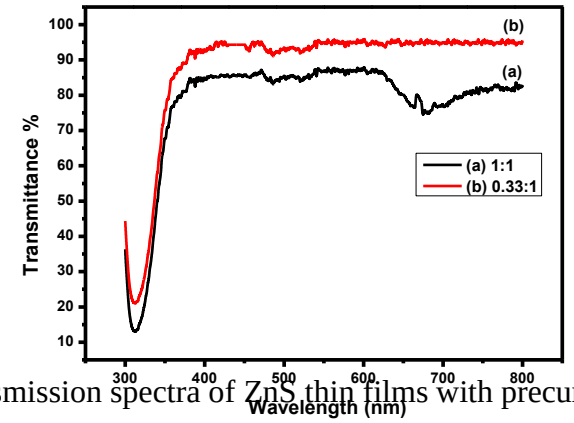


Fig. 4.11 Transmission spectra of ZnS thin films with precursor concentration ratio (a) 1:1and (b) 0.33:1.

Figure 4.11 shows an increase in transmittance of the ZnS thin films with a decrease in the zinc precursor concentration. The transmittance of the ZnS films was found to be in the order of 82% and 95% for the films deposited with precursor concentration ratio 1:1 and 0.33:1, respectively. The absorption coefficient 'α' of the film was found to be of the order $10^2$ $cm^{-1}$, calculated using the equation 2.14 (Beddek et al. 2016). The band gap of the material was determined using the Tauc's relation 2.13 (Tauc 1974). Figure 4.12 shows the Tauc's plot for direct transition of the films deposited with precursor concentration ratios 1:1 and 0.33:1.

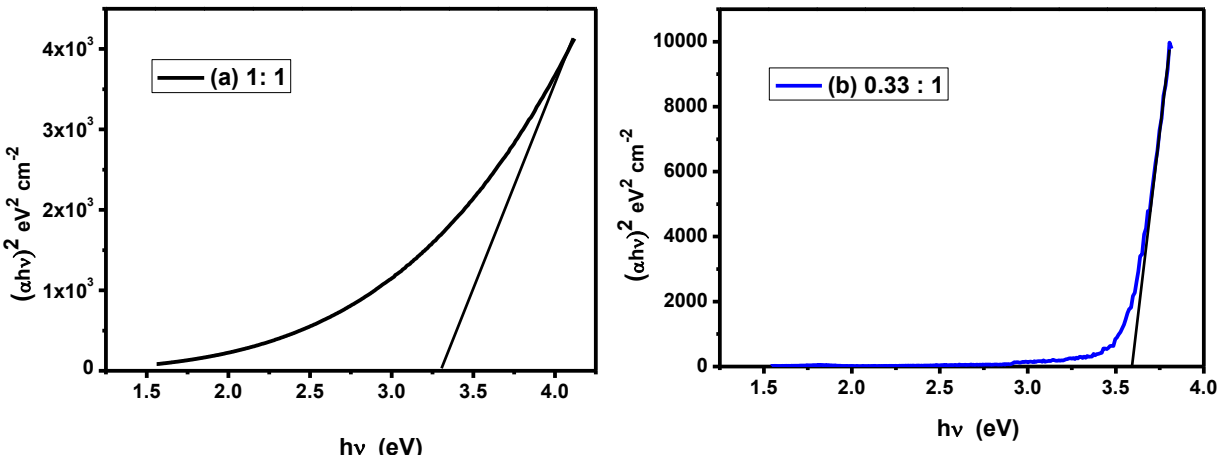


Fig. 4.12 Tauc plot of ZnS thin films with precursor concentration ratio (a) 1:1and (b) 0.33:1.

The direct optical energy band of the ZnS films is found to be in the order of 3.38 eV and 3.54 eV for the films deposited with precursor concentration ratio 1:1 and 0.33:1, respectively (Hernandez et al. 2008, Meshram et al. 2012). No changes in the optical parameters have been observed after annealing the zinc sulphide films.

4.3.4 Electrical studies

The linear nature of I-V characteristics (Fig. 4.13) confirms that silver makes ohmic contact with ZnS films. The measured resistivity of the ZnS thin films was found to be in the order of $10^7$ Ω cm.

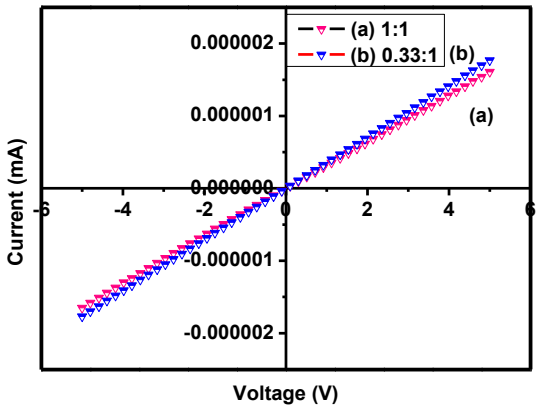


Fig. 4.13 I-V plots of ZnS thin films with precursor concentration ratio (a) 1:1and (b) 0.33:1.

The Fig. 4.14 shows Arrhenius plot (variation of log R with 1/T) of the ZnS films. The decrease in resistance with increase in the temperature shows the semiconducting nature of the films. The slope of the plot shows the presence of conduction mechanism in extrinsic

region (Ravishankar et al. 2016). The activation energy was found to be 0.82 ± 0.05 eV. Hot probe measurement showed the +ve value of $V_{DC}$ which indicates ZnS thin films were n-type semiconductors. No changes in the electrical behavior have been observed after annealing the zinc sulphide films.

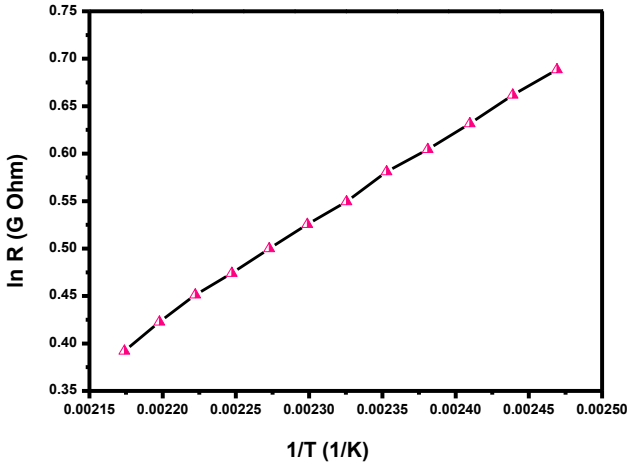


Fig. 4.14 ln R verses 1/T plot for Zn:S thin film with precursor concentration ratio of 0.33:1.

# CHAPTER 5

# PREPARATION AND CHARACTERIZATION OF LEAD ZINC SULPHIDE THIN FILMS

This chapter deals with the preparation of mixed lead zinc sulphide thin films using spray pyrolysis technique and characterization of these films.

## 5.1 SYNTHESIS OF LEAD ZINC SULPHIDE THIN FILMS

Lead zinc sulphide thin films were deposited on glass substrates at various deposition conditions. Aqueous solutions of lead acetate ($Pb(CH_3COO)_2$), zinc acetate ($Zn(CH_3COO)_2$) and thiourea ($CS(NH_2)_2$) were utilized as precursor solutions. The optimized parameters used for the synthesis of binary compounds (PbS and ZnS) were considered and utilized to synthesize ternary PbZnS films. According to Hume-Rothery rules, strengthening of solid solutions depends on concentration of solute atoms, size of solute atoms and valency of solute atoms (for ionic materials). Thus considering these rules for the formation of solid solution, lead zinc sulphide films were synthesized by controlling lead acetate and zinc acetate molar ratios in precursor as mentioned in Table 5.1.

Table 5.1 Precursor ratio used to synthesize $Pb_xZn_{1-x}S$ thin films.

| **Composition** | **Precursor Ratio Pb:Zn:S (0.1M)** |
|---|---|
| PbS | 1.25:0:1 |
| $Pb_{0.8}Zn_{0.2}S$ | 1:0.066:1 |
| $Pb_{0.6}Zn_{0.4}S$ | 0.75:0.132:1 |
| $Pb_{0.5}Zn_{0.5}S$ | 0.625:0.165:1 |
| $Pb_{0.4}Zn_{0.6}S$ | 0.5:0.198:1 |
| $Pb_{0.2}Zn_{0.8}S$ | 0.25:0.264:1 |
| ZnS | 0:0.33:1 |

After deposition, the films were allowed to cool at room temperature before taking them out of the deposition system. The films were subjected to dry air blower before carrying out characterization studies. The adhesion of the films on the substrate was quite good. Lead zinc sulphide thin film is formed according to the following chemical reaction.

$$Pb_x\ (CH_3COO)_2\ .3H_2O + Zn_{1-x}(CH_3COO)_2.2H_2O + NH_2CSNH_2 \xrightarrow{200°C-450°C,\ decompose} Pb_xZn_{1-x}S + NH_3\uparrow + NH_4\uparrow + 7CO_2\uparrow + 4CH_4\uparrow + 2H_2\uparrow + steam\uparrow \quad (5.1)$$

## 5.2 PREPARATIVE PARAMETERS

To prepare films of the required composition, the precursor were mixed in appropriate concentrations mentioned in Table 5.1 up to a total volume of 50 ml and sprayed on to substrates. Other parameters relevant to the preparation are mentioned in the Table 5.2. It may be mentioned that all the parameters were maintained at the specified values. However, the substrate temperature was chosen by experimentation for different compositions.

Table 5.2 Preparative parameters for $Pb_xZn_{1-x}S$ thin films.

| Parameter | Values |
|---|---|
| Precursor | Lead acetate, zinc acetate and thiourea |
| Volume | 50 ml |
| Substrate temperature | 250˚C to 450˚C |
| Spray rate | 1.5 ml/min |
| Nozzle to substrate distance | 16 cm |
| Carrier gas | Air |
| Pressure of carrier gas | 1.8 bar |
| Thickness | 550± 20 nm |

## 5.3 EFFECT OF SUBSTRATE TEMPERATURE

### 5.3.1 Compositional and morphological analysis

$Pb_xZn_{1-x}S$ (x=0.8, 0.6, 0.5, 0.4 and 0.2) thin films were prepared at different substrate temperatures to obtain stoichiometric films. The elemental composition of lead, zinc and sulphur in $Pb_xZn_{1-x}S$ (x=0.8, 0.6, 0.5, 0.4 and 0.2) thin films were estimated by EDAX analysis as given in Tables (5.3, 5.5, 5.7, 5.9 and 5.11) respectively. The growth of thin films

using solution processing techniques involves the coating of wet precursors which should be performed in advance and followed by thermal annealing at high temperature for their decomposition and reaction. Hence, for solution based techniques, annealing process is indispensible. Owing to the advantages offered by annealing, stoichiometric films were annealed for 30 min and 60 min at the synthesized temperature itself to maintain stoichiometry. The elemental composition for annealed $Pb_xZn_{1-x}S$ thin films (x=0.8, 0.6, 0.5, 0.4 and 0.2) is given in Tables (5.4, 5.6, 5.8, 5.10 and 5.12) respectively.

Table 5.3 Elemental compositions of $Pb_{0.8}Zn_{0.2}S$ at different substrate temperature.

| **Ratio** | **Substrate temperature (˚C)** | **Lead (At %)** | **Zinc (At %)** | **Sulphur (At %)** |
|---|---|---|---|---|
| (1:0.066:1) | 250 | 41.11 | 4.07 | 54.82 |
| | 300 | 40.84 | 6.48 | 52.68 |
| | 350 | 40.14 | 10.13 | 49.75 |

Table 5.4 Elemental compositions of annealed $Pb_{0.8}Zn_{0.2}S$ thin films.

| **Ratio** | **Substrate temperature (˚C)** | **Annealed temperature (˚C)** | **Duration (min)** | **Lead (At %)** | **Zinc (At %)** | **Sulphur (At %)** |
|---|---|---|---|---|---|---|
| 1:0.066:1 | 350 | 350 | 30 | 39.94 | 10.42 | 49.64 |
| | | | 60 | 39.85 | 11.83 | 48.32 |

Table 5.5 Elemental compositions of $Pb_{0.6}Zn_{0.4}S$ at different substrate temperature.

| **Ratio** | **Substrate temperature (˚C)** | **Lead (At %)** | **Zinc (At %)** | **Sulphur (At %)** |
|---|---|---|---|---|
| (0.75:0.132:1) | 300 | 30.72 | 16.65 | 52.63 |
| | 350 | 30.14 | 20.29 | 49.57 |

Table 5.6 Elemental compositions of annealed $Pb_{0.6}Zn_{0.4}S$ thin films.

| Ratio | Substrate temperature (˚C) | Annealed temperature (˚C) | Duration (min) | Lead (At %) | Zinc (At %) | Sulphur (At %) |
|---|---|---|---|---|---|---|
| 0.75:0.132:1 | 350 | 350 | 30 | 29.12 | 16.65 | 49.44 |
| | | | 60 | 29.88 | 21.43 | 48.69 |

Table 5.7 Elemental compositions of $Pb_{0.5}Zn_{0.5}S$ at different substrate temperature.

| Ratio | Substrate temperature (˚C) | Lead (At %) | Zinc (At %) | Sulphur (At %) |
|---|---|---|---|---|
| (0.625:0.165:1) | 300 | 33.66 | 13.28 | 53.06 |
| | 350 | 24.95 | 24.75 | 50.48 |

Table 5.8 Elemental compositions of annealed $Pb_{0.5}Zn_{0.5}S$ thin films.

| Ratio | Substrate temperature (˚C) | Annealed temperature (˚C) | Duration (min) | Lead (At %) | Zinc (At %) | Sulphur (At %) |
|---|---|---|---|---|---|---|
| 0.625:0.165:1 | 350 | 350 | 30 | 24.84 | 25.03 | 50.13 |
| | | | 60 | 24.82 | 25.40 | 49.78 |

Table 5.9 Elemental compositions of $Pb_{0.4}Zn_{0.6}S$ at different substrate temperature.

| Ratio | Substrate temperature (˚C) | Lead (At %) | Zinc (At %) | Sulphur (At %) |
|---|---|---|---|---|
| (0.5:0.198:1) | 300 | 21.92 | 23.91 | 54.17 |
| | 350 | 21.47 | 26.48 | 52.05 |
| | 400 | 20.03 | 29.97 | 50.00 |

Table 5.10 Elemental compositions of annealed $Pb_{0.4}Zn_{0.6}S$ thin films.

| Ratio | Substrate temperature (˚C) | Annealed temperature (˚C) | Duration (min) | Lead (At %) | Zinc (At %) | Sulphur (At %) |
|---|---|---|---|---|---|---|
| 0.5:0.198:1 | 400 | 400 | 30 | 19.98 | 30.15 | 49.87 |
| | | | 60 | 19.23 | 31.82 | 48.95 |

Table 5.11 Elemental compositions of $Pb_{0.2}Zn_{0.8}S$ at different substrate temperature.

| Ratio | Substrate temperature (˚C) | Lead (At %) | Zinc (At %) | Sulphur (At %) |
|---|---|---|---|---|
| (0.25:0.264:1) | 300 | 11.77 | 34.88 | 53.35 |
| | 350 | 10.91 | 37.78 | 51.31 |
| | 400 | 9.98 | 39.84 | 49.78 |

Table 5.12 Elemental compositions of annealed $Pb_{0.2}Zn_{0.8}S$ thin films.

| Ratio | Substrate temperature (˚C) | Annealed temperature (˚C) | Duration (min) | Lead (At %) | Zinc (At %) | Sulphur (At %) |
|---|---|---|---|---|---|---|
| 0.25:0.264:1 | 400 | 400 | 30 | 9.12 | 41.53 | 49.35 |
| | | | 60 | 8.25 | 42.79 | 48.96 |

Table 5.13 Elemental compositions for stoichiometric $Pb_xZn_{1-x}S$ (x=0.8-0.2) thin films with substrate temperature.

| Composition | Substrate temperature (˚C) | Atomic % | | |
|---|---|---|---|---|
| | | Lead | Zinc | Sulphur |
| $Pb_{0.8}Zn_{0.2}S$ | 350 | 40.14 | 10.13 | 49.72 |
| $Pb_{0.6}Zn_{0.4}S$ | 350 | 29.90 | 20.30 | 49.80 |
| $Pb_{0.5}Zn_{0.5}S$ | 350 | 24.95 | 24.74 | 50.48 |
| $Pb_{0.4}Zn_{0.6}S$ | 400 | 20.03 | 29.97 | 50.00 |
| $Pb_{0.2}Zn_{0.8}S$ | 400 | 9.98 | 39.84 | 49.78 |

It is observed that lead and sulphur content in the film decreases as the substrate temperature and/or annealing duration is increased. Sulphur has a greater affinity towards oxygen and might have escaped from the surface of the film as $SO_2$ (Raviprakash et al. 2009). Table 5.13 shows the elemental compositions of $Pb_xZn_{1-x}S$ thin films with corresponding substrate temperature in which films were stoichiometric. Figure 5.1 shows representative SEM and EDAX spectra of stoichiometric $Pb_xZn_{1-x}S$ (x=0.8) thin films. SEM

images show homogeneous, smooth and network structures due to increased volumetric stress in the films caused by $Zn^{2+}$ ions incorporation into lead sites (Yilmaz et al. 2015). It has been observed that there is no influence on morphology of the thin films as a result of the change in substrate temperature and annealing duration.

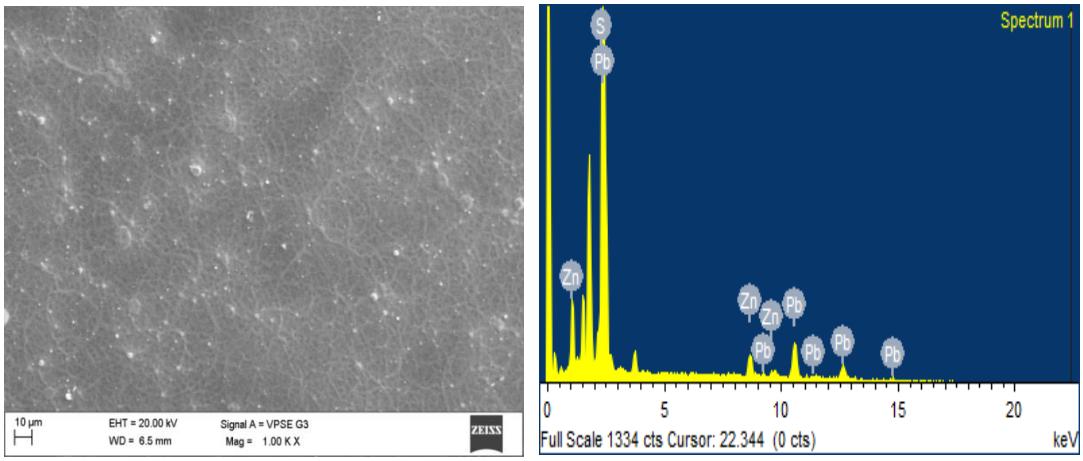


Fig. 5.1 Representative SEM image and EDAX spectra for annealed $Pb_{0.2}Zn_{0.8}S$ thin films.

5.3.2 Structural analysis

XRD patterns of $Pb_xZn_{1-x}S$ (x=0.8, 0.6, 0.5, 0.4 and 0.2) thin films prepared at different substrate temperature are shown in Figures (5.2, 5.3, 5.4, 5.5 and 5.6) respectively. It shows that the $Pb_xZn_{1-x}S$ thin films are polycrystalline in nature with face-centered cubic structure. The structure of the deposited films was confirmed by comparing the observed diffraction angles with the standard data (JCPDS file PbS: 00-005-0592 and ZnS: 00-005-0566). There was no additional diffraction peak observed in the diffraction patterns which indicate the formation of a single phase compound. The crystallite size for maximum intensity peak is determined by using Scherrer formula (equation 2.6). The lattice parameters were estimated using the combination of Bragg's law and the interplanar spacing equation for the cubic structure (equation 2.2).

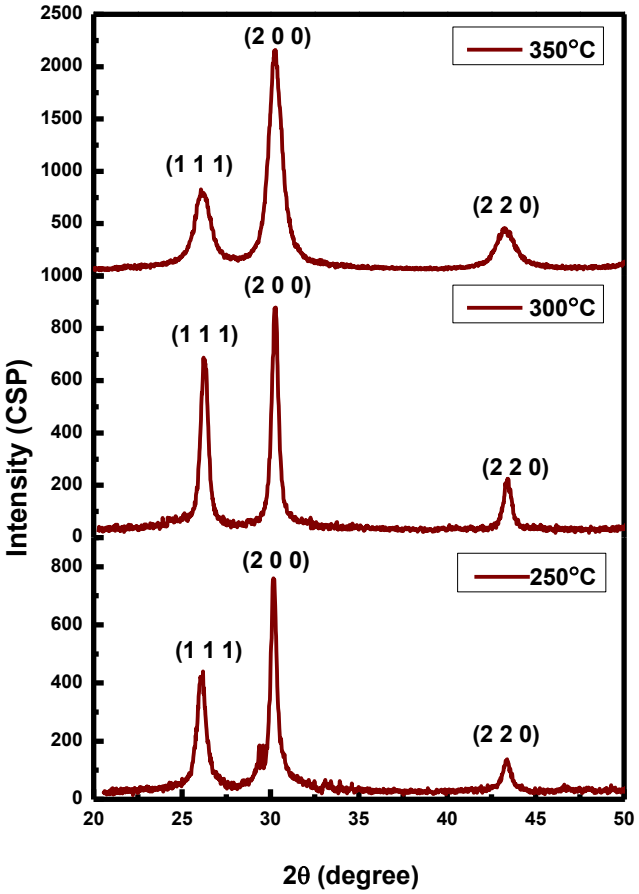


Fig. 5.2 XRD patterns of $Pb_{0.8}Zn_{0.2}S$ films deposited at different substrate temperatures.

Table 5.14 Structural parameters of stoichiometric $Pb_{0.8}Zn_{0.2}S$ thin films.

| Composition | Ratio | Substrate temperature (˚C) | 2θ (degree) | (h k l) value | d (Å) | a (Å) | (D) (nm) |
|---|---|---|---|---|---|---|---|
| $Pb_{0.8}Zn_{0.2}S$ | 1:0.066:1 | 250 | 30.15 | (2 0 0) | 3.407 | 5.901 | 14.31 |
| | | 300 | 30.15 | | 3.407 | 5.901 | 18.82 |
| | | 350 | 30.15 | | 3.407 | 5.901 | 19.58 |

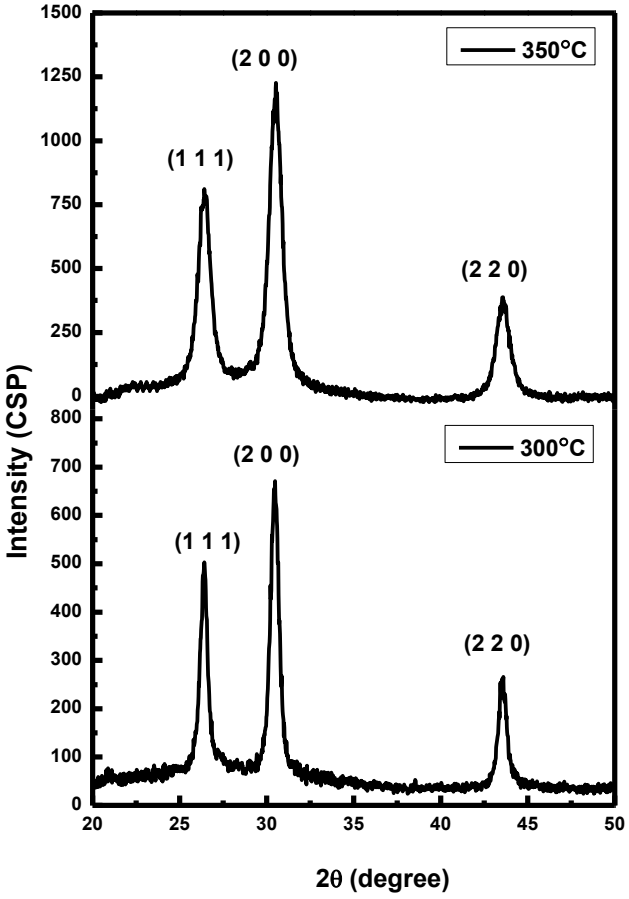


Fig. 5.3 XRD patterns of $Pb_{0.6}Zn_{0.4}S$ films deposited at different substrate temperatures.

Table 5.15 Structural parameters of stoichiometric $Pb_{0.6}Zn_{0.4}S$ thin film.

| **Composition** | **Ratio** | **Substrate temperature (˚C)** | **2θ (degree)** | **(h k l) value** | **d (Å)** | **a (Å)** | **D (nm)** |
|---|---|---|---|---|---|---|---|
| $Pb_{0.6}Zn_{0.4}S$ | 0.75:0.132:1 | 300 | 30.59 | (2 0 0) | 2.923 | 5.846 | 12.71 |
| | | 350 | 30.59 | | 2.923 | 5.846 | 18.09 |

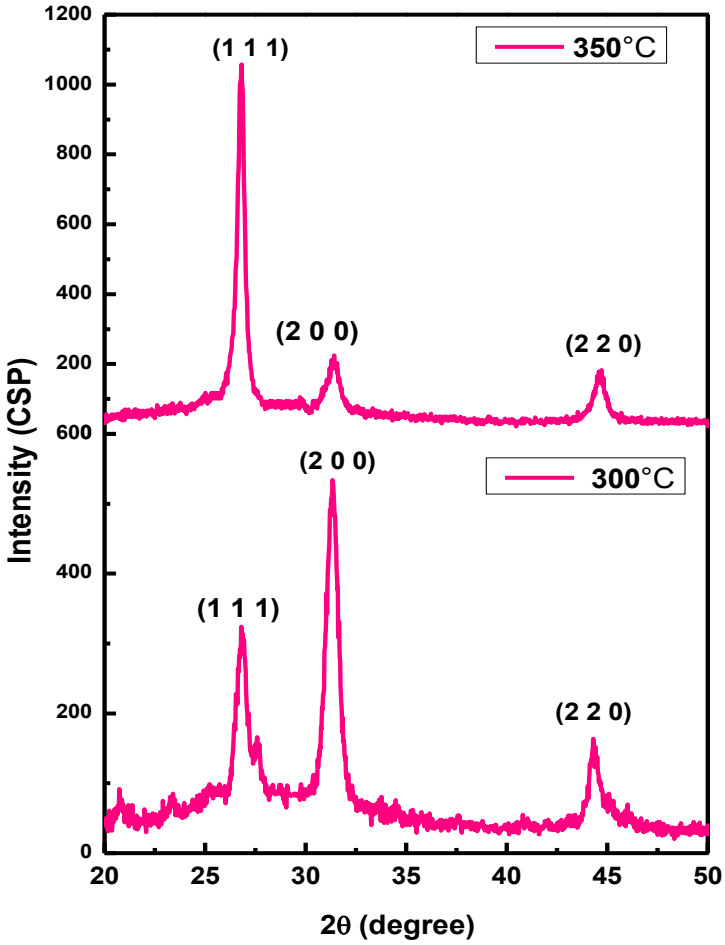


Fig. 5.4 XRD patterns of $Pb_{0.5}Zn_{0.5}S$ films deposited at different substrate temperatures.

Table 5.16 Structural parameters of stoichiometric $Pb_{0.5}Zn_{0.5}S$ thin films**.**

| **Composition** | **Ratio** | **Substrate temperature (˚C)** | **2θ (degree)** | **(h k l) value** | **d (Å)** | **a (Å)** | **D (nm)** |
|---|---|---|---|---|---|---|---|
| $Pb_{0.5}Zn_{0.5}S$ | 0.625:0.165:1 | 300 | 31.20 | (2 0 0) | 2.850 | 5.745 | 11.35 |
| | | 350 | 26.82 | (1 1 1) | 3.324 | 5.752 | 17.85 |

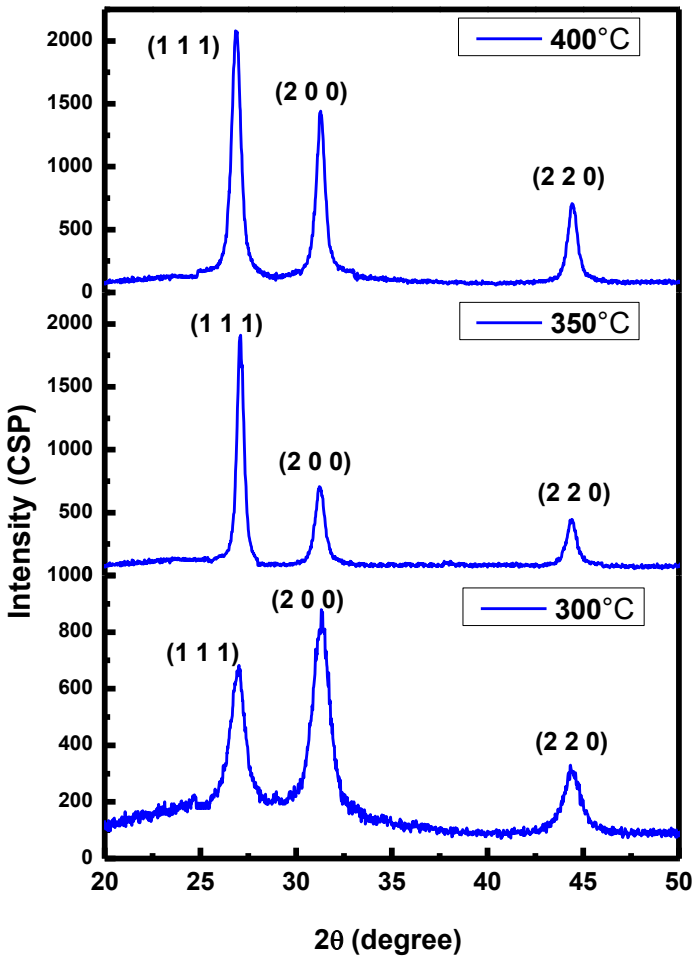


Fig. 5.5 XRD patterns of $Pb_{0.4}Zn_{0.6}S$ films deposited at different substrate temperatures.

Table 5.17 Structural parameters of stoichiometric $Pb_{0.4}Zn_{0.6}S$ thin films.

| **Composition** | **Ratio** | **Substrate temperature (˚C)** | **2θ (degree)** | **(h k l) value** | **d (Å)** | **a (Å)** | **D (nm)** |
|---|---|---|---|---|---|---|---|
| $Pb_{0.4}Zn_{0.6}S$ | 0.5:0.198:1 | 300 | 31.35 | (2 0 0) | 2.853 | 5.705 | 7.011 |
| | | 350 | 27.08 | (1 1 1) | 3.293 | 5.704 | 13.53 |
| | | 400 | | | | | 16.42 |

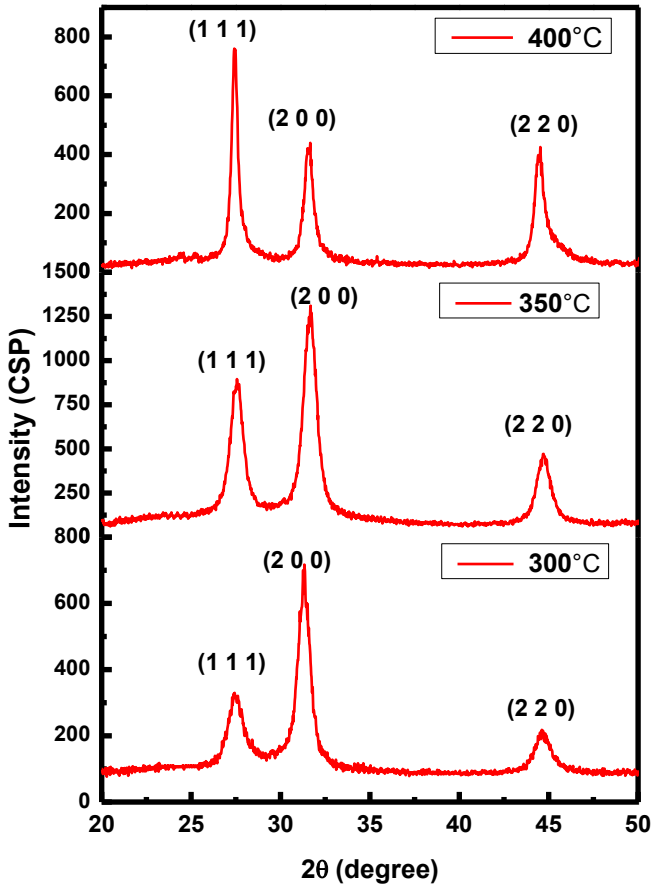


Fig. 5.6 XRD patterns of $Pb_{0.2}Zn_{0.8}S$ films deposited at different substrate temperatures.

Table 5.18 Structural parameters of stoichiometric $Pb_{0.2}Zn_{0.8}S$ thin films.

| **Composition** | **Ratio** | **Substrate temperature (˚C)** | **2θ (degree)** | **(h k l) value** | **d (Å)** | **a (Å)** | **D (nm)** |
|---|---|---|---|---|---|---|---|
| $Pb_{0.2}Zn_{0.8}S$ | 0.25:0.264:1 | 300 | 31.55 | (2 0 0) | 2.837 | 5.679 | 9.75 |
| | | 350 | | | | | 11.89 |
| | | 400 | 27.50 | (1 1 1) | 3.244 | 5.675 | 12.75 |

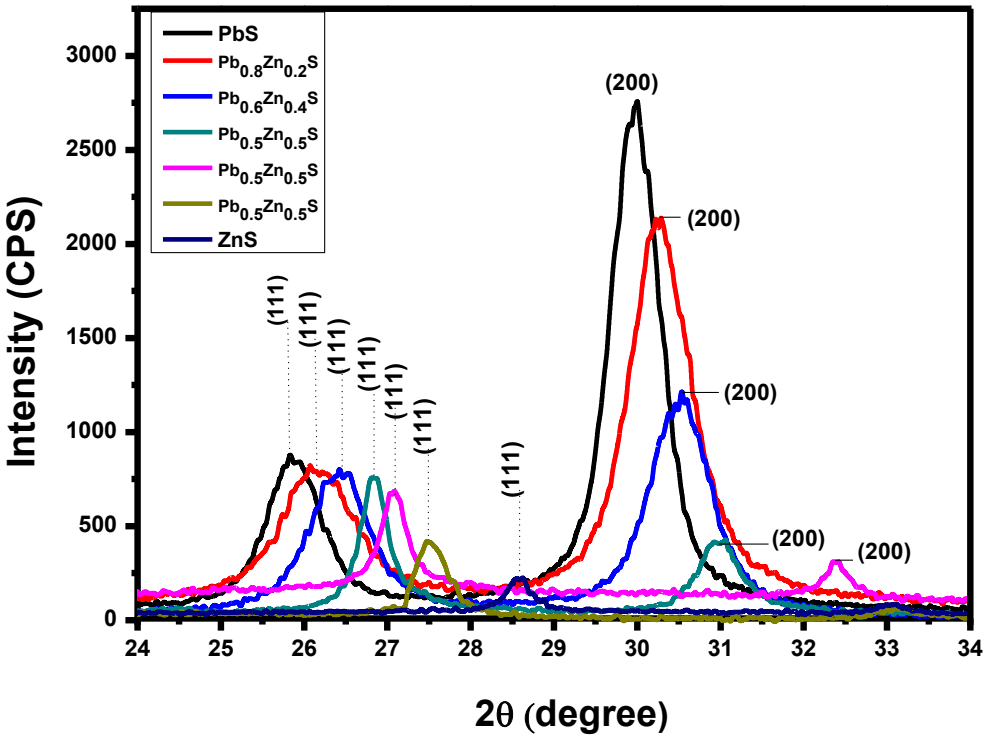


Fig. 5.7 Shift in the (111) and (200) peak for $Pb_xZn_{1-x}S$ (x=0-1) thin films.

Table 5.19 Structural parameters of stoichiometric $Pb_xZn_{1-x}S$ thin films.

| Composition | Maximum intensity | | For (111) plane | | | |
|---|---|---|---|---|---|---|
| | 2θ (degree) | (h k l) plane | 2θ (degree) | d (Å) | a (Å) | D (nm) |
| $Pb_{0.8}Zn_{0.2}S$ | 30.26 | (2 0 0) | 26.15 | 3.408 | 5.905 | 19.58 |
| $Pb_{0.6}Zn_{0.4}S$ | 30.59 | (2 0 0) | 26.49 | 3.345 | 5.793 | 18.09 |
| $Pb_{0.5}Zn_{0.5}S$ | 26.82 | (1 1 1) | 26.82 | 3.324 | 5.760 | 17.85 |
| $Pb_{0.4}Zn_{0.6}S$ | 27.08 | (1 1 1) | 27.08 | 3.293 | 5.704 | 16.42 |
| $Pb_{0.2}Zn_{0.8}S$ | 27.5 | (1 1 1) | 27.5 | 3.244 | 5.619 | 12.75 |

As the $Zn^{2+}$ ions incorporated in lead sites of the PbS films, a slight shift in the position of the diffraction peaks to higher angles has been observed which confirms the formation of a solid solution. It can be observed that preferential orientation of the $Pb_xZn_{1-x}S$

thin-films ($x \leq 0.5$) changed from (200) to (111) plane as the $Zn^{2+}$ ions in the films increased. This is due to the ionic radius of $Pb^{2+}$ (1.19 Å) which is larger compare to ionic radius of $Zn^{2+}$ (0.74 Å). Similar behavior of zinc has been reported by (Abiodun et al. 2015), (Monacada et al. 2013) and (Touati et al. 2015) for $Zn_xPb_{1-x}S$, $Cd_{1-x}Zn_xS$ and Zn: PbS ternary alloys respectively. The computed lattice parameter and crystallite size of the $Pb_xZn_{1-x}S$ films are given in Table 5.19. Crystallite size decreased with increased $Zn^{2+}$ ions in lead sites. It is due to the formation of structural disorder in the crystal with the increased of $Zn^{2+}$ ions in the films (Monacada et al. 2013).

The intensity of the peaks increased with increase in substrate temperature which reveals that crystallinity of the film improves at elevated substrate temperature. It might be due to the reduction of microstrain values at a higher temperature (Thangaraju et al. 2000). The variation in lattice parameters and crystallite size as a function of substrate temperature for $Pb_xZn_{1-x}S$ (x=0.8, 0.6, 0.5, 0.4 and 0.2) thin films are shown in Tables (5.14, 5.15, 5.16, 5.17 and 5.18) respectively. Figure 5.8 shows the increase in the lattice constant with increase in Pb ion concentration of the films. The variation is far from linear dependence. This indicates that metallic solid solutions rarely obey Vegard's law precisely. The lattice constant as a function of composition is reported to exhibit negative curvature (Chaure et al. 2008, Matt ford et al. 2011). There were no significant changes observed in the structural properties of the films after annealing.

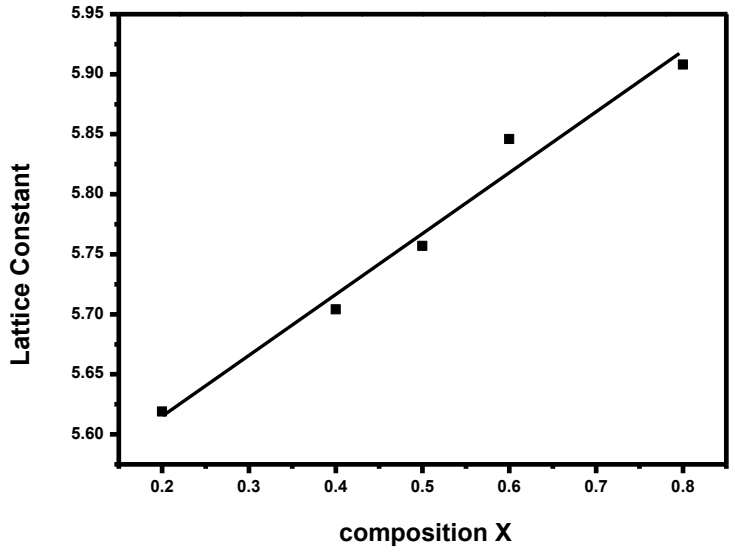


Fig. 5.8 Variation of lattice constant with composition x in $Pb_xZn_{1-x}S$ thin films.

The composition of solid solution has been evaluated using Nelson relay extrapolation method by plotting lattice constant obtained against Nelson-Relay function (f(θ)) (Nelson et al.1945, Matt ford et al. 2011).

$$f(\theta) = \left(\frac{cos\theta^2}{sin\theta} + \frac{cos\theta^2}{\theta}\right) \quad (5.2)$$

Figure 5.9 shows the Nelson–Relay extrapolation curve which confirms the substitution of more than 50mol% Zn ions in PbS lattice. A chemically deposited $Zn_{1-x}Pb_xS$ with maximum zinc content of 4.2 mol% in the solid solution has been reported (Maskaeva et al. 2008). In the present work, more than 50 mol% Zn in PbS has been achieved.

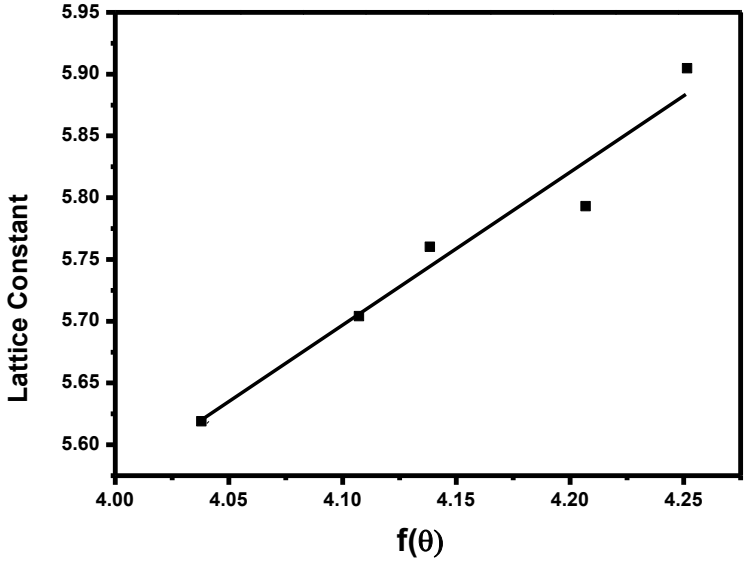


Fig. 5.9 Plot of lattice constant against the Nelson-Relay function.

5.3.3 Optical studies

The optical absorption spectra of the $Pb_xZn_{1-x}S$ thin films were recorded for x = 0.2, 0.4, 0.5, 0.6 and 0.8 as a function of the wavelength ranging from 300 nm to 3000 nm. Figure 5.10 shows the variation of optical absorbance of $Pb_xZn_{1-x}S$ (x=0.8, 0.6, 0.5, 0.4 and 0.2) thin films with the wavelength of the light. As shown in Figure 5.10, all films exhibit non-interference fringes is an evidence for the effect of network structures formed on the surface of the prepared thin films. The absorption edge shifts towards the shorter wavelength side i.e., from 352 nm to 3044 nm as the lead content increases in the $Pb_xZn_{1-x}S$ films from x=0 to 1. The increase of absorbance with increase in lead content of the film may be due to the fact that the ionic radii and electronegativity of $Pb^{2+}$ ion is higher than those of zinc ions

which leads to the formation of defects in the lattice and thereby creating new energy levels due to more free electrons (Ashraf et al. 2012).

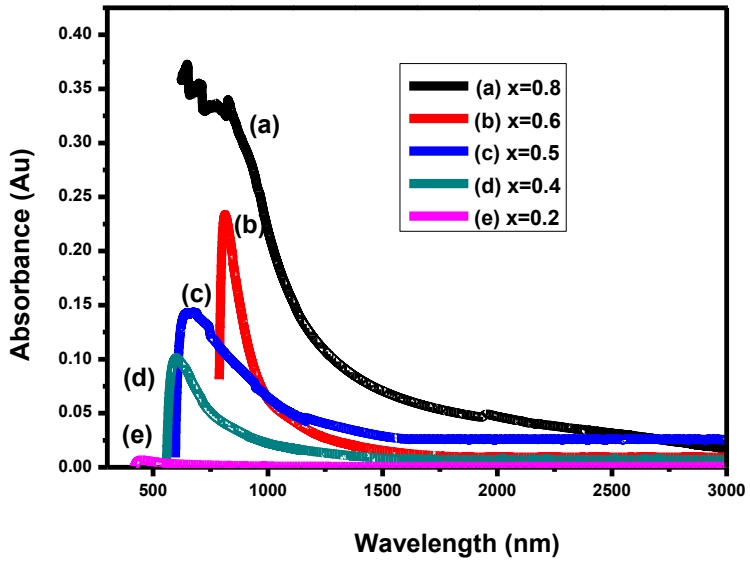


Fig. 5.10 Absorbance spectra of stoichiometric $Pb_xZn_{1-x}S$ thin films.

The absorption coefficient ($\alpha$) of the film was calculated using the equation 2.14 (Padiyan et al. 2004). The absorption coefficient is found to be in the order of $10^6$ $cm^{-1}$ and decreased to $10^2$ $cm^{-1}$ as Pb ion concentration decreased in $Pb_xZn_{1-x}S$ thin-films. According to the band to band transition theory, the absorption begins at $h\nu = E_g$ which gives the relation between the absorption coefficient ($\alpha$) and the photon energy ($h\nu$). The optical energy band gap of the films was calculated by using the Tauc relation given in equation 2.13 (Padiyan et al. 2004). Schoolar et al. (1965), Charles et al. (1986), Preetha et al. (2011) and Douri et al. (2008) have reported that PbS thin films have both allowed direct and indirect energy band gaps. Kennedy et al. (2014) and Fenollosa et al. (2008) observed allowed direct transition for ZnS thin films. Hence, a detailed study of the energy band gap of $Pb_xZn_{1-x}S$ thin-films was carried out considering both direct and indirect transition.

The mode of optical transitions in these films have been confirmed by equation (Kamruzaman et al. 2012, Pal et al. 1993)

$$\ln(\alpha h\nu) = \ln K + n \ln(h\nu - E_g) \qquad (5.3)$$

The plot of ln(αhν) v/s ln(hν-$E_g$) shown in Figure 5.11 is a straight line with two linear regions whose slope gives the power factor n for the films x=0-0.5. The value of n has been found to be ~0.5 for lower wavelength region indicating direct transition whereas for higher wavelength, n is approximately 2 indicating indirect transition. Further, for thin films x≤0.5, the plot shows a single straight line and value of n has been found to be ~0.5 indicating direct transition. This confirms the fact that the complete change from indirect to direct transition for thin films x≤0.5. The obtained values of n in lower wavelength and higher wavelength suggest that the fundamental absorption edge in the film is formed by the direct and indirect allowed transition.

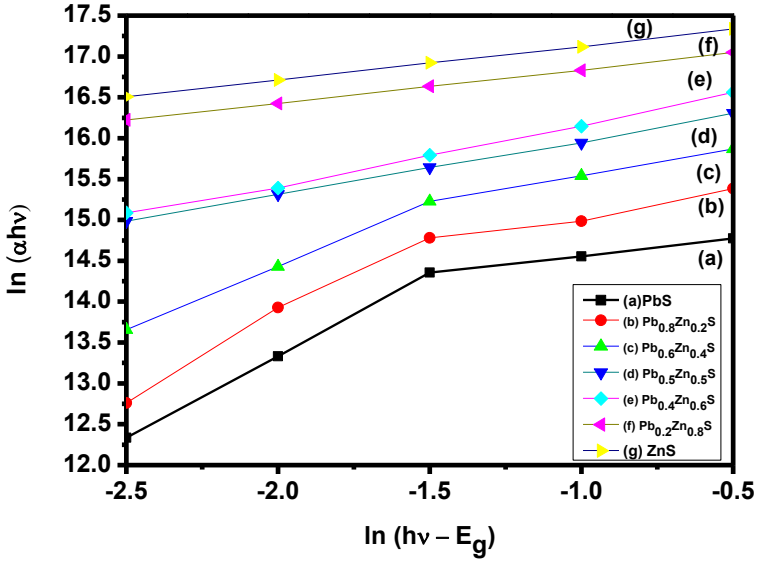


Fig. 5.11 Plot of ln (αhν) Vs. ln (hν-$E_g$) for $Pb_xZn_{1-x}S$ thin films.

Figures 5.12 and 5.13 show the Tauc's plots for both direct and indirect transition respectively. These figures show the dependence of the optical energy band gap on the composition x in $Pb_xZn_{1-x}S$ thin films. It can be observed that $Pb_xZn_{1-x}S$ thin films have direct band gap energy varying between 1.22 eV and 3.54 eV as x varies from 1 to 0 and indirect band gap varies between 0.4 eV to 0.83 eV for x > 0.5. It has been observed that indirect transition has changed to direct transition completely for x ≤ 0.5.

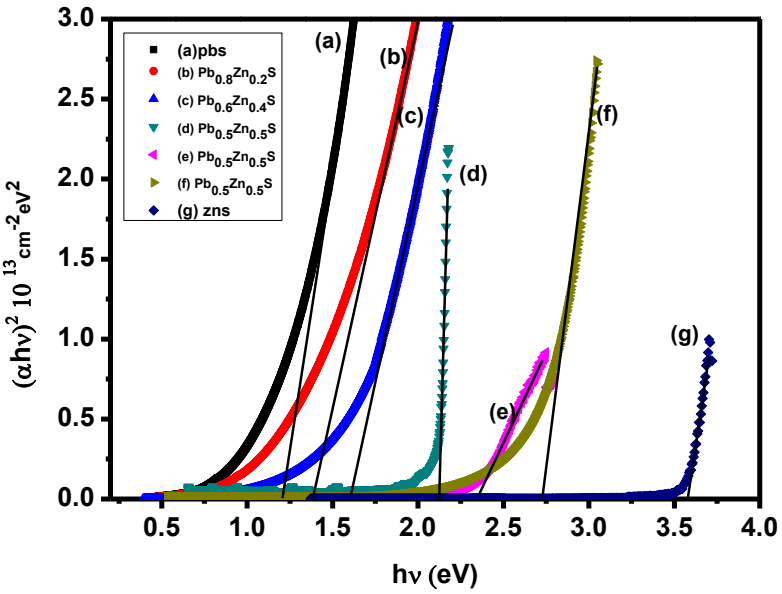


Fig. 5.12 Tauc plot of the $Pb_xZn_{1-x}S$ thin film (direct transition).

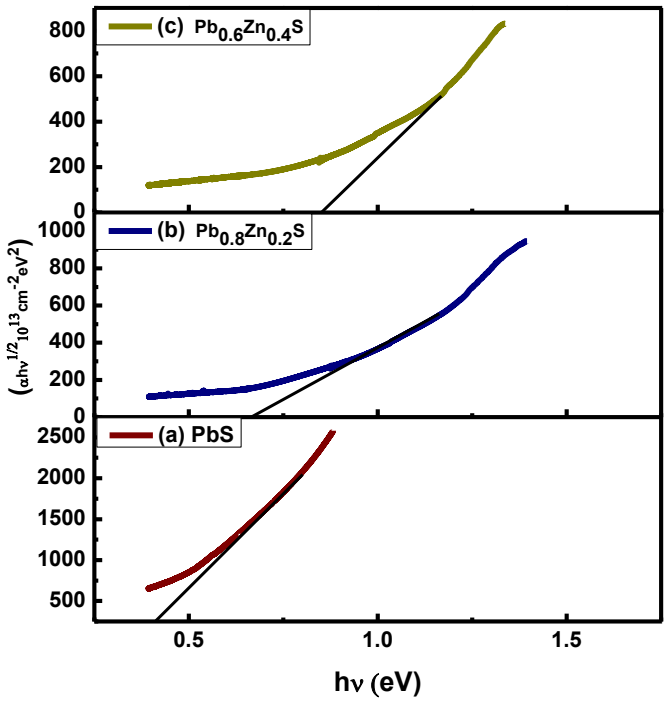


Fig. 5.13 Tauc plot of $Pb_xZn_{1-x}S$ (x=1, 0.8 and 0.6) thin film (indirect transition).

Table 5.20 Optical energy band gap $Pb_xZn_{1-x}S$ (x = 0.2, 0.4, 0.5, 0.6 and 0.8) thin film.

| Composition | Energy band gap (eV) |
|---|---|
| $Pb_{0.8}Zn_{0.2}S$ | 1.39($E_{gd}$)/0.64($E_{gid}$) |
| $Pb_{0.6}Zn_{0.4}S$ | 1.59($E_{gd}$)/0.83($E_{gid}$) |
| $Pb_{0.5}Zn_{0.5}S$ | 2.1($E_{gd}$) |
| $Pb_{0.4}Zn_{0.6}S$ | 2.40($E_{gd}$) |
| $Pb_{0.2}Zn_{0.8}S$ | 2.87( $E_{gd}$) |

Table 5.20 shows the direct and indirect band gap energy values of $Pb_xZn_{1-x}S$ thin films. The increase in band gap energy is observed with increase in the zinc content. This is attributed to the fact that the force bond of Zn-S is greater than the force bond of Pb-S due to the difference in electronegativity of zinc and lead. The difference in electronegativity for Zn-S bond is 0.9 while for Pb-S bond is 0.3 ($Pb^{2+}$ ions and $Zn^{2+}$ ions have electronegativity 2.33 and 1.65 respectively). Therefore the energy required to break the Zn-S bond is higher than the energy required to break the Pb-S bond, in addition, lead has atomic number (82) larger than zinc (30) which means the transfer of an electron in an atom level of lead is easier than electrons transfer to levels of an atom of zinc (Suhail 2012). Figure 5.14 shows that the optical energy band gap increases with increase in Zn content of $Pb_xZn_{1-x}S$ thin films. The variation in the band gap with Pb concentration is far from a linear dependence. It confirms that the optical properties show a greater dependence on the zinc ion concentration in the lead zinc sulphide thin films.

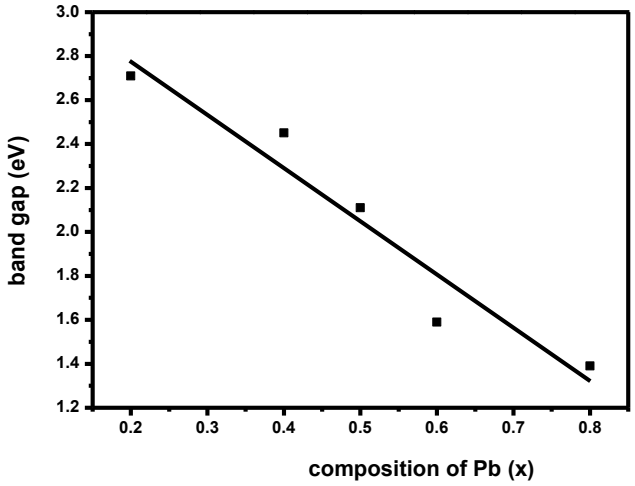


Fig. 5.14 Variation of direct energy band gap with composition x in $Pb_xZn_{1-x}S$ thin film.

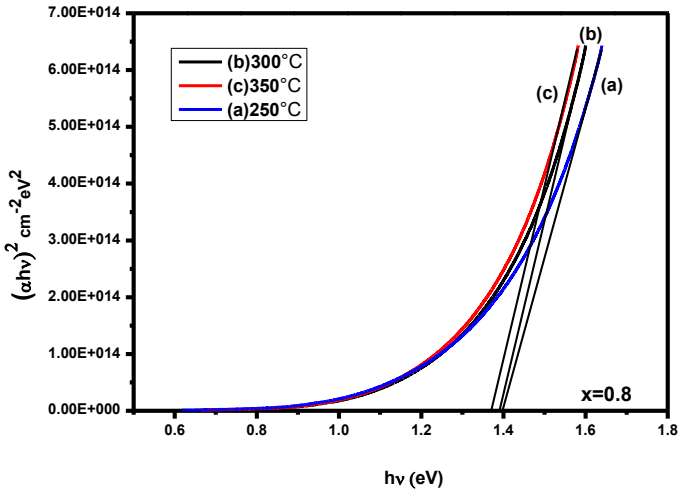


Fig. 5.15 Tauc plot of $Pb_{0.8}Zn_{0.2}S$ thin film at different substrate temperature.

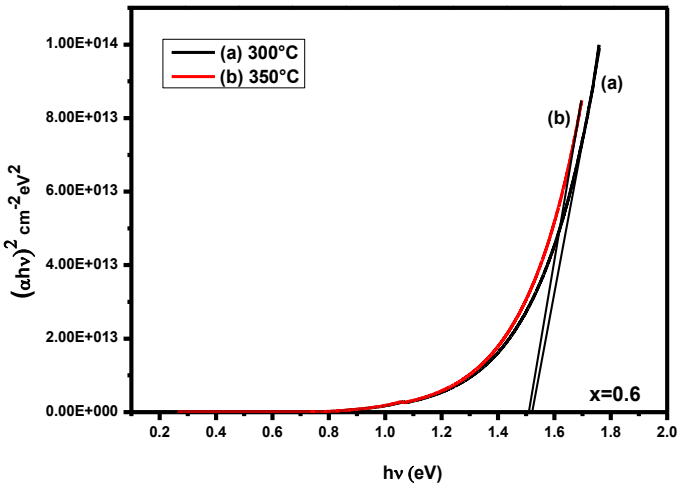


Fig. 5.16 Tauc plot of $Pb_{0.6}Zn_{0.4}S$ thin film at different substrate temperature.

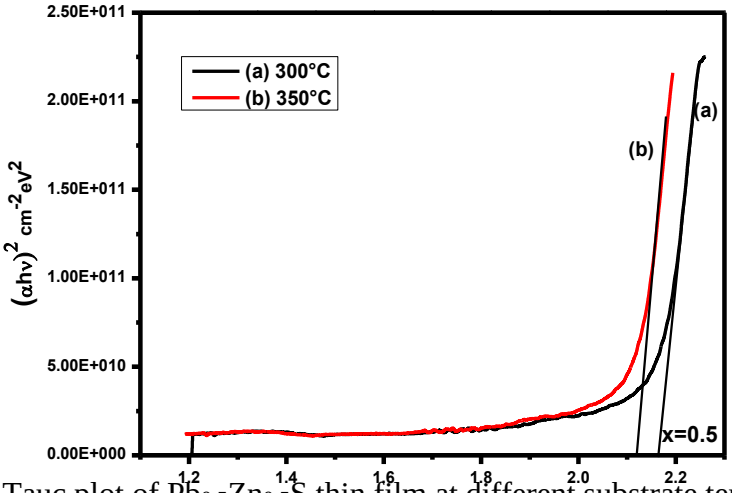


Fig. 5.17 Tauc plot of $Pb_{0.5}Zn_{0.5}S$ thin film at different substrate temperature.

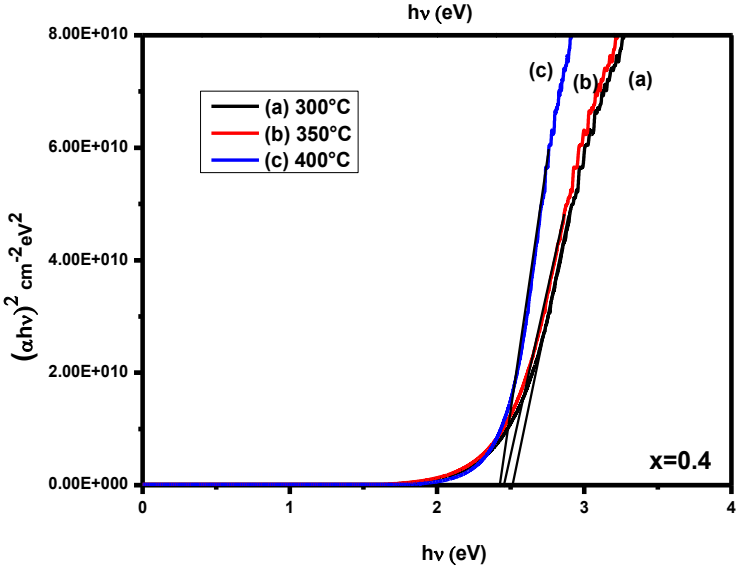


Fig. 5.18 Tauc plot of $Pb_{0.4}Zn_{0.6}S$ thin film at different substrate temperature.

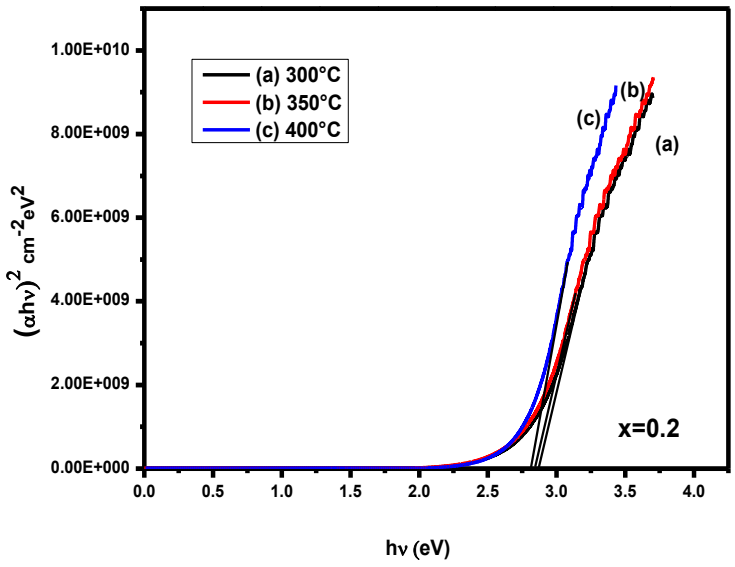

Fig. 5.19 Tauc plot of $Pb_{0.2}Zn_{0.8}S$ thin film at different substrate temperature.

Figures (5.15, 5.16, 5.17, 5.18 and 5.19) shows the Tauc's plots for $Pb_xZn_{1-x}S$ (x=0.8, 0.6, 0.5, 0.4 and 0.2) thin films respectively at different substrate temperature for the direct transition. It is evident that the optical band gap of the $Pb_xZn_{1-x}S$ films decreased with increased substrate temperature. Table 5.21 shows the band gap values at various substrate temperature of $Pb_xZn_{1-x}S$ (x=0.8, 0.6, 0.5, 0.4 and 0.2) thin films respectively. In the present study, a clear blue shift is observed in nanocrystalline $Pb_xZn_{1-x}S$ thin films deposited at different substrate temperatures which can be related to the effect of quantum confinement. It has been observed that as the band gap decreases the crystallite size increases. This decrease in band gap may be attributed to an increase in crystallite size with corresponding increase in substrate temperature. Annealing the films show a negligible effect in altering the originally observed band gap.

Table 5.21 Band gap value of $Pb_xZn_{1-x}S$ thin film at different substrate temperature.

| **Composition** | **Substrate temperature (˚C)** | **Band gap (eV)** |
|---|---|---|
| $Pb_{0.8}Zn_{0.2}S$ | 250 | 1.396 |
| | 300 | 1.389 |
| | 350 | 1.370 |
| $Pb_{0.6}Zn_{0.4}S$ | 300 | 1.524 |
| | 350 | 1.518 |
| $Pb_{0.5}Zn_{0.5}S$ | 300 | 2.164 |
| | 350 | 2.114 |
| $Pb_{0.4}Zn_{0.6}S$ | 300 | 2.493 |
| | 350 | 2.472 |
| | 400 | 2.439 |
| $Pb_{0.2}Zn_{0.8}S$ | 300 | 2.851 |
| | 350 | 2.842 |
| | 400 | 2.815 |

5.3.4 Electrical analysis

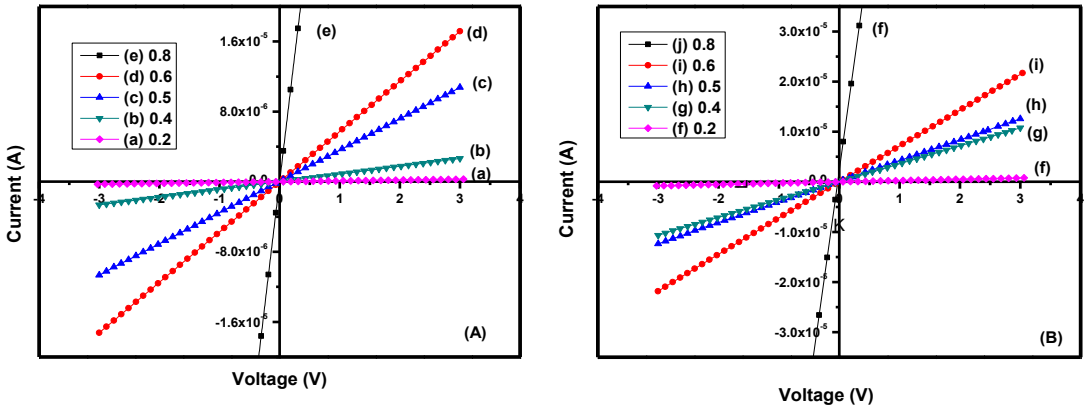


Fig. 5.20 I-V curves of (A) as deposited (B) annealed stoichiometric $Pb_xZn_{1-x}S$(x=0-1) thin films.

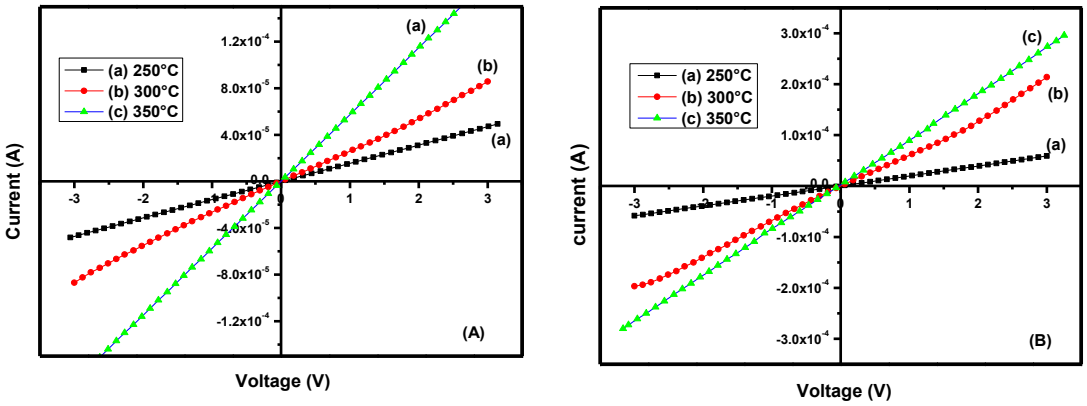


Fig. 5.21 I-V curves of $Pb_{0.8}Zn_{0.2}S$ (A) as deposited (B) annealed thin film at different substrate temperature.

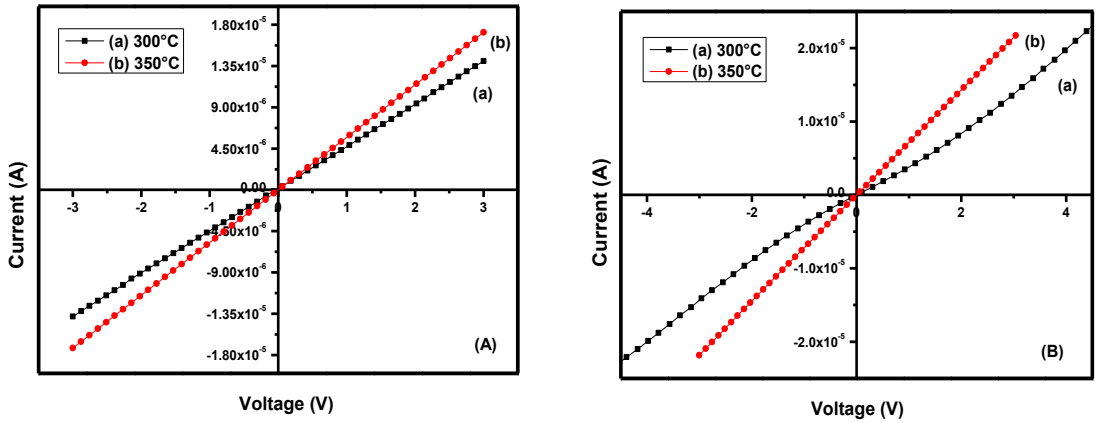


Fig. 5.22 I-V curves of $Pb_{0.6}Zn_{0.4}S$ (A) as deposited (B) annealed thin film at different substrate temperature.

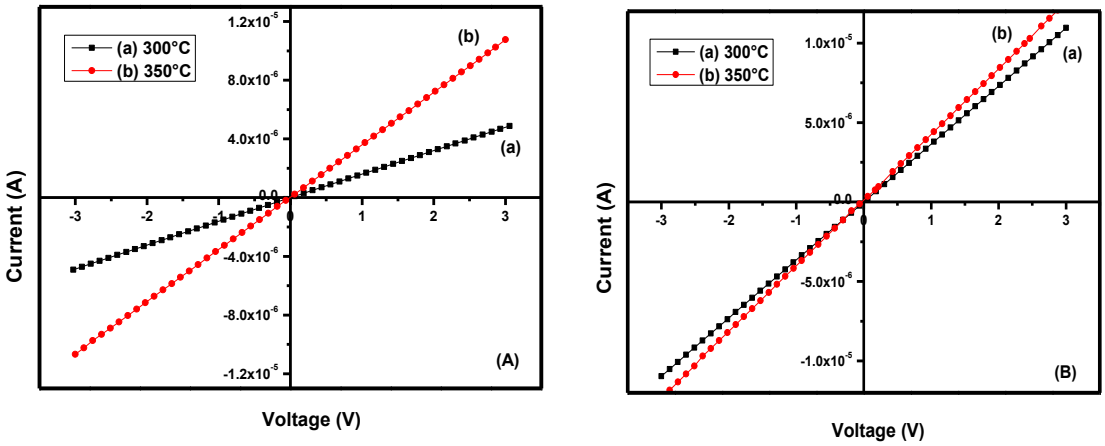


Fig. 5.23 I-V curves of $Pb_{0.5}Zn_{0.5}S$ (A) as deposited (B) annealed thin film at different substrate temperature.

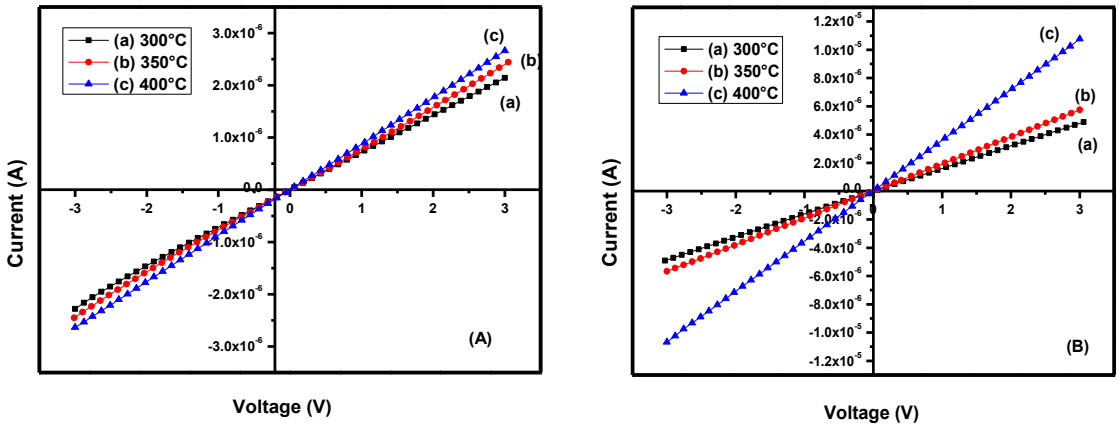


Fig. 5.24 I-V curves of $Pb_{0.4}Zn_{0.6}S$ (A) as deposited (B) annealed thin film at different substrate temperature.

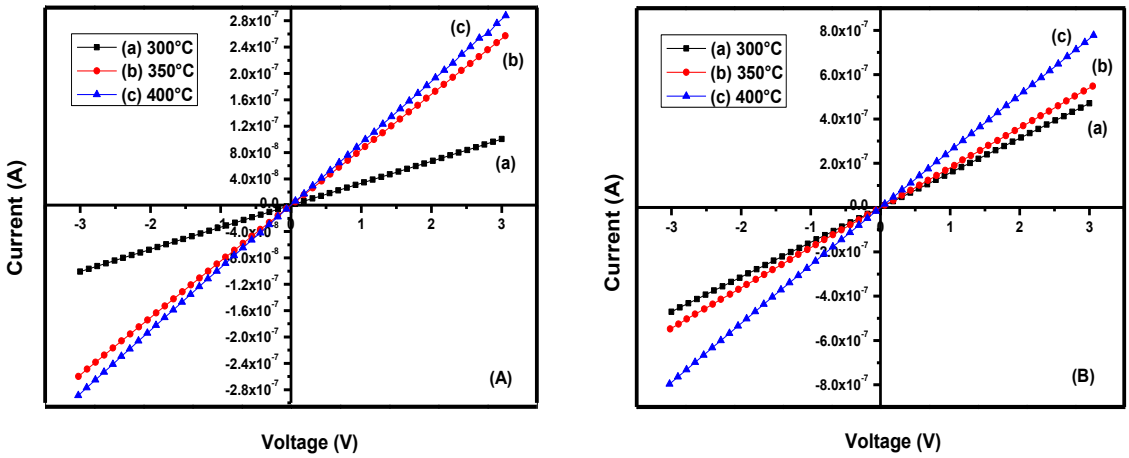

Fig. 5.25 I-V curves of $Pb_{0.2}Zn_{0.4}S$ (A) as deposited (B) annealed thin film at different substrate temperature.

I-V plots of the $Pb_xZn_{1-x}S$ films with silver contact are shown in Figure 5.20. The linear nature of I-V characteristics confirms that silver makes ohmic contact with $Pb_xZn_{1-x}S$ indicating that the work function of silver is higher than the $Pb_xZn_{1-x}S$ thin film (Ibrahim et al. 2014). Figures 5.21, 5.22, 5.23, 5.24 and 5.25 show the I-V curves for $Pb_xZn_{1-x}S$ (x=0.8, 0.6, 0.5, 0.4 and 0.2) thin films respectively at different substrate temperatures. It is evident that the resistivity of the $Pb_xZn_{1-x}S$ films decreases with increase in substrate temperature and annealing duration. Table 5.22 shows the resistivity of the films calculated at different substrate temperature using the equation 2.15.

Table 5.22 Resistivity values of the $Pb_xZn_{1-x}S$ thin film at different substrate temperature.

| **Composition** | **$T_s$ (˚C)** | **Resistance (Ω)** | | **Resistivity (Ω cm)** | |
|---|---|---|---|---|---|
| | | **As deposited** | **Annealed** | **As deposited** | **Annealed** |
| $Pb_{0.8}Zn_{0.2}S$ | 250 | 6.39E+04 | 5.11E+04 | 0.35145 | 0.281 |
| | 300 | 3.61E+04 | 1.48E+04 | 0.19855 | 0.0814 |
| | 350 | 1.74E+04 | 1.12E+04 | 0.0957 | 0.0616 |
| $Pb_{0.6}Zn_{0.4}S$ | 300 | 2.17E+05 | 2.05E+05 | 1.1935 | 1.1275 |
| | 350 | 1.74E+05 | 1.39E+05 | 0.957 | 0.7645 |
| $Pb_{0.5}Zn_{0.5}S$ | 300 | 6.22E+05 | 2.74E+05 | 3.421 | 1.507 |
| | 350 | 2.81E+05 | 2.42E+05 | 1.5455 | 1.331 |
| $Pb_{0.4}Zn_{0.6}S$ | 300 | 1.38E+06 | 6.22E+05 | 7.59 | 3.421 |
| | 350 | 1.26E+06 | 5.25E+05 | 0.63 | 0.2625 |
| | 400 | 1.11E+06 | 2.81E+05 | 6.105 | 1.5455 |
| $Pb_{0.2}Zn_{0.8}S$ | 300 | 2.99E+07 | 6.38E+06 | 164.45 | 35.09 |
| | 350 | 1.18E+07 | 5.54E+06 | 64.9 | 30.47 |
| | 400 | 1.06E+07 | 3.88E+06 | 58.3 | 21.34 |

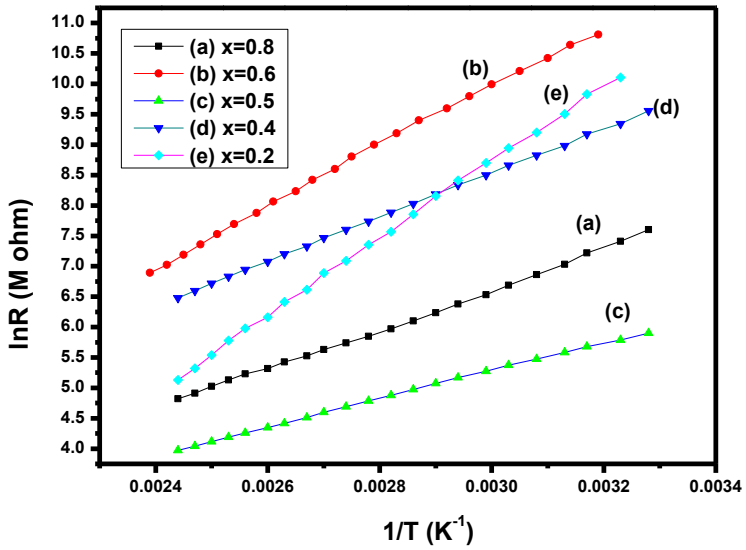


Fig. 5.26 Variation in ln R with the inverse of temperature for $Pb_xZn_{1-x}S$ thin-films.

Table 5.23 Activation energy of $Pb_xZn_{1-x}S$ (x=0.2-0.8) thin films.

| **Composition** | **Activation energy (eV)** |
|---|---|
| $Pb_{0.8}Zn_{0.2}S$ | 0.32 (intrinsic) |
| $Pb_{0.6}Zn_{0.4}S$ | 0.41 (intrinsic) |
| $Pb_{0.5}Zn_{0.5}S$ | 0.28 (extrinsic) |
| $Pb_{0.4}Zn_{0.6}S$ | 0.39 (extrinsic) |
| $Pb_{0.2}Zn_{0.8}S$ | 0.54 (extrinsic) |

The plot of the ln R versus the inverse of absolute temperature ranging from 313K to 400K is shown in Figure 5.26. The decrease in resistance with an increase in temperature indicates its semiconducting nature. The activation energy was calculated by using the equation 2.16. Table 5.23 shows the activation energy for the various compositions, calculated from the ln R Vs 1/T plots. Figure 5.26 shows variation in ln R with the inverse of

temperature for $Pb_xZn_{1-x}S$ thin-films in the temperature range from 313K to 400K. The plots show extrinsic conduction in $Pb_xZn_{1-x}S$ thin-film with $x \leq 0.5$ and intrinsic conduction for the film with $x > 0.5$ is due to interband transition. Hot probe measurement indicates n-type nature of conductivity of the films. The carrier concentration and mobility determined for annealed films deposited at various substrate temperatures are calculated using equations 2.24 and 2.25 respectively. Hall Effect analysis shows that the films were n-type which confirms the results of hot probe measurements. The conductivity of the films increases with increase in substrate temperature. This change can be related to the improvement in the crystallinity of the films at higher substrate temperatures. Since annealing also improves the crystallinity the same reason holds good for the observed increase in the conductivity of the annealed films (Gowrish et al. 2005). Annealing of the films minimizes the native defects such as dislocations, vacancies, and interstitial atoms etc which act as carrier traps. Hence, the reduction in the defects certainly enhances the conductivity. The excess sulphur atoms in the films deposited at lower temperatures, act like scattering centers impeding the flow of carriers (Suhail 2012). The conductivity, carrier concentration and mobility of the films decreased with increase in Zn composition as shown in Table 5.24 which is attributed to the reduced crystallite size of the films which results in the increasing defects that can act as carrier traps (Yilmaz et al. 2015).

Table 5.24 Electrical properties of stoichiometric $Pb_xZn_{1-x}S$ (x= 0.2-0.8) thin films.

| **Ratio** | **Conductivity (S/cm)** | | **Carrier Concentration ($/cm^3$)** | | **Mobility ($cm^2/VS$)** | |
|---|---|---|---|---|---|---|
| | **As** | **An** | **As** | **An** | **As** | **An** |
| $Pb_{0.8}Zn_{0.2}S$ | 0.1044932 | 0.162338 | $3.534X10^{17}$ | $1.316X10^{17}$ | 7.653 | 7.706 |
| $Pb_{0.6}Zn_{0.4}S$ | 0.0097752 | 0.01308 | $1.289X10^{17}$ | $1.596X10^{17}$ | 5.064 | 5.116 |
| $Pb_{0.5}Zn_{0.5}S$ | 0.0055772 | 0.007513 | $9.989X10^{16}$ | $1.166X10^{17}$ | 4.021 | 4.026 |
| $Pb_{0.4}Zn_{0.6}S$ | 0.001638 | 0.00378 | $3.896X10^{16}$ | $1.499X10^{16}$ | 2.651 | 2.696 |
| $Pb_{0.2}Zn_{0.8}S$ | 0.0001715 | 0.000469 | $6.613X10^{15}$ | $1.76\ X10^{15}$ | 1.621 | 1.663 |

# CHAPTER 6

# SUITABILITY FOR DEVICE APPLICATIONS

This chapter deals with the photoconductivity measurements and heterojunction studies, carried out for the $Pb_xZn_{1-x}S$ thin films to find the suitability for device applications such as optoelectronic devices.

## 6.1 PHOTOCONDUCTIVITY MEASUREMENTS

It is well known that since 1946 PbS is an $A_4$ $B_6$ semiconductor compound with very good photoconductive properties in the 1000-3000nm (IR domain) spectral range at room temperature (Cashman 1946). The Pb ions were replaced by Zn ions to enhance the photoconductive properties of the PbS films from IR domain to UV – IR domain. Hence, the photoconductive properties of $Pb_xZn_{1-x}S$ thin films were studied and reported. The relative sensitivity of the photoconductive material depends on the wavelength of the incident radiation. A plot of relative response as a function of wavelength is called a spectral response curve. The position of the peak response normally corresponds to the band gap energy of the material. On the longer wavelength side, the photoresponse goes down because the photons will not have enough energy to create electron-hole pairs. However, it is frequently observed that the photoresponse goes on the shorter wavelength side even though the absorption coefficient is high in this spectral region. This is because the photons of these energies are absorbed in or near the surface of the semiconductor where the recombination is very high (Gowrish et al. 2010).

The normalized spectral response curves of the $Pb_xZn_{1-x}S$ (x= 0.8, 0.6, 0.5, 0.4 and 0.2) films at different substrate temperature are shown in Figures (6.1, 6.2, 6.3, 6.4 and 6.5) respectively. The $Pb_{0.8}Zn_{0.2}S$, $Pb_{0.6}Zn_{0.4}S$, $Pb_{0.5}Zn_{0.5}S$, $Pb_{0.4}Zn_{0.6}S$ and $Pb_{0.2}Zn_{0.8}S$ spectra show a peak at about 890 nm, 780nm, 590nm, 516nm and 451nm respectively which corresponds to the band gap energy (1.39 eV, 1.59eV, 2.11eV, 2.4eV and 2.75eV) of the material. The spectral response curves of the stoichiometric $Pb_xZn_{1-x}S$ (x= 1, 0.8, 0.6, 0.5, 0.4 and 0.2) films are shown in Figure 6.6. It is observed that for PbS films, photoconductivity

lies in NIR region whereas it is shifted towards visible region with addition of zinc to lead sites. This may be due to shifting of lattice parameters towards lower diffraction angle. The decrease in photocurrent with the increase in zinc ion concentration is caused by the decrease in the crystallite size and mobility of the charge carriers. The increase in photocurrent with the increase in substrate temperature in each $Pb_xZn_{1-x}S$ (x=0.8, 0.6, 0.5, 0.4 and 0.2) films is caused by the increased crystallite size and higher mobility of the charge carriers. The ratios of film resistance under dark ($R_d$) and illuminated ($R_i$) conditions are given in Tables 6.1 and 6.2. The decrease in photosensitivity with the increase in zinc ion concentration is due to decrease in photocurrent which is caused by decreased crystallite size and mobility of the charge carriers. The increase in photosensitivity with the increase in substrate temperature in each $Pb_xZn_{1-x}S$ (x=0.8, 0.6, 0.5, 0.4 and 0.2) films is due to increase in photocurrent which is caused by increased crystallite size and mobility of the charge carriers.

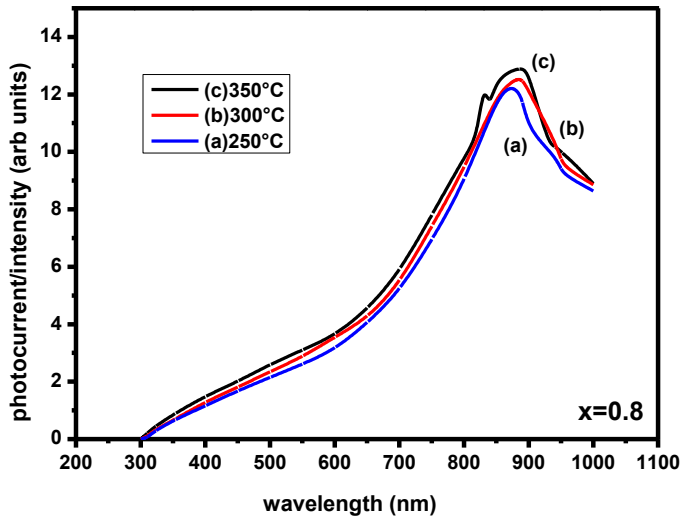


Fig. 6.1 Spectral response curves of $Pb_{0.8}Zn_{0.2}S$ films deposited at a different substrate temperature.

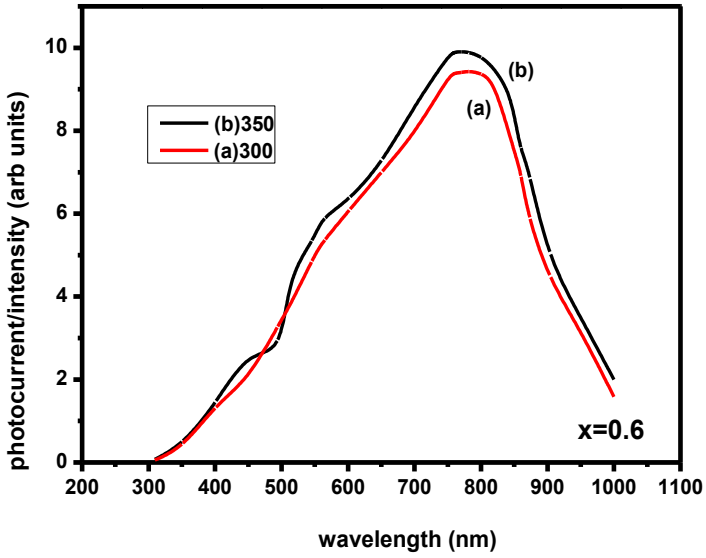

Fig. 6.2 Spectral response curves of $Pb_{0.6}Zn_{0.4}S$ films deposited at a different substrate temperature.

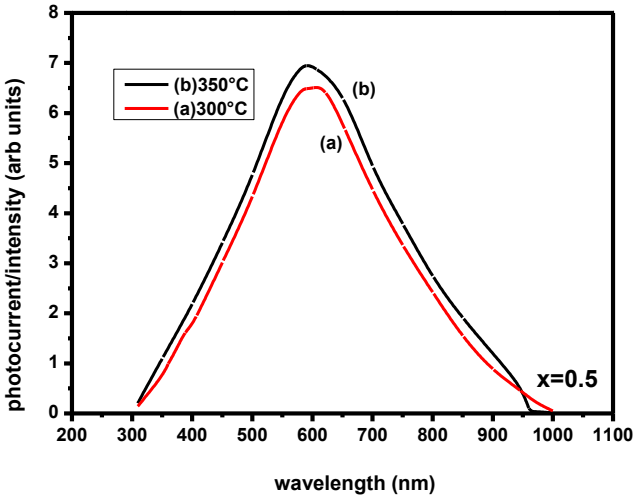


Fig. 6.3 Spectral response curves of $Pb_{0.5}Zn_{0.5}S$ films deposited at a different substrate temperature.

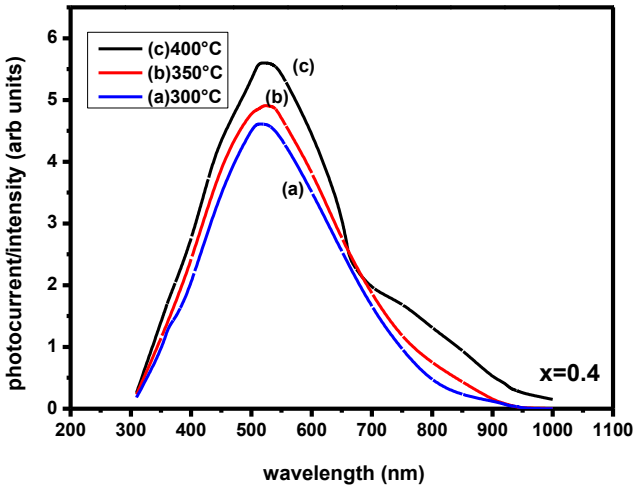


Fig. 6.4 Spectral response curves of $Pb_{0.4}Zn_{0.6}S$ films deposited at a different substrate temperature.

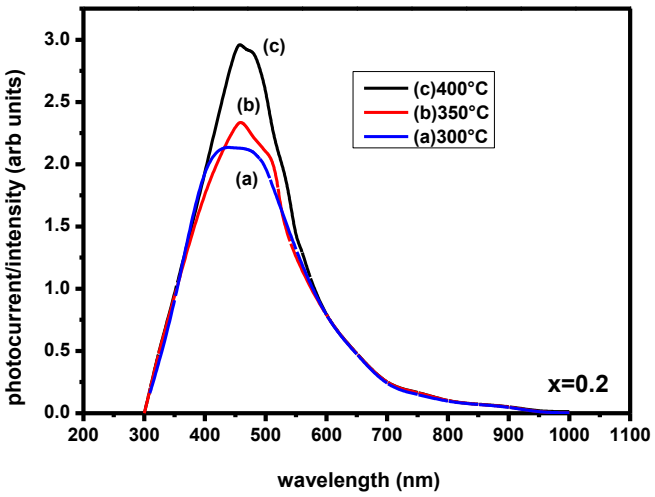

Fig. 6.5 Spectral response curves of $Pb_{0.2}Zn_{0.8}S$ films deposited at a different substrate temperature.

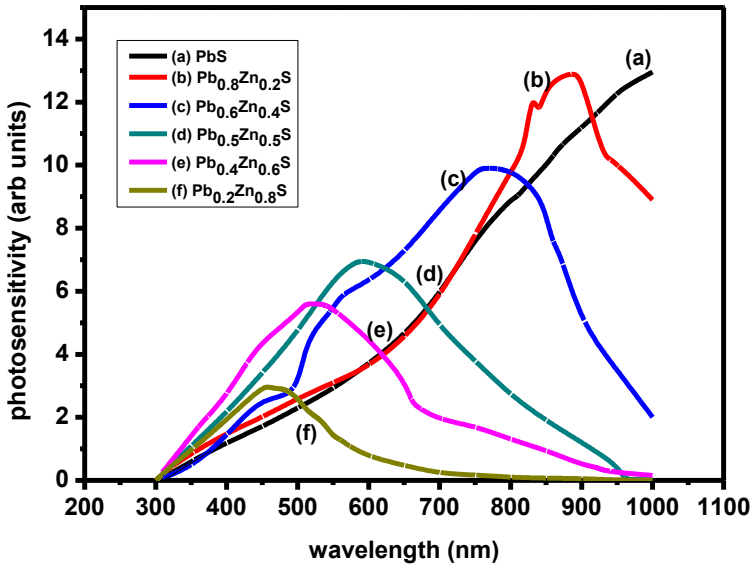


Fig. 6.6 Spectral response curves of stoichiometric $Pb_xZn_{1-x}S$ films.

Table 6.1 Ratios of film resistance under dark ($R_d$) and illuminated ($R_i$) conditions for $Pb_xZn_{1-x}S$ films deposited at different substrate temperature.

| | **Substrate temperature (˚C)** | **Dark resistance $R_D$(KΩ)** | **illuminated resistance $R_i$ (KΩ)** | **$R_D/R_i$ Sensitivity** |
|---|---|---|---|---|
| PbS | 225 | 1.68 | 0.0796 | 21.1 |
| $Pb_{0.8}Zn_{0.2}S$ | 250 | 51.1 | 3.194 | 15.995 |
| | 300 | 14.8 | 0.869 | 17.02 |
| | 350 | 11.2 | 0.613 | 18.242 |
| $Pb_{0.6}Zn_{0.4}S$ | 300 | 20.5 | 13.047 | 15.72 |
| | 350 | 13.9 | 8.559 | 16.24 |
| $Pb_{0.5}Zn_{0.5}S$ | 300 | 274 | 26.76 | 10.24 |
| | 350 | 242 | 20.35 | 11.89 |
| $Pb_{0.4}Zn_{0.6}S$ | 300 | 622 | 68.05 | 9.14 |
| | 350 | 525 | 54.01 | 9.72 |
| | 400 | 481 | 44.13 | 10.9 |

| | | | | |
|---|---|---|---|---|
| $Pb_{0.2}Zn_{0.8}S$ | 300 | 6380 | 1724.32 | 3.7 |
| | 350 | 5544 | 788.09 | 7.12 |
| | 400 | 3882 | 461.36 | 8.41 |

Table 6.2 Ratios of film resistance under dark ($R_d$) and illuminated ($R_i$) conditions for stoichiometric $Pb_xZn_{1-x}S$ films.

| | **Substrate temperature (˚C)** | **Dark resistance $R_D$(KΩ)** | **illuminated resistance $R_i$ (KΩ)** | **$R_D/R_i$ Sensitivity** |
|---|---|---|---|---|
| PbS | 225 | 1.68 | 0.0796 | **21.1** |
| $Pb_{0.8}Zn_{0.2}S$ | 350 | 11.2 | 0.6139 | **18.24** |
| $Pb_{0.6}Zn_{0.4}S$ | 350 | 13.9 | 8.559 | **16.24** |
| $Pb_{0.5}Zn_{0.5}S$ | 350 | 242 | 20.35 | **11.89** |
| $Pb_{0.4}Zn_{0.6}S$ | 400 | 481 | 44.128 | **10.9** |
| $Pb_{0.2}Zn_{0.8}S$ | 400 | 3882 | 461.355 | **8.41** |

## 6.2. HETEROJUNCTION STUDIES

P-N junctions form the basis of all semiconductor devices. Hence, it is necessary to check the diode characteristics of materials to use them in various device applications. It is well known from the literature (Hussain et al. 2016, Luther et al. 2010, Hernandez et al. 2011, Rath et al. 2011, Elabd et al. 1980, Steckl et al. 1980, Joshi et al. 2004 and Hussain et al. 2013) that PbS is compatible to form better heterojunction with various compounds. Hence, to check the performance of $Pb_xZn_{1-x}S$ (x=1, 0.8, 0.6, 0.5, 0.4 and 0.2) thin films with Si substrate to form a junction, diode characteristics of n-PbS/p-Si have been studied.

Heterojunctions are formed by joining two different semiconductors having different energy band gap is accommodated by discontinuities in valence and conduction band edges i.e., $\Delta E_v$ and $\Delta Ec$. Band bending on either side of the interface is seen in p-n and metal-semiconductor junctions, but band discontinuity is unique to heterojunctions. Such discontinuity plays an important role in determining carrier transport and confinement

properties of the heterojunctions. It offers a wide range of design choice for novel semiconductor devices such as transistors, diodes, detectors etc (Achuthan 2007).

Based on the conductivity type of the semiconductors involved, in heterojunctions, they can be classified into two types: isotype (both have the same type of conductivity e.g p-p, n-n) and an-isotype (having a different type of conductivity such as p-n junctions). Three different kinds of heterojunctions are possible depending on band alignment at the interface of constituent compounds they are type I (straddled alignment Fig. 6.7 a), type II (staggered alignment Fig. 6.7 b) and type III (broken alignment Fig. 6.7 c).

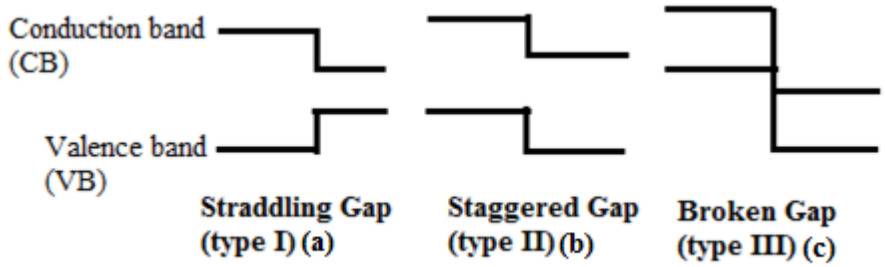


Fig. 6.7 Schematic representation of three possible band alignments to hetero-interface.

Type I: the band gap of one semiconductor is completely contained in the band gap of the other one. The discontinuities of the bands are such that both types of carriers need the energy to change from the material with the smaller band gap to the one with the larger gap – the carriers from the other side gain this energy which is advantageous for diode applications.

Type II: the conduction band and valence band edge of one material is lower than the corresponding band edge of the material. This feature of the heterojunction enhances the spatial separation of photogenerated charge carriers, which makes them potential candidates for solar cell applications. Thus, desired device characteristics can be achieved by a suitable combination of the compound.

In order to get the advantage of lead zinc sulphide thin films in the fabrication, the possibility of integrating lead zinc sulphide based optoelectronics with the widely used silicon – base microelectronics must be thoroughly investigated. This type of investigation would primarily require a thorough study of PbZnS-Si heterojunction. To form n- $Pb_xZn_{1-x}S$ /p-Si heterojunction; Boron doped p-type silicon wafers were taken as the substrates and PbZnS films were deposited on them at various substrate temperature using spray

pyrolysis technique. The silicon wafers used for the fabrication of n-$Pb_xZn_{1-x}S$ /p-Si heterojunction are mirror like p-type (100) orientation with resistivity 8-12 Ω cm and 525 μm thickness. The deposition of lead zinc sulphide thin films on silicon wafers is similar to the deposition of lead zinc sulphide thin films on glass substrates as discussed in chapter 5. The aluminium electrodes (diameter 0.1 cm) are deposited on the surface of silicon wafers by vacuum evaporation for ohmic contact. The metal silver (diameter 0.1 cm) electrodes are vacuum deposited on the PbZnS film through a suitable mask to form the structure Al/(p)Si/(n)PbZnS/Ag as shown in Figure 6.8.

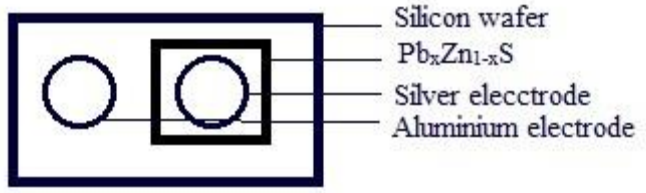


Fig. 6.8 Schematic diagram of Al/(p)Si/(n)PbZnS/Ag structure.

I-V curves of n- $Pb_xZn_{1-x}S$ (x=1, 0.8, 0.6, 0.5, 0.4 and 0.2)/p-Si heterojunction at various ambient temperatures are shown in Figures 6.9 (a, b, c, d, e and f) respectively. Fig. 6.9 (g) shows the I-V curve of n-ZnS /p-Si heterojunction at room temperature. It is observed that the forward current is very small comparable with the reverse current. This is because of the high resistivity of undoped zinc sulphide film which makes the heterojunction unsuitable for any application. The junctions with mixed $Pb_xZn_{1-x}S$ films exhibit rectifying characteristics with small reverse current indicating the existence of a barrier between the interface of p-Si wafer and n- $Pb_xZn_{1-x}S$ (x=1, 0.8, 0.6, 0.5, 0.4 and 0.2) thin film. Under forward bias condition, the height of the potential barrier will be lowered by the applied forward voltage 'V'. The equilibrium initially established between the forces tending to produce diffusion of majority carriers and the restraining influence of the potential energy barrier at the junction will be disturbed. Hence, for a forward bias, the holes cross the junction from p-type to n-type region, where they constitute an injected minority current. Similarly, the electrons cross the junction in reverse direction and become a minority current injected into the p-region. Under reverse bias, the height of the potential energy barrier is increased by an amount $qV$ where $q$ is the elementary charge and $V$ is the applied reverse voltage. This increase in the barrier height reduces the flow of majority carriers whereas the

minority carrier flow is uninfluenced which constitutes a small reverse current Reddy (2012) and Hussain (2013).

The conduction mechanism in a heterojunction diode usually follows the model proposed by Sze and Crowell (Crowell 1966, Rhoderick 1988 and Lamberti 2008). According to this model, the conduction occurs mainly due to thermionic emission and carrier diffusion. The forward current varies with the voltage according to the equation,

$$I = I_S \exp \frac{qV}{nkT} \tag{6.1}$$

where $I_s$ is the reverse saturation current, $k$ is Boltzmann's constant, $n$ is the diode ideality factor, $T$ is the temperature and $q$ are the elementary charges.

In order to verify the conduction mechanism in the present heterojunction, a graph showing the variation of $lnI$ with voltage '$V$' was drawn as shown the Fig. 6.10. Such variation should be linear if the conduction is by thermionic emission according to the equation 6.1. Fig. 6.11 and Fig. 6.12 show the variations in the low and high forward bias conditions respectively for $Pb_xZn_{1-x}S$ (x=1, 0.8, 0.6, 0.5, 0.4 and 0.2) thin films. The linear nature of the graph at low voltages suggests that the thermionic emission is the dominant conduction mechanism at low voltages. The ideality factor for the diode determined from the slope of the graph is summarized in Table 6.3. The ideality factor decreased marginally with the increase in ambient temperature and Zn ion concentration. The non-linear nature of the graph in Fig. 6.12 hints at the possibility of a different conduction mechanism in operation at higher voltages. The variation of current with the square of the voltage was studied and it was found to be linear as shown in Figure 6.13 for $Pb_xZn_{1-x}S$ (x=0.5). This linear variation implies the space charge limited conduction (SCLC) mechanism at higher voltages. The conduction through SCLC mechanism can be expressed by the equation 6.2.

$$I = \left(\frac{AV^2 N_C \mu \varepsilon_0 \varepsilon_r}{8L^3 N_t}\right) \exp\left(\frac{-E_t}{kT}\right) \tag{6.2}$$

where $\varepsilon_r$ is the relative permittivity, $N_c$ is the effective density of states, $N_t$ is the concentration of traps with activation energy $E_t$, $L$ is the thickness of the film and $\mu$ is the electron mobility. The barrier height of the heterojunction can be determined by the equation for thermionic emission. The reverse saturation current '$I_s$' is given by

$$I_s = AA^*T^2 \exp(\frac{-\Phi_b}{kT}) \qquad (6.3)$$

where $A$ is the device area, $A^*$ is the Richardson's constant and $\Phi_b$ is the barrier height. The variation of ln ($I_s/T^2$) with $1/T$ was found to be linear for n- $Pb_xZn_{1-x}S$ /p-Si heterojunction as shown in Fig. 6.14. The barrier height $\Phi_b$ calculated from the slope of the graph is summarized in Table 6.3.

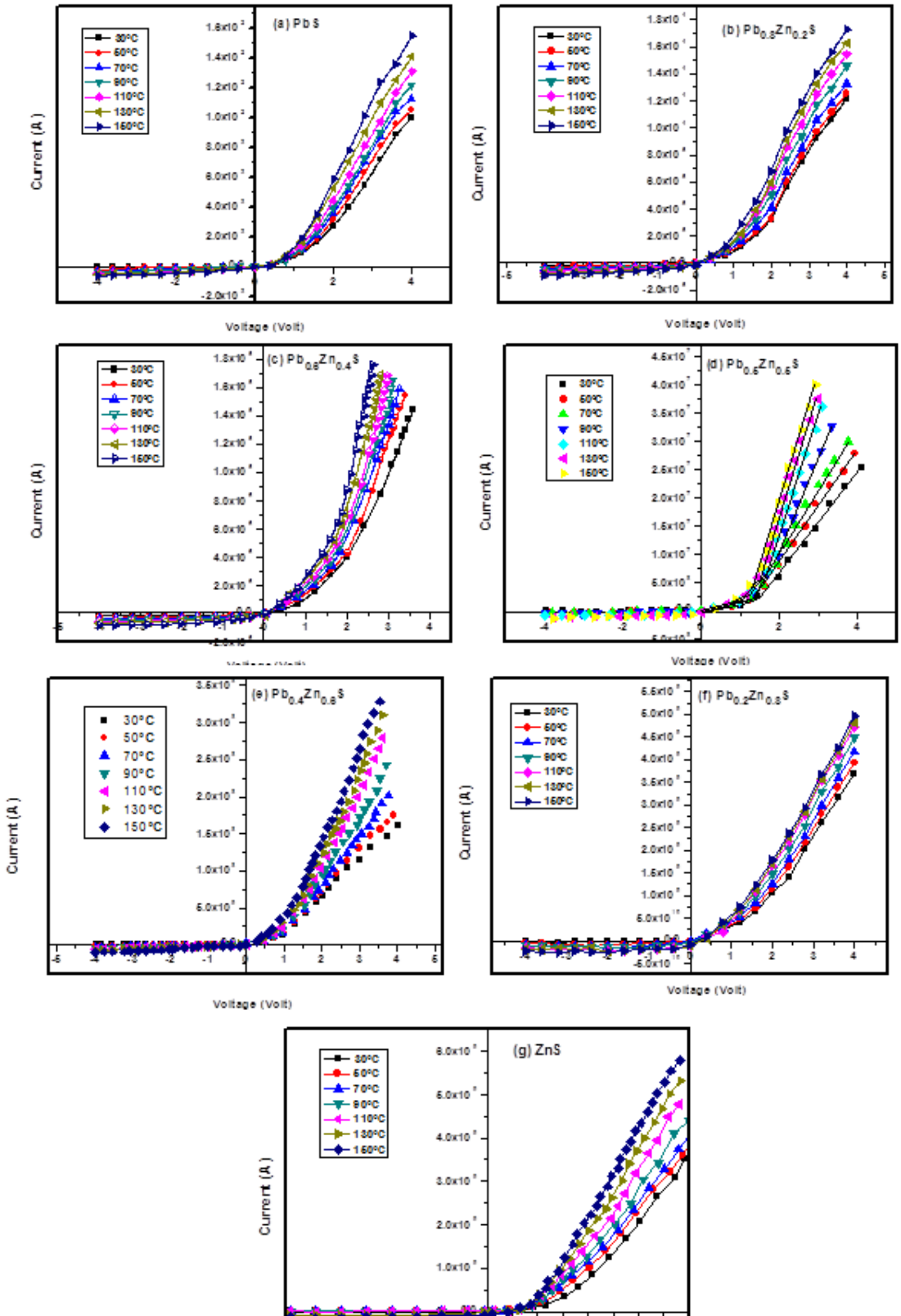

Fig. 6.9 (a to g) I-V characteristics of n- $Pb_xZn_{1-x}S$ (x=0-1) /p-Si heterojunction at a different temperature.

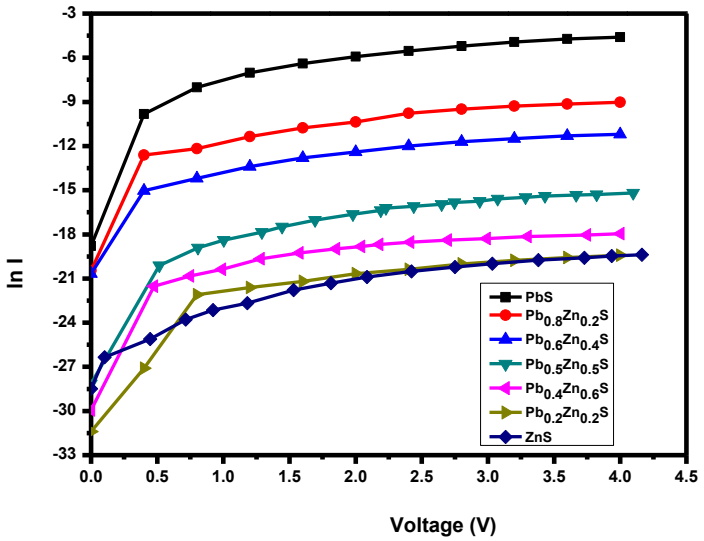


Fig. 6.10 Variation of ln I with voltage for n- $Pb_xZn_{1-x}S$ /p-Si heterojunction.

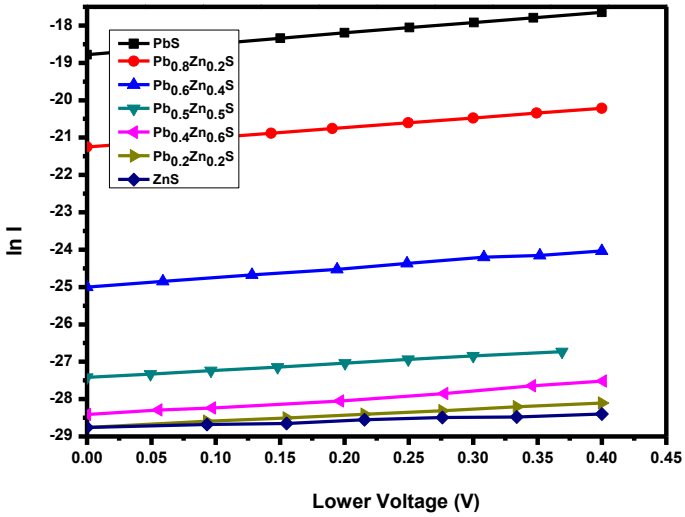


Fig. 6.11 Variation of ln I with voltage for n- $Pb_xZn_{1-x}S$ /p-Si heterojunction in lower voltage region.

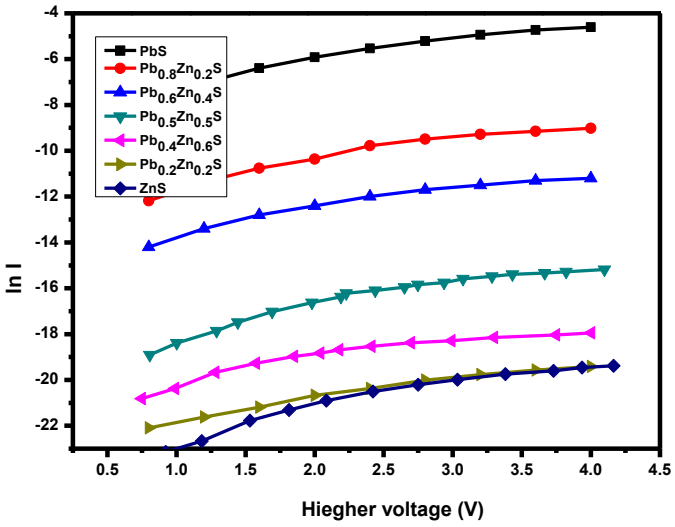

Fig. 6.12 Variation of ln I with voltage for n- $Pb_xZn_{1-x}S$ /p-Si heterojunction in higher voltage region.

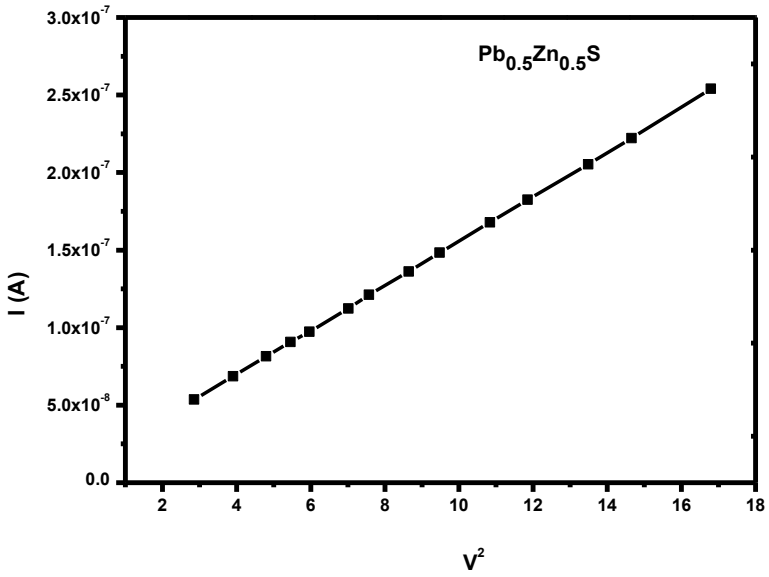


Fig. 6.13 Variation of I with $V^2$ for n- $Pb_xZn_{1-x}S$ (x=0.5) /p-Si heterojunction in higher voltage region.

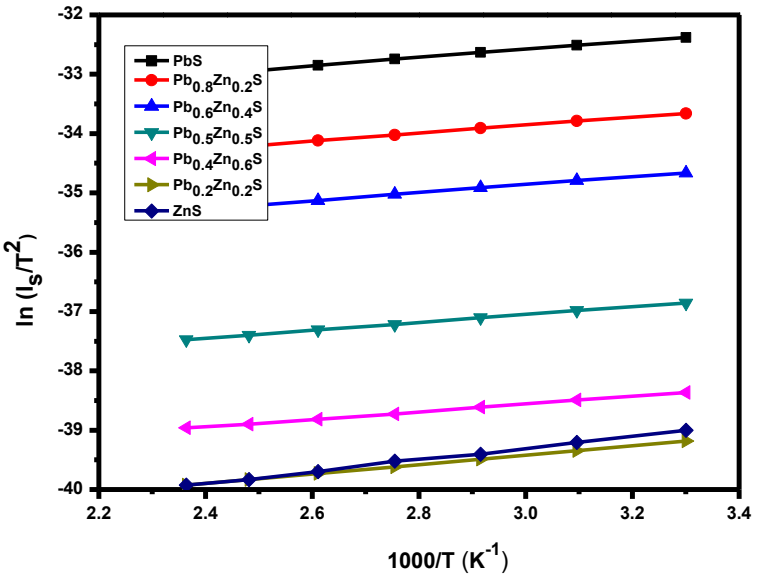


Fig. 6.14 Variation of ln $(I_s/T^2)$ with 1/T for n- $Pb_xZn_{1-x}S$ /p-Si heterojunction.

Table 6.3 summarizes the optical and electrical characteristics of lead zinc sulphide thin films. It shows a change in the energy band gap from indirect to direct electron transition and

shifted towards higher values with decrease in Pb ion concentration. It has been observed that transmittance % in the visible region of the films increased with decreased Pb ion concentration. Barrier height and resistance found to increase with decrease in Pb ion concentration.

Table 6.3. Optical and electrical characteristics of n- $Pb_xZn_{1-x}S$ /p-Si heterojunction.

| **Composition (x)** | **Energy band gap (eV)** | **T (%)** | **λ (nm)** | **R (Ω)** | **Ideality factor** | **Barrier height** |
|---|---|---|---|---|---|---|
| 1 | 1.22(d)/0.4(in) | 45 | >1016 (NIR) | 1.69E+03 | 2.83 | 0.647 |
| 0.8 | 1.39(d)\0.64(in) | 48 | >891 (NIR) | 1.74E+04 | 2.59 | 0.658 |
| 0.6 | 1.59(d)\0.53(in) | 52 | >779.77 (NIR) | 1.86E+05 | 2.25 | 0.679 |
| 0.5 | 2.1(d) | 59 | >590.4 (VIS) | 3.26E+05 | 1.87 | 0.684 |
| 0.4 | 2.4(d) | 63 | >516.6 (VIS) | 1.11E+06 | 1.813 | 0.714 |
| 0.2 | 2.81(d) | 75 | >441.94 (VIS) | 1.06E+07 | 1.63 | 0.79 |
| 0 | 3.54(d) | 95 | >354 (UV) | 0.2E+09 | 1.1 | 0.81 |

.

Increasing concerns on the toxicity of Pb-based materials has initiated research activities on the exploration of novel, environmentally friendly materials and replacing lead with zinc appears to be a welcome step. A variety of non-toxic materials have been synthesized and introduced as candidates for solar cell devices. Present results suggest that lead zinc sulphide thin films with composition x<0.5have suitable characteristics that can be employed for solar window applications.

# CHAPTER 7

# SUMMARY AND CONCLUSIONS

This chapter outlines the summary of the work presented in thesis along with the conclusions pertaining to the research work. Scope for the future work also has been included in the chapter.

## 7.1 SUMMARY OF THE PRESENT WORK

The work presented in this thesis is categorized into seven chapters with various sections in each chapter. The first chapter deals with a brief introduction to the topics covered in the thesis namely thin films, various deposition techniques, lead sulphide, zinc sulphide and lead zinc sulphide thin films. The existing literature on these topics, scope and objectives of the work were reported. The detailed procedure of experimental technique and characterization techniques employed in the work has been covered in the second chapter. The preparation of stoichiometric lead sulphide thin films using spray pyrolysis technique and characterization of these films were discussed in the third chapter. The preparation of stoichiometric zinc sulphide thin films using spray pyrolysis technique and corresponding results obtained by characterization of these films were reported in the fourth chapter. The fifth chapter contains the detailed studies about the preparation of mixed lead zinc sulphide thin films using spray pyrolysis technique and characterization of these films. The sixth chapter concerned with the photoconductivity measurements and heterojunction studies, carried out for the $Pb_xZn_{1-x}S$ thin films to find the suitability for optoelectronic devices. The seventh chapter deals with the summary of the work presented in thesis along with the conclusions. Scope for the future work also has been included.

Stoichiometric and homogeneous PbS, ZnS and PbZnS thin films were successfully prepared using optimized conditions by chemical spray pyrolysis technique. The substrate temperature (150˚C to 350˚C), Pb precursor concentration (1 to 2) and annealing (300˚C to 350˚C with various duration) were varied to obtain stoichiometric PbS films. Similarly, Zn precursor concentrations (1 to 0.25) were varied to synthesize ZnS films. The effect of substrate temperature (250˚C to 450˚C) on the compositional, morphological, structural,

optical and electrical properties of the mixed PbZnS films have been studied using EDAX, SEM, XRD, UV-VIS-IR spectroscopy and Keithley instruments respectively.

A detailed study of the photoconductivity of the PbS and PbZnS films was performed. The PbS, $Pb_{0.8}Zn_{0.2}S$, $Pb_{0.6}Zn_{0.4}S$, $Pb_{0.5}Zn_{0.5}S$, $Pb_{0.4}Zn_{0.6}S$ and $Pb_{0.2}Zn_{0.8}S$ photoconductive spectra show a peak at about 1034 nm, 890 nm, 780 nm, 590 nm, 516 nm and 451 nm respectively which corresponds to the band gap energy (1.22 eV, 1.39 eV, 1.59 eV, 2.11 eV, 2.4 eV and 2.75 eV) of the material.

The heterojunctions involving PbS, ZnS and PbZnS films were fabricated using spray pyrolysis technique and characterized in detail. The study of n- $Pb_xZn_{1-x}S$(x=1, 0.8, 0.6, 0.5, 0.4, 0.2 and 0) /p-Si heterojunction is important as it would be beneficial in integrating PbS and PbZnS with Si-based devices such as solar cell and optoelectronic devices. The heterojunction parameters such as ideality factor and barrier height were determined by detailed study of their I-V characteristics.

## 7.2 CONCLUSIONS

### 7.2.1 PbS thin films

- The films were polycrystalline in nature with face-centered cubic structure oriented along (200) plane. The crystallite size of the film was found to increase with an increase in Pb precursor concentration also with an increase in the substrate temperature as well as annealing.
- The Pb:S films synthesized with precursor concentration ratio 1.25:1 with substrate temperature 225˚C and annealed at 350˚C for four hours were found to be stoichiometric.
- SEM images showed that the films were smooth, homogeneous and uniform.
- The absorption coefficient, direct and indirect band gap energy of the stoichiometric PbS films were found to be $10^2$ $cm^{-1}$, 1.22 eV and 0.41 eV respectively.
- The resistivity of stoichiometric PbS films is found to be in the order of $10^2\,\Omega$ cm.

- ❖ Both hot probe and Hall Effect analysis revealed n-type conductivity in the stoichiometric PbS films.
- ❖ The thermal activation energy of the stoichiometric PbS films found to be 0.20 eV.

7.2.2 ZnS thin films

- ❖ The films were polycrystalline with cubic structure oriented along (111) plane. The crystallite size of the film was found to increase with the decrease in Zn precursor concentration.
- ❖ The ZnS films synthesized with precursor concentration ratio 0.33:1 was found to be stoichiometric.
- ❖ SEM images showed that the ZnS films were granular and homogeneous.
- ❖ The absorption coefficient and optical band gap energy of the stoichiometric ZnS films were found to be $10^2$ $cm^{-1}$ and 3.54 eV respectively.
- ❖ The resistivity and activation energy of the stoichiometric ZnS films were found to be $10^7$ $\Omega^{-1}$ $cm^{-1}$ and 0.82 eV respectively.
- ❖ Hot probe analysis revealed n-type conductivity in the ZnS films.

7.2.3 $Pb_xZn_{1-x}S$ thin films

- ❖ The films were polycrystalline in nature with face-centered cubic structure. The lattice parameter varied from 5.944 (PbS) to 5.364 (ZnS) for $0.2 \leq x \leq 0.8$.
- ❖ The crystallite size of the films decreases with the increase in $Zn^{2+}$ ion concentration. No significant changes in crystallite size due to increase in substrate temperature and annealing.
- ❖ The increase in zinc ion concentration in the $Pb_xZn_{1-x}S$ films changes the preferred orientation from (200) to (111) plane.
- ❖ SEM images show that the substitution of $Zn^{2+}$ ions to the lead sites modifies the morphology of the films.
- ❖ The optical band gap energy of the $Pb_xZn_{1-x}S$ films varies between 1.39eV and 2.81 eV for $0.2 \leq x \leq 0.8$.
- ❖ The absorption coefficient of the $Pb_xZn_{1-x}S$ films decreases as zinc content increases. No significant changes in optical properties due to increase in substrate temperature.

- The resistivity of as-deposited and annealed films increased with an increase in Zn ion concentration and decreases with increase in substrate temperature.
- Both hot probe and Hall Effect analysis indicate that the films show n-type conductivity.
- The resistance of the films decreases with increase in temperature confirming the semiconductor nature of the films. The thermal activation energy for conduction in the films has been determined.
- The carrier concentration and mobility of as-deposited and annealed films are found to decrease with increase in Zn ion concentration and increase with an increase in substrate temperature.
- These results indicate the possibility of band gap tuning associated with lattice parameter variation through a variation of Pb composition for the mixed films.

7.2.4 Photoconductivity studies

- Films were photoconductive in NIR region for PbS and shifted towards visible region while adding zinc ions to lead sites in the PbS films.
- Photocurrent and photosensitivity were decreased with increase in zinc ion concentration and increased with increase in substrate temperature in each $Pb_xZn_{1-x}S$ (x=0.8, 0.6, 0.5, 0.4 and 0.2) films.

7.2.5 Heterojunction studies

- The electrical conduction in the diodes was found to takes place by thermionic emission at low voltages and by space charge limited conduction at high voltages.
- The ideality factor of the diodes determined were varied from 2.85 to 1.63 for $Pb_xZn_{1-x}S$ (x=1, 0.8, 0.6, 0.5, 0.4 and 0.2) thin films.
- Barrier height of the heterojunctions varied from 0.647 to 0.79 for $Pb_xZn_{1-x}S$ (x=1, 0.8, 0.6, 0.5, 0.4 and 0.2) thin films.
- Results suggest that lead zinc sulphide thin films with composition $x<0.5$have suitable characteristics that can be employed for solar window applications.

## 7.3 SCOPE FOR FUTURE WORK

The present work is mainly focused on synthesizing device quality PbS, ZnS and PbZnS films using spray pyrolysis technique. Photoconductivity and heterojunction studies of the films were investigated. In order to enhance the performance of the devices incorporating these compounds, special treatments like specific thermal treatments, radiation annealing, etc may be performed. Doping the samples with various dopants and different extents of doping are very effective in producing drastic effects on the characteristics of the films. Studies including doping to deactivate the compensating defects in order to use the compound in optoelectronic devices can be investigated further. Ternary alloys of PbS, ZnS and PbZnS with different composition are useful in the fabrication of such devices. Selectivity of suitable composition with favorable bandgap and lattice parameters is critical in fabricating heterostructures for specific applications. The other properties such as sensing, mechanical and thermoelectric properties of the films can be studied. Various techniques can be used to evaluate these compounds which prove to be helpful in the mass production of the device quality films.

**REFERENCES**


Abbas, M., Shehab, A., Hassan, N., & Al-Samuraee, A. (2011). Effect of temperature and deposition time on the optical properties of chemically deposited nanostructure PbS thin films. *Thin Solid Films, 519*(15), 4917-4922.

Achuthan, M. K. and Bhat, K. N. (2007) "*Fundamentals of semiconductor devices*", Mc-Graw Hill, Inc. NEW DELHI.

Adeoye, A., Ajenifuja, E., Taleatu, B., & Fasasi, A. (2015). Rutherford Backscattering Spectrometry Analysis and Structural Properties of ZnxPb1-xSThin Films Deposited by Chemical Spray Pyrolysis. *Journal Of Materials, 2015,* 1-8. http://dx.doi.org/10.1155/2015/215210

Afifi, H., Mahmoud, S., and Ashour, A. (1995). "Structural study of ZnS thin films prepared by spray pyrolysis." *Thin Solid Films*, *263*(2), 248-251.

Al-Douri, A., Alias, M., Makadsi, M., Mohammed, G., and Alnajjar, A. (2008). The role of annealing temperature and lead content on optical properties of $Pb_xS_{1-x}$ films. *Thin Solid Films, 517*(2), 881-885.

Altıokka, B. (2015). "Effects of inhibitor on PbS thin films obtained by chemical bath deposition." *Ar. J. Sci. Eng., 40*(7), 2085-2093.

Andersen, J. C. (1965). *"The use of thin films in physical investigations."* New York: Academic press Inc.

Ashraf, M., Akhtar, S., and Qayyum, A. (2012). "Characterization of ternary $Mg_xZn_{1-x}O$ thin films deposited by electron beam evaporation." *Mater. Sci. Semicond. Process., 15*(3), 251-257.

Axelevitch, A., and Golan, G. (2013). "Hot-probe method for evaluation of majority charged carriers concentration in semiconductor thin films." *Facta universitatis - series: Electronics and Energetics, 26*(3), 187-195.

Bardeen, J., Blatt, F. J. and Hall, L. H. (1956). "*In proceedings of photoconductivity." conference held at Atlantic city, eds.* John Wiley, New York, 146.

Barman, J., Sarma, K. C., Sarma, M. and Sarma, K. (2008). Chemically prepared nanocrystalline thin films. *Indian J. Pure Appl. Phys.*, 46, 333.

Barote, M. A., Yadav, A. A., Deshmukh, L. P. and Masumdar, E. U. (2010). "Synthesis and characterization of chemically deposited $Cd_{1-x}Pb_xS$ thin films." *J. Non-Oxide Glasses.* 2, 151-165.

Basak, D., Amin, G., Mallik, B., Paul, G. K. and Sen, S. K. (2003). "Photoconductive UVdetectors on sol–gel-synthesized ZnO filmS." *J. Cr. Growth,* 256, 73–77.

Berry, N. T., Kamoun, N. and Guash, C. (2008). "Physical properties of ZnS thin films prepared by chemical bath deposition." *Appl. Surf. Sci.,* 254, 5039-5043.

Berry, R. W., Hall, P. M. and Harris, M. T. (1968) "*Thin film technology"* New jersey: D. Van No strand Company, Ltd.

Bouderbala, M., Hamzaoui, S., Amrani, B., Reshak, A., Adnane, M., Sahraoui, T., and Zerdali, M. (2008). "Thickness dependence of structural, electrical and optical behaviour of undoped ZnO thin films." *Physica B: Condensed Matter*, *403*(18), 3326-3330.

Bouderbala, M., Hamzaoui, S., Amrani, B., Reshak, A.H. Adnane, M., Sahraoui, T., Zerdali. M., Thickness dependence of structural, electrical and optical behavior of undoped ZnO thin films Physica B, 403, (2008) 3326-3330.

Broderick, N. N. (2003). "*Solid State Electronics*" Electronics book, 47-48.

Bube, R. H. (1963). "*In: Photoconductivity in solids*" (Jhon Wiley, New York), (1963).

Bube, R.H. (1960). "*Photoconductivity of solids*" John Wiley & Sons, Inc., NY. 211-214.

Bube, R.H. (1988). "*in: Electron in Solids: An Introductory Survey*." 2 nd edition, Academic Press Inc.

Cashman, J. R. No title, (1946) *J. Opt. Soc*. 36 356.

Chamberlin R. R. and Skarman J. S. (1966) “Chemical spray deposition process for inorganic films.” *J. Electrochem. Soc.* 113, 86-89.

Chandra, S. and Dhaka, M. S. (2015) “Optimization of physical properties of vacuum evaporated CdTe thin films with the application of thermal treatment for solar cells.” *Mater. Sci. Semicond. Process.* 40, 708-712.

Charles, P., Poole, J. and Owens, F. J. (2003) “*Introduction to Nanotechnology*”, Wiley-interscience publication, 90.

Chaure, N. B., Chaure, S. and Pandey, R. K. (2008). “$Cd_{1-x}Zn_xTe$ thin films formed by non-aqueous electrochemical route.” *Electrochemica Acta.,* 54, 296-304.

Chopra, K. L. (1969). “*Thin film phenomena*.” Tata McGraw-Hill Company Ltd.

Chopra, K. L. and Malhotra, K. L. (1984). “*Thin film technology and applications*.” Tata McGraw-Hill Company Ltd.

Crowell, C. R. and Sze, S. Z. (1966) Current transport in metal semiconductor barriers, solid state electronics 9, 1035-1048.

Cullity, B. D. (1956). “*Elements of X-ray Diffraction*.” Addison wesley Publ. Co.

Daranfed, W., Aida, M. S., Hafdallah, A and H. Lekiket., (2009). “Substrate temperature influence on ZnS thin films prepared by ultrasonic spray.” *Thin Solid Films*, 518, 1082-1084.

Devore, H. B. No title, Phys. Rev., 102 (1956) 86.

Drift, V. A. (1967). “Evolutionary selection, a principle governing growth orientation in vapour-deposited layers.” *Philps Res. Rep.*, 22, 267-288.

Elabd, H. and Steckl, A. J. Structural and compositional properties of the PbS-Si heterojunction. J. *Appl. Phys*. 5 (1980) 726-737.

Erbarut, E. (2003). “Optical response functions of ZnS, ZnSe, ZnTe by the LOM method.” *Sol. State Commun.,* 127, 515-519.

Ezema, F. I. and Osuji, R. U. (2006).“Preparation and optical characterization of chemical bath deposited. $CdCoS_2$ thin films,” *J. App. Sci.* 6, 1827.

Ford, M., Nill, M. and Bryant, A. (2011). "*Precision X-Ray diffractometry*." MSE 104 Spring 2011.

Fraj, M. G. and Omar, H. D. (2014). "The effect of substrate temperature on the structural properties of spray pyrolysed lead sulphide thin films." ARO, The scientific journal of koya university, 92

Fujimura, N., Nishihara, T. and Goto, S. (1993). Control of preferred orientation for ZnOx films: control of self-texture, *J. cryst. Growth.* 130, 269-279.

Gode, F., Guneri, E. and Emen, F. M. "Synthesis, structural, optical, electrical and thermoluminescence properties of chemically deposited PbS thin films." J. Lumi. 147 (2014) 41-48.

Goudarzi, A., Aval, G., Sahraei, R., & Ahmadpoor, H. (2008). Ammonia-free chemical bath deposition of nanocrystalline ZnS thin film buffer layer for solar cells. *Thin Solid Films*, *516*(15), 4953-4957.

Guneri, E., Gode, F. and Cevik, S. (2015). "Influence of grain size on structural and optical properties of PbS thin films produced by SILAR method." *Thin Solid Films*, 589, 578-83.

Hass, G. (1963). "*Physics of thin films*." New York: Academic press Inc.

Hernandez-Borja, J., Vorobiev, Y. V. and Ramirez-Bon, R. (2011). "Thin film ***solar cells*** of CdS/PbS chemically ... by an ammonia-free process." *Sol. Energy Mater. Sol. Cells* 95, 1882-1888.

Hernández-Fenollosa, M., López, M., Donderis, V., González, M., Marí, B., and Ramos-Barrado, J. (2008). "Role of precursors on morphology and optical properties of ZnS thin films prepared by chemical spray pyrolysis." *Thin Solid Films*, *516*(7), 1622-1625.

Hussain, A., and Rahman, A. (2013). "Synthesis and electrical characteristics of Al/(p)PbS schottky barrier junction." *Mater. Sci. Semicond. Process.*, *16*(6), 1918-1924.

Hussain, A., Begum, A. and Rahman, A. (2012). "Electrical & optical properties of nanocrystalline lead sulfide thin films prepared by CBD." *In. J. Phys.* 86, (8), 697-701.

Hussain, A., Singh, H. S. and Rahman, A. (2016). “Electrical characteristics of (n)Si/(p)PbS heterojunction prepared by chemical bath deposition technique, Superlattices and Microstructures.” 89, 43-52.

Ibrahim, S. G. and Ubale, A. U. (2014). “Structural, electrical and optical properties of nanostructured $Cd_{1-x}Fe_xS$ thin films deposited by a chemical spray pyrolysis technique.” *J. Mol. Str*. 1076, 291-298.

Ibrahim, S., and Ubale, A. (2014). “Structural, electrical and optical properties of nanostructured Cd1−xFexS thin films deposited by chemical spray pyrolysis technique.” *Journal of Molecular Structure, 1076,* 291-298.

Ivanov, P. S. (1984). *“Introduction to Solid State Electronics”*, Mir Publishers, Moscow, 385-387.

Ji, J., Ji, H., Wang, J., Zheng, X., Lai, J., Liu, W., and Li, T. et al. (2015). “Deposition and characteristics of PbS thin films by an in-situ solution chemical reaction process.” *Thin Solid Films, 590,* 124-133.

Jiang, X., Jia, C. L. and Zyszka, B. S. (2002). “Manufacture of specific structure of aluminum-doped zinc oxide films by patterning the substrate surface.” *Appl. Phys Lett.,* 80 3090.

Joshi, R. K., Kanjilal, A. and Sehgal, H. K. (2004). “Solution grown PbS nanoparticle films.” *Appl. Surf. Sci*. 221, 43-47.

Kamruzzaman, M., Dutta, R. and Podder, J. (2012). “Synthesis and characterization of the as deposited $Cd_{1-x}Pb_xS$ thin films prepared by spray pyrolysis technique.” *J. Turkish Phys.,* 46, 7.

Kashani, S. (1996). “Production and evaluation of ZnS thin films by the MOCVD technique as alpha-particle detectors.” *Thin Solid Films,* 288, 50-56.

Kennedy, J., Murmu, P. P., Gupta, P. S., Carder, D. A., Chong, S. V., Leveneur, J. and Rubanov, S. (2014). “Effects of annealing on the structural and optical properties of zinc sulphide thin films deposited by ion beam sputtering.” *Mater. Sci. Semicond. Process.,* 26, 561-566.

Khan, A., Mehmood, M., Rana, A., & Muhammad, T. (2010). “Effect of annealing on structural, optical and electrical properties of nanostructured Ge thin films.” *App. Sur. Sci., 256*(7), 2031-2037.

Kittel, C. (1986). “*Introduction to solid state physics*.” 6th ed. New York: wiki and sons. 34-35.

Kiyotaka, W., Kitabatake, M. and Adachi, H. (2004) “*Thin films materials of technology: sputtering of compound materials*.” William Andrew, Inc

Kumar, K., Pasha, S., Muhammad, G., Chidambaram, K., and Deshmukh, K. (2016). “Influence of nickel on the structural, optical and magnetic properties of PbS thin films synthesized by successive ionic layer adsorption and reaction (SILAR) method.” *Mater. Lr, 164*, 108-110.

Lakhdar M.H. Ouni, B., Amlouk, M., Thickness effect on the structural and optical constants of stibnite thin films prepared by sulfidation annealing of antimony films, Optik, 125 (2014) 2295-2301.

Lamberti, C. (2008). “Characterization of semiconductor heterostructures and nanostructures.” Elsevier publications, Netherlands.

Leaver, K. D. and Chapman, B. N. (1971) *“Thin films.”* London: Wykeham publications.

Lenggoro, I. Okuyama, W. K., Mora, J. F. and Tohge, N. (2000). “Preparation of ZnS nanoparticles by electro spray pyrolysis.” *J. Aerosol Sci*. 31, 121-136.

Lopez, M. C., Espinos, J. P. Martin. F. Lienen, D. and Ramos, B. J. R. (2005). “Growth of ZnS thin films obtained by chemical spray pyrolysis the influence of precursors” *J. Cryst. Growth.*, 285, 66-75.

Lopez, M. C., Espinos, J. P., Martin, F., Leinen, D. and Barrado, J. R. R. “ Growth of ZnS thin films obtained by chemical spray pyrolysis: The influence of precursors.” *J. Cry. Growth.* 285, 6-75 (2005).

Luther, J. M., Gao, J., Lioyd, M. T., Semonin, O. E., Beard, M. C. and Nozik, A. J. (2010). "Stability assessment on a 3% bilayer PbS/ZnO quantum dot heterojunction solar cell," *Adv. Mater.* 22, 3704-3707.

Martucci, A., Fic, J., Schell, J., Battaglini, G. and Guglielmi, M. (1999). "The IV characteristic of an ITO/PbS NCs-zirconia/PbS bulk/Au structure ex." *J. App. Phys.* 86 7.

Maskaeva, L. N., Markov, V. F. and Poverkhnost, G. A. (2004). "Hydrochemical deposition of metal sulfide films: modeling and experiment." , *Technical Phys. Lts.,* 2, 100**.**

Maskaeva, L. N., Markov, V. F., Morozova, I. M., Barbin, N. M., Shur, V., Shishkin, E. I. and Samilova, E. S. (2007). "Composition and submicron structure of thin films of supersaturated $Zn_xPb_{1-x}S$ solid solutions." *Technical Phys. Lts.,* 34, 472-474.

Meshram, R. S. and Thombre, R. M. (2012). "Structural & optical properties of ZnS thin films deposited by spray pyrolysis technique" *In. J. Comput. App.,* 22-25.

Mohamed, S. H. (2010). "Photocatalytic, optical and electrical properties of copper-doped zinc sulfide thin films." *J. Phys. D: Appl. Phys.* 43.

Moncada, C., Gonzlez, L. A., Pech-canul, M. I. and Ramirez – Bon, R. (2013). "$Cd_{1-x}Zn_xS$ thin films with low Zn content obtained by an ammonia-free chemical bath deposition process." *Thin Solid Films,* 548, 270-274.

Moss, T. S. (1953), No Title, Research 6, 258.

Nada, M. S. (2011). "Structural and optical properties of ZnS thin ilms prepared by spray. pyrolysis technique." *J. Al-Nahrain Univ.,* 14, 86-92.

Nair, P. K. and Nair, M. T. S. (1989). "Versatile solar control characteristics of chemically deposited PbS-$Cu_xS$ thin film combinations." *Semicond. Sci. Technol.,* 4, 807.

Nelson, J. B. and Riley, J. P. (1945). "An experimental investigation of extrapolation methods in the derivation of accurate unit cell dimensions of crystals." *Proc. Phys. Soc. London..,* 321, 160-177.

Nemec. P. and Frumar, M. (2003). “Chalcogenide-based amorphous thin films pre- pared by pulsed laser deposition.” *J. Optoelec. Adv. Mater.* 5, 1047-1058.

Offer, P. O., Okorie, B. A., Ezekoye, B. A., Ezekoye, V. A. and Ezema, J. I. “Chemical spray pyrolysis synthesis of zinc sulphide (ZnS) thin films via double source precursors.” *J. Ovonic Research.,* 11, 73-77 (2015).

Padiyan, D. P., Marikani, A. and Murali, K. R. (2004). “Structural, optical and photoelectrical properties of vacuum evaporated $Cd_{0.3}Sn_{0.7}Se$ thin films.” *J. Alloys. Comp.,* 365, 8-14.

Pal, U., Samanta, D., Ghorai, S. and Chaudhri, A.K. (1993). “Electrical and optical properties of nanocrystalline lead sulphide thin films prepared by chemical bath deposition.” *J. Appl. Phys.* 74, 63-68.

Pankove, J. I. (1971).“*Optical Processes in Semiconductors*” Dover publications Inc., NY.

Pauw, J. V. (1958). "A method of measuring specific resistivity and Hall Effects of discs of arbitrary shape.", *Philips Research Reports,* 13, 1.

Petritz R. L. (1956) Theory of photoconductivity in semiconductor films, *Phys. Rev.* 104, 1508-1516.

Pike, R. D., Cui, H., Kershaw, R., Dwight, K. and Wold, A. *Thin Solid Films*, 224, 221 – 226 (1993).

Pike, R. D., Cui, H., Kershaw, R., Dwight, K. and Wold, A. (1993). “Preparation of ZnS thin films by ultrasonic spray pyrolysis from bis (diethyl dithio carbamato) Zinc (II).” *J. Appl. Phys.* 23, 452.

Pillai, P. O. (2005). “*Solid State Physics*”, 6 th Edition, New age international (P) limited, publishers, New Delhi.

Popa, A., Lisca, M., Stancu, V., Buda, M., Pentia, E. and Botila, T. (2006).“ Electrical characteristics of nano-PbS/SiO2/Si heterostructures.” *J. Optoelectron. Adv. Mater.,* 8(1), 43–45.

Popescu, M. (2006). “Chalcogenides–past, present, future.” *J. Non-Cryst. Solids*. 352, 887-891

Popescu, V., Nascu, H .J. and Darvasi, E. (2006). “Optical properties of PbS-CdS multilayers and mixed (CdS+PbS) thin films deposited on glass substrate by spray pyrolysis.” *J. Opt. Electron. Adv. Mater.*, 8, 1187-1193.

Preetha, K. C., Murali, K. V., Ragina, A. J., Deepa, K. and Ramadevi, T. L. (2011). “Effect of cationic precursor PH on optical and transport properties of SILAR deposited nano crystalline PbS thin films.” *Cur. App. Phys*., 12, 53.

Preetha, K., Murali, K., Ragina, A., Deepa, K., and Remadevi, T. (2012). “Effect of cationic precursor pH on optical and transport properties of SILAR deposited nano crystalline PbS thin films.” *Cr. App. Phys.*, *12*(1), 53-59.

Rajashree, C., Balu, A., & Nagarethinam, V. (2016). Influence of Al doping on the structural, morphological and opto-electrical properties of spray deposited lead sulfide thin films. *J. Mater. Sci.: Mater. Electrons.*, *27*(8), 7876-7882.

Rajathi, S., Kirubavathi, K. and Selvaraju, K. “Structural, morphological, optical, and photoluminescence properties of nano crystalline PbS thin films grown by chemical bath deposition method. (2014). *Arab. J. Chem.*, 11, 057.

Rath, A., Bernechea, M., Martinez, L., and Konstantatos, G. (2011). “Solution-Processed Heterojunction Solar Cells Based on p-type PbS Quantum Dots and n-type Bi2S3 Nanocrystals.” *Adv. Mater.*, *23*(32), 3712-3717.

Raviprakash, Y., Bangera, K. V. and Shivakumar, G. K. (2009). “Preparation and characterization of $Cd_xZn_{1-x}S$ thin film by spray pyrolysis technique for photovoltaic applications.” *Solar Energy* 83, 1645-1651.

Raviprakash, Y., Bangera, K. V. and Shivakumar, G. K. (2009). “Preparation and characterization of $Cd_xZn_{1-x}S$ thin film by spray pyrolysis technique for photovoltaic applications.” *Solar Energy* 83 (2009) 1645-1651.

Ravishankar, S., Balu, A. R., Anbarasi, M. and Nagarethinam, V. S. (2015). " Influence of precursor molar concentration on the structural morphological, optical and electrical properties of PbS thin films deposited by spray pyrolysis technique using perfume atomizer." *Optic*. 926, 2550-2555.

Ray, S. C., Karanjai , M. K. and Gupta, D. D. (1998). "Fabrication of high quality nanocrystalline thin films for optoelectronic Applications." *Thin Solid Films*, 322, 117-122 .

Reddy K. L. (2011). "*Principle of engineering metallurgy*." New age international Ltd. 78-80.

Reddy, N. N. K. and Reddy, V. R. (2012). "Temperature dependent current–voltage and photovoltaic properties of chemically prepared (p)Si/(n)$Bi_2S_3$ heterojunction." Bull. Mater. Sci. 35 (1), 53-61.

Revathi, N., Prathap, P., Miles, R. W. and Ramakrishna Reddy, K. T. (2010). "Annealing effect on the physical properties of evaporated $In_2S_3$ films, solar energy materials and solar cells." 94, 148-1491.

Rhoderick, E. H. and Williams, R.H. (1988) Metal-semiconductor contacts. Oxford Science Publications, okford.

Rose, A. (1955). "Space-charge-limited currents in solids." *Phys. Rev*; 97, 1538.

Rose, A. (1963). "I*n: Concept in Photoconductivity and Allied Problems."* (Inter science, New York).

Rosenberg, H. M. (1965). "*Low temperature Solid State Physics*", Oxford Clarendon Press, 247.

S. M. Sze, (1985). "*SemiconductorDevices-Physics& Technology*", John Willey& Sons, NY. 22.

Sagade, A., Sharma, R., and Sulaniya, I. (2009). "Enhancement in sensitivity of copper sulfide thin film ammonia gas sensor: Effect of swift heavy ion irradiation." *J. App. Phys., 105*(4), 043701.

Sahraei, R. and Darafarin, S. (2015). “An investigation on optical characteristics of nanocrystalline ZnS:Ni thin films prepared by a chemical deposition method.” *Spectrochimica Acta Part A: Moler. Biomoler. Spectro.*, 149, 941–948.

Sahraei, R. and Darafarin, S. “An investigation on optical characteristics of nanocrystalline ZnS:Ni thin films prepared by chemical deposition method.” *Spectrochimica acta A: molecular and biomolecular spectroscopy*, 149, 941-948 (2015).

Sahraei, R., Abbasi, S., Daneshfar, A., Majles Ara, M.H., Goudarzi, A. and Rahimi, F. (2013). “Optical properties of nanocrystalline ZnS: Mn thin films prepared by a chemical bath deposition method.” *J Mater Sci: Mater Electron*., 24, 260–266.

Sakhare, Y., Thakare, N., and Ubale, A. (2016). “Influence of quantity of spray solution on the physical properties of spray deposited nanocrystalline MgSe thin films.” *St. Petersburg Polytechnical University Journal: Physics and Mathematics*, *2*(1), 17-26.

Seghaier, S., Kamoun, N., Brini, R. and Amara, A. (2006). “Structural and optical properties of PbS thin films deposited by chemical bath deposition.” *Mater. Chem. Physics.*, *97*(1), 71-80.

Seghier, S., Kamoun, N., Brini, R. and Amara, A.B. (2006). “Growth and characterization of lead sulphide thin film for solar cell fabrication.” *Mater. Chem. Phys*, 97, 71-80.

Sharma, A. B., Sharma, M. and Pandey, R.K. (2009). “ *Asian journal of Chemistry*, 21(10), 33-38.

Simpson, O. (1951). “Photoconductivity in the Infra-Red region of the spectrum. Part II. The mechanism of photoconductivity in lead telluride.” *Phil. Trans. R. Soc. A.* 243, 547-564.

Slater, J. C. (1956). “Barrier theory of the photoconductivity of lead sulphide.” *phys. Rev*. 103, 1631-1644.

Slonopas, A., Alijabbari, N., Saltonstall, C., Globus, T., and Norris, P. (2015). “Chemically deposited nanocrystalline lead sulfide thin films with tunable properties for use in photovoltaics.” *Electrochimica Acta, 151*, 140-149.

Smith, W. F. and Hasheni, J. (2006). "*Foundations of material science and engineering*." 4th ed. *Mc. Grawhill.* 139-140.

Steckl, A., Elabd, H., Ka-Yee Tam, Shey-Ping Sheu, and Motamedi, M. (1980). "The optical and detector properties of the PbS-Si heterojunction." *IEEE Transactions On Electron Devices*, *27*(1), 126-133.

Suchea, M., Christoulakis, S., Katharakis, M., Vidakis, N., & Koudoumas, E. (2009). Influence of thickness and growth temperature on the optical and electrical properties of ZnO thin films. *Thin Solid Films, 517*(15), 4303-4306.

Sudad, S., Eman, A., Hassan, K. and F. Emad. "PbS nano thin film photoconductive detector." *Int. J. of Phys. Res*. 3 (2013) 21-26.

Suhail, M. H. (2012). "Structural and optical properties of ZnS, PbS, $Zn_{1-x}Pb_xS$, $Zn_xPb_{1-x}S$ and $PbZn_xS_{1-x}$ thin films." *In. J. Pure App. Phy*., 50, 380-386.

Thangaraju, B. and Kaliannan, P. (2000). "Spray pyrolytically deposited PbS thin films by CBD technique." *Semicond. Sci. Technol.,* 15, 849-853.

Tohidi, T., Ghaleh, K. J., Namdar, A. R. and Ghaleh, R. A. (2013). "Effect of deposition time on lead selenide thermoelectric thin films prepared by chemical bath deposition technique." *Mater. Sci. Semicond. Process.*, 1369, 8001 (2013).

Tong, H., Deng, Z. H., Huang, Z. C., Huang, Hailan, J. and Yongge C. W., (2011) Effects of post annealing on structural, optical and electrical properties of Al-doped ZnO thin films. *App. Sur. Sci.* 257 (2011) 4906-4911.

Touati, B., Gassoumi, A., Alfaify, S. and Kamoun-Turki, N. (2015). "Optical, morphological and electrical studies of Zn: PbS thin films." *Mater. Sci. Semicond. Process.*, 34, 82–87.

Veena, E., Bangera, K. V. and Shivakumar, G. K. (2016). " Effect of substrate temperature on the structural and electrical properties of spray deposited lead sulphide thin films." *Mater. Today Proced.*. , 3, 2225-2231.

Wang, Y., Park, S., John., Yeow, T.W., Langner, A. and Müller, F. (2010). " A capacitive humidity sensor based on ordered macro porous silicon with thin film surface coating." *Sensors and Actuators B,* 149, 136–142.

Watchman, J. B. and Kalman J. H. (1928). "*Characterization of materials*." Butterworth Heinemann, Boston.

Wells, O. C. (1974) "*Scanning electron microscopy*", Mc-Graw Hill, Inc. USA

Yang, P, Lu, M. and Hu. D. (2003). "Study of Bi -Doped ZnS quantum dots synthesized by chemical capping method." *J. Phys. Chem. Sol.,* 155, 64-67.

Yilmaz, M. and Aydogun, S. (2015). "The effect of Pb doping on the characteristic properties of spin-coated ZnO thin films: Wrinkle structures." *Mater. Sci. Semicond. Process*. 40, 162-170.

Yuan, Z., Zhu, X., Wang, X., Cai, X., Zhang, B., Qiu, D., and Wu, H. (2011). Annealing effects of In2O3 thin films on electrical properties and application in thin film transistors. *Thin Solid Films, 519*(10), 3254-3258.

Yücel, E., Yücel, Y., and Beleli, B. (2015). "Optimization of synthesis conditions of PbS thin films grown by chemical bath deposition using response surface methodology." *J. Alloys. Comp., 642*, 63-69.

**RESEARCH OUTPUTS**

**NATIONAL CONFERENCES**

1. Veena, E., Bangera, K. V. and Shivakumar, G. K. (2015). "Effective role of annealing temperature on the structural properties of spray deposited lead sulphide thin films." National Conference on Condensed Matter Physics and Applications, held at Manipal Institute of Technology, during March 27 -28.

**INTERNATIONAL CONFERENCES**

1. Veena, E., Bangera, K.V. and Shivakumar, G. K. (2015). **"**Effect of substrate temperature on the structural and electrical properties of spray deposited lead sulphide thin films." International Conference on Recent Advances in Nano Science and Technology-2015, held at Sathyabama University, Chennai during July 8 – 10, secured **best paper** award.
2. Veena, E., Bangera, K.V. and Shivakumar, G. K. (2015). "Growth & Characterization of $Pb_xZn_{1-x}S$ thin films by spray pyrolysis." International Conference $4^{th}$ nano today conference – 2015, held in Dubai, during December 6 – 10.
3. Veena, E., Bangera, K.V. and Shivakumar, G. K. (2017). "Influence of zinc precursor concentration on the properties spray deposited lead sulphide thin films." International conference on functional materials, characterization, solid state physics, power, thermal and combustion energy, held in Elur, Andra Pradesh, during April 7 – 8, secured **best presentation** award.

## CONFERENCE PROCEEDINGS

1. Veena, E., Bangera, K. V. and Shivakumar, G.K. (2016). "Effect of substrate temperature on the structural and electrical properties of spray deposited lead sulphide thin films." ***Materials Today Proceedings.*** **3, 2225-2231.**
2. Veena, E., Bangera, K.V. and Shivakumar, G. K. (2017). "Influence of zinc precursor concentration on the properties spray deposited lead sulphide thin films." ***AIP Conference Proceedings*****. 1859, 020115-1-7.**

**INTERNATIONAL JOURNAL PUBLICATIONS**

1. Veena, E., Bangera, K. V. and Shivakumar, G.K. (2016). "Influence of lead precursor concentration on the properties spray deposited lead sulphide thin films." ***International journal of pure and applied physics,* 12, 2, 97-112.**
2. Veena, E., Bangera, K. V. and Shivakumar, G.K. (2017). "Effect of annealing on the properties of spray pyrolysed lead sulphide thin films for solar cell application." ***Applied physics A,* 123:366.**
3. Veena, E., Bangera, K. V. and Shivakumar, G.K. (2017). "Effective role of thickness on structural, electrical and optical properties of lead sulphide thin films for photovoltaic applications." ***Materials science and engineering B,* 223, 64-69.**
4. Veena, E., Bangera, K. V. and Shivakumar, G.K. (2017). "Study on structural, optical and electrical properties of spray pyrolysed $Pb_xZn_{1-x}S$ thin films for optoelectronic applications. ***Optics* 144, 528-538.**

# BIO DATA


| | | |
|---|---|---|
| NAME | : | VEENA E. |
| PERMENENT ADDRESS | : | 103, 34 GANGA BLOCK<br>BDA GNANA BHARATHI ENCLAVE<br>MYISANDRA, NEAR KENGERI MAIN<br>BUS STOP, NEAR KENGARI MAIN<br>ROAD, BANGALORE 60. |
| Tel. No. | : | 9036549243 |
| EMAIL ADDRESS | : | veenaphy.e@ gmail.com |


## EDUCATIONAL QUALIFICATIONS

July 2013- National Institute Of Technology Karnataka, Surathkal, India.

Present Ph.D., Physics (pursuing) (Course work CGPA: 7.67)

**Growth and characterization of spray deposited lead zinc sulfide thin films.**

Jan 2008- Tumkur university, Tumkur, Karnataka, India.

July 2010 M.Sc., Physics (condensed matter physics) (65.20%)

## JOURNAL PUBLICATIONS

1. Veena, E., Bangera, K. V. and Shivakumar, G.K. (2016). "Influence of lead precursor concentration on the properties spray deposited lead sulphide thin films." ***International journal of pure and applied physics,* 12, 2, 97-112.**

2. Veena, E., Bangera, K. V. and Shivakumar, G.K. (2017). "Effect of annealing on the properties of spray pyrolysed lead sulphide thin films for solar cell application." ***Applied physics A,* 123:366**.

3. Veena, E., Bangera, K. V. and Shivakumar, G.K. (2017). "Effective role of thickness on structural, electrical and optical properties of lead sulphide thin films for photovoltaic applications." ***Materials science and engineering B,*** **223, 64-69.**

4. Veena, E., Bangera, K. V. and Shivakumar, G.K. (2017). "Study on structural, optical and electrical properties of spray pyrolysed $Pb_xZn_{1-x}S$ thin films for optoelectronic applications. ***Optics*** **144, 528-538.**

**CONFERENCE PROCEEDINGS**

1. Veena, E., Bangera, K. V. and Shivakumar, G.K. (2016). "Effect of substrate temperature on the structural and electrical properties of spray deposited lead sulphide thin films." ***Materials today proceedings.,*** **3, 2225-2231.**

2. Veena, E., Bangera, K.V. and Shivakumar, G. K. (2017). "Influence of zinc precursor concentration on the properties spray deposited lead sulphide thin films." **AIP conference proceedings 1859, 020115-1-7.**

**INTERNATIONAL CONFERENCES**

1. Veena, E., Bangera, K.V. and Shivakumar, G. K. (2015). **"**Effect of substrate temperature on the structural and electrical properties of spray deposited lead sulphide thin films." International conference on Recent Advances in Nano Science and Technology-2015, held at Sathyabama University, Chennai during July 8-10, secured **best paper** award.
2. Veena, E., Bangera, K.V. and Shivakumar, G. K. (2015). "Growth & characterization of $Pb_xZn_{1-x}S$ thin films by spray pyrolysis." International Conference $4^{th}$ nano today conference – 2015, held in Dubai, during December 6-10.
3. Veena, E., Bangera, K.V. and Shivakumar, G. K. (2017). "Influence of zinc precursor concentration on the properties spray deposited lead sulphide thin films." International conference on functional materials, characterization, solid

state physics, power, thermal and combustion energy, held in Elur, Andra Pradesh, during April 7-8, secured **best presentation** award.

**NATIONAL CONFERENCES**

1. Veena, E., Bangera, K. V. and Shivakumar, G. K. (2015)."Effective role of annealing temperature on the structural properties of spray deposited lead sulphide thin films." National conference on Condensed Matter Physics and Applications, held at Manipal Institute of Technology, during March 27-28.

**WORK SHOPS**

1. Workshop on "Recent advances in optoelectronic materials and devices," $30^{th}$ - $31^{st}$, July 2014, N. M. A. M. Institute of Technology, NITTE, Karnataka, India.
2. Work shop on "Novel functional materials for energy conversion," $4^{th}$-$7^{th}$, October 2016, National Institute of Technology Karnataka, Surathkal, India.